# INJECTABLE SELF-HEALING BIOPOLYMER-BASED HYDROGEL CONTAINING HERBAL EXTRACT FOR CHRONIC WOUND TREATMENT

**MUEANCHAN CHANMONTRI**

**DOCTOR OF PHILOSOPHY**
**IN**
**APPLIED CHEMISTRY**

**SCHOOL OF SCIENCE**
**MAE FAH LUANG UNIVERSITY**
**2024**

# INJECTABLE SELF-HEALING BIOPOLYMER-BASED HYDROGEL CONTAINING HERBAL EXTRACT FOR CHRONIC WOUND TREATMENT

**MUEANCHAN CHANMONTRI**

**THIS DISSERTATION IS A PARTIAL FULFILLMENT OF THE REQUIREMENTS FOR THE DEGREE OF DOCTOR OF PHILOSOPHY IN APPLIED CHEMISTRY**

**SCHOOL OF SCIENCE**
**MAE FAH LUANG UNIVERSITY**
**2024**

**DISSERTATION APPROVAL**

**MAE FAH LUANG UNIVERSITY**

**FOR**

**DOCTOR OF PHILOSOPHY IN APPLIED CHEMISTRY**

**Dissertation Title:** Injectable Self-healing Biopolymer-based Hydrogel Containing Herbal Extract for Chronic Wound Treatment

**Author:** Mueanchan Chanmontri

**Examination Committee:**

| | |
|---|---|
| Assistant Professor Datchanee Pattavarakorn, Ph. D. | Chairperson |
| Associate Professor Orawan Suwantong, Ph. D. | Member |
| Professor Lisbeth Grøndahl, Ph. D. | Member |
| Assistant Professor Anyarat Watthanaphanit, Ph. D. | Member |
| Assistant Professor Chuleeporn Thanomsilp, Ph. D. | Member |

**Advisors:**

.....Advisor

(Associate Professor Orawan Suwantong, Ph. D.)

.....Co-Advisor

(Professor Lisbeth Grøndahl, Ph. D.)

**Dean:**

.....

(Professor Surat Laphookhieo, Ph. D.)

# ACKNOWLEDGEMENTS

Completing this dissertation has been a significant milestone in my academic journey, and I am deeply grateful to many people who have supported me along the way. First and foremost, I would like to express my sincere thanks to my supervisor, Assoc. Prof. Dr. Orawan Suwantong, from School of Science, Mae Fah Luang University and my co-advisor, Prof. Dr. Lisbeth Grondahl, School of Chemistry and Molecular Biosciences, University of Queensland, Australia. Moreover, I am also deeply grateful to Asst. Prof. Dr. Datchanee Pattavarakorn, Assoc. Prof. Dr. Anyarat Watthanaphanit, and Asst. Prof. Dr. Chuleeporn Thanomsilp for their thoughtful comments and suggestions.

I would like to thank the facilities and the scientific and technical assistance, the Australian Microscopy & Microanalysis Research Facility at the Centre for Microscopy & Microanalysis, the University of Queensland. Moreover, I would like to thank Dr. Ahmed Eid Elsayed Swilem, Dr. Alexandra Mutch, and Jiankun Yang for helping with the facilities and recording the data of XPS, $^{1}$H NMR, and viscosity.

I would like to thank my laboratory members in room 204 in S2 building: Dr. Porntipa Pankongadisak, Dr. Kitipong Kiti, Mr. Tanawat Buntum, Miss Kanyawadee Bureekeaw, and Miss Phanawat Charoensuk for all the enjoyment and and helping in the last few years. I would like to acknowledge the Postgraduate Scholarship (MFU-2020) for tuition fees and the Graduate Research Grant, Mae Fah Luang University for financially supporting this research. Moreover, I would like to thank the scholarship under the Outbound Research Exchange for Excellence Research Collaboration Programme, which allowed me to visit the University of Queensland. This dissertation has received funding support from the National Science, Research and Innovation Fund (NSRF). Furthermore, I would like to thank Scientific and Technological Instruments Center (STIC), Mae Fah Luang University for laboratory facilities. Without their funding, this study would not have been possible.

Mueanchan Chanmontri

| | |
|---|---|
| **Dissertation Title** | Injectable Self-Healing Biopolymer-Based Hydrogel Containing Herbal Extract for Chronic Wound Treatment |
| **Author** | Mueanchan Chanmontri |
| **Degree** | Doctoral of Philosophy (Applied Chemistry) |
| **Advisor** | Associate Professor Orawan Suwantong, Ph. D. |
| **Co-Advisor** | Professor Lisbeth Grøndahl, Ph. D. |

## ABSTRACT

The treatment of chronic wounds such as full-thickness wounds is crucial for preventing infection, which can result in severe conditions and potential amputation. Injectable self-healing hydrogel has gained much interesting for full-thickness wound healing because the hydrogel material can be injected directly and fulfill the wound site. Moreover, the hydrogel material has self-healing properties, which prolongs the healing process due to the recovery ability after damage to the hydrogel. For the first study, quaternized chitosan (QCS) was modified to improve the solubility and antibacterial activity. Also, oxidized pectin (OPEC) was modified to achieve aldehyde groups for Schiff's base reaction with the amino groups from QCS. Then, the hydrogel was optimized by varied concentrations and volumes of QCS and OPEC. The gelation of the hydrogels was evaluated and displayed for less than 1 min. Furthermore, the self-healing of hydrogels was studied and showed 30 min after cutting and continuous self-healing. The mechanical properties of the pure hydrogels were characterized. The compressibility was 162 and 117, which was not significantly different for pure hydrogel. However, the HG_0.6:0.4 showed a significantly higher hardness than HG_0.8:0.2. Moreover, the adhesiveness of HG_0.6:0.4 was 133 Pa within a suitable range for application as a wound dressing. The cytotoxicity and cell migration of pure hydrogels exhibited no cytotoxicity to NCTC clone 929 cells, and HG_0.6:0.4 showed higher cell migration than HG_0.8:0.2 and control. Meanwhile, the extraction media from the pure hydrogels displayed no antibacterial properties against *E. coli* and *S.*

*aureus*. From the result, HG_0.6:0.4 has the best potential use for the wound dressing material for the treatment.

For the second study was to improve the biological activities of hydrogels by incorporating with the α-mangostin (MT) or curcumin (CM)-β-cyclodextrin (CD) inclusion complex (MTx and CMx, respectively). MTx and CMx were prepared to improve the water solubility. The water solubility and XRD of drug-β-CD inclusion complexes were evaluated in this study. Moreover, the antioxidant and anti-inflammatory activities of drug-β-CD inclusion complexes were also evaluated. The results showed that the gelation time of the hydrogels containing drug-β-CD inclusion complexes was within 1 min, and the gel fraction was 81-85%. The injectable self-healing hydrogel containing drug-β-CD inclusion complexes promoted mechanical properties and good performance in antioxidant and anti-inflammatory activities. Furthermore, the antibacterial activity of these hydrogels against *E. coli* and *S. aureus* was up to 80% bacterial inhibition. The hydrogels containing drug-β-CD inclusion complexes were non-toxic to the cells and showed faster wound closure than the pure hydrogels. Thus, these injectable self-healing hydrogels containing MTx or CMx are good candidates for use as wound dressing materials.

**Keywords:** Quaternized Chitosan, Oxidized Pectin, Self-healing, Curcumin, α-Mangostin, Wound Healing

# TABLE OF CONTENTS


| CHAPTER | Page |
|---|---|
| **1 INTRODUCTION** | **1** |
| 1.1 Background and Significant of Research Problem | 1 |
| 1.2 Research Objectives | 4 |
| 1.3 Scope of Research | 5 |
| **2 LITERATURE REVIEWS** | **6** |
| 2.1 Wound | 6 |
| 2.2 Wound Dressings | 8 |
| 2.3 Injectable Hydrogel Dressings | 10 |
| 2.4 Self-Healing Hydrogels | 11 |
| 2.5 Chitosan | 15 |
| 2.6 Pectin | 16 |
| 2.7 Natural Product Extracts | 17 |
| 2.8 Cyclodextrin Inclusion Complex | 18 |
| 2.9 Cyclodextrin Inclusion Complex with Natural Product Extracts | 20 |
| **3 RESEARCH METHODOLOGY** | **22** |
| 3.1 Materials | 22 |
| 3.2 Methodology | 22 |
| **4 RESULTS AND DISCUSSION** | **39** |
| 4.1 Characterization of QCS and OPEC Polymers | 39 |
| 4.2 Fabrication of QCS/OPEC Hydrogels | 42 |
| 4.3 Characterization of QCS/OPEC Hydrogels | 43 |
| 4.4 Rheological Analysis of QCS/OPEC Hydrogels | 45 |
| 4.5 Self-Healing Properties of QCS/OPEC Hydrogels | 46 |
| 4.6 Mechanical Properties of QCS/OPEC Hydrogels | 48 |
| 4.7 *In Vitro* Cytotoxicity of OPEC, QCS, and Hydrogels | 49 |
| 4.8 *In Vitro* Cell Migration of QCS/OPEC Hydrogels | 50 |
| 4.9 Antibacterial Activity of OPEC, QCS, and Hydrogels | 52 |

# TABLE OF CONTENTS


| CHAPTER | Page |
|---|---|
| 4.10 Characterization of MTx and CMx | 54 |
| 4.11 Fabrication of QCS/OPEC Hydrogels Containing Drug-β-CD Inclusion Complexes | 56 |
| 4.12 Swelling and Mass Loss of Hydrogels Containing Drug-β-CD Inclusion Complexes | 57 |
| 4.13 Rheological Analysis of Hydrogels Containing Drug-β-CD Inclusion Complexes | 58 |
| 4.14 Self-Healing Analysis of Hydrogels Containing Drug-β-CD Inclusion Complexes | 60 |
| 4.15 Mechanical Properties and Adhesiveness of Hydrogels Containing Drug-β-CD Inclusion Complexes | 62 |
| 4.16 Cytotoxicity | 64 |
| 4.17 Anti-Inflammatory Activity | 65 |
| 4.18 Antioxidant Activity | 68 |
| 4.19 Antibacterial Activity | 70 |
| 4.20 *In Vitro* Wound Healing of Hydrogels Containing MTx, CMx, and MTx/CMx | 72 |
| **5 CONCLUSIONS** | **74** |
| **REFERENCES** | **76** |
| **APPENDIX** | **90** |
| **CURRICULUM VITAE** | **93** |

# LIST OF TABLES


| Table | Page |
|---|---|
| 2.1 The Development of the Self-Healing Hydrogels | 12 |
| 4.1 Gel Formation Ability of Mixtures of QCS and OPEC | 43 |
| 4.2 Compressibility, Hardness, and Adhesiveness of HG_0.6:0.4 and HG_0.8:0.2 | 49 |
| 4.3 Minimum Inhibition Concentration (MIC) and Minimum Bactericidal Concentration (MBC) Values[1] Against *E. coli* TISTR 527 and *S. aureus* TISTR 746 | 53 |
| 4.4 Compositions, Gel Fraction, Adhesiveness of Injectable Self-Healing QCS/OPEC Hydrogels Containing Drug-β-CD Inclusion Complexes. | 57 |
| 4.5 Antioxidant and Anti-Inflammatory Activities of MTx, CMx, and MTx/CMx (n=3) | 68 |
| 4.6 Antibacterial Activity of MTx, CMx, and MTx/CMx and Amoxicillin Against *E. coli* TISTR 527 and *S. aureus* TISTR 746 (n=3) | 71 |

# LIST OF FIGURES


| Figure | Page |
|---|---|
| 4.1 FTIR Spectra of (A) Chitosan and QCS (B) Pectin and OPEC | 41 |
| 4.2 $^{1}$H NMR Spectra of (A) Chitosan and QCS (B) Pectin and OPEC | 41 |
| 4.3 1D DOSY NMR Spectra of (A) Chitosan and QCS and (B) Pectin and OPEC | 42 |
| 4.4 XPS Survey Spectra of (A) Chitosan and QCS; (B) Pectin and OPEC. Trace Amounts (< 0.7% of Other Elements Such as Ca and Si were Also Observed) | 42 |
| 4.5 Schematic Representation of Potential Intra and Intermolecular Interactions Between QCS and OPEC. Visual Observation of the Self-Healing Behavior of the Injectable Hydrogel HG_0.6:0.4. Part of Diagram with BioRender.com | 44 |
| 4.6 The Rheological Analysis of the HG_0.6:0.4 and HG_0.8:0.2 Samples (A) Storage Modulus G' and Loss Modulus G" Analysis During the Gelation Process (37 ºC, Frequency 1.0 Hz, Strain 1%); (B) G' and G" Strain Sweep (37 ºC, Frequency 1.0 Hz, Strain 1%) | 46 |
| 4.7 Continuous Step Strain Analysis of the HG_0.6:0.4 and HG_0.8:0.2 Sample. Low Strain of 1% and High Strain of 2000% were Applied with 100 s Intervals | 48 |
| 4.8 Indirect Cytotoxicity of (A) OPEC, (B) QCS, and (C) HG_0.6:0.4 and HG_0.8:0.2 Hydrogels (n = 3). *p < 0.05 Compared with the Control at Any Given Extraction Ratio | 50 |
| 4.9 Examples of Images Taken of Scratch Assay to Evaluate the Wound Closure of the Extraction Media for the Two Hydrogels | 51 |
| 4.10 Selected Images of Minimal Bacterial Concentration (MBC) Against *E. coli* TISTR 527 and *S. aureus* TISTR 746 of (A) Chitosan, (B) QCS, (C) Pectin, (D) OPEC, (E) HG_0.6:0.4, and (F) HG_0.8:0.2 | 54 |

# LIST OF FIGURES


| Figure | Page |
|---|---|
| 4.11 XRD Patterns of (A) MT, MTpm, MTx, and β-CD and (B) CM, CMpm, CMx, and β-CD | 55 |
| 4.12 The Solution of MT, MTpm, MTx, CM, CMpm, and CMx in Water at the Concentration of 10 mg/mL | 56 |
| 4.13 A) Swelling Ratio and (B) Mass Loss of HG, HG_MTx, HG_CMx and HG_MTx/CMx (n = 3). *p < 0.05 Compared with HG at Any Given Day (n = 3). #p < 0.05 Compared with Day 1 at Any Given Sample Type (n = 3) | 58 |
| 4.14 Representative Data for Rheological Analysis of the HG (A and E), HG_MTx (B and F), HG_CMx (C and G), and HG_MTx/CMx (D and H) Samples. (A - D) Storage Modulus G' and Loss Modulus G" Analysis During the Gelation Process (37 °C, Frequency 1.0 Hz, Strain: 1 %); (E - H) G' and G" Strain Sweep (37 °C, Frequency 1.0 Hz) | 59 |
| 4.15 Photographs of (A and D) HG_MTx, (B and E) HG_CMx, and (C and F) HG_MTx/CMx Before (Upper) and After (Lower) Self-Healing | 61 |
| 4.16 Representative Data for Continuous Step Strain Analysis of (A) HG, (B) HG_MTx, (C) HG_CMx, and (D) HG_MTx/CMx. Low Strain of 1% and High Strain of 3000% were Applied with 100 s Intervals | 62 |
| 4.17 (A) Compressive Strength, (B) Compressibility, and (C) Hardness of Hydrogel Samples Before and After Self-Healing (n = 3). *p < 0.05 Compared with HG Before or After Healing. #p < 0.05 Compared with the Hydrogels Before Healing at Any Given Sample Type | 64 |
| 4.18 Indirect Cytotoxicity of MTx (A), CMx (B), and HG, HG_MTx, and HG_CMx (C) (n=3). *p < 0.05 Compared with HG at Any Given Extraction Ratio | 65 |

# LIST OF FIGURES


| Figure | Page |
|---|---|
| 4.19 UV Spectra of Extraction Media From HG, HG_MTx (A), HG_CMx (B), and HG_MTx/CMx. Extraction Media (500 mg/mL) of Hydrogels were Prepared in PBS for 24 h. (C) UV Spectra of QCS and OPEC Solutions | 67 |
| 4.20 (A) Anti-Inflammatory Activity of MTx, CMx, and MTx/CMx (n=3). *p < 0.05 Compared with MTx at Any Given Concentration. (B) Anti-Inflammatory Activity of HG, HG_MTx, HG_CMx, and HG_MTx/CMx (n=3). *p < 0.05 Compared with HG at Any Given Extraction Ratio | 68 |
| 4.21 (A) Antioxidant Activity of MTx, CMx, and MTx/CMx (n=3). *p < 0.05 Compared with MTx at Any Given Concentration. (B) Antioxidant Activity of HG, HG_MTx, HG_CMx, and HG_MTx/CMx (n=3). *p < 0.05 Compared with HG at Any Given Extraction Ratio | 69 |
| 4.22 Antibacterial Activity of HG, HG_MTx, HG_CMx, and HG_MTx/CMx (n=3). *p < 0.05 Compared with HG at Any Given Extraction Ratio | 72 |
| 4.23 Representative Light Microscope Images of *In Vitro* Scratch Wound Healing Assay at 0 and 24 h Using NHDF Cells (n=3) | 73 |

# ABBREVIATIONS AND SYMBOLS

| | |
|---|---|
| QCS | Quaternized chitosan |
| OPEC | Oxidized pectin |
| GTMAC | Glycidyl trimethylammonium chloride |
| CM | Curcumin |
| MT | Mangostin |
| β-CD | 2-Hydroxylpropyl- β-cyclodextrin |
| MTx | Mangostin-β-cyclodextrin inclusion complex |
| CMx | Curcumin-β-cyclodextrin inclusion complex |
| HG | Pure hydrogel |
| HG_MTx | Hydrogel containing mangostin-β-cyclodextrin inclusion complex |
| HG_CMx | Hydrogel containing curcumin-β-cyclodextrin inclusion complex |
| % v/v | Percent of volume by volume |
| % w/v | Percent of weight by volume |
| °C | Degree Celsius |
| mL | Milliliter |
| $cm^{-1}$ | Unit of wavenumber |
| $cm^2$ | Square centimeter |
| Mg | Milligram |
| G | Gram |
| Kg | Kilogram |
| N | Newton |
| mg/mL | Milligram per millilitter |
| Mm | Micrometer |
| μL | Microlitter |
| Nm | Nanometer |

# ABBREVIATIONS AND SYMBOLS

| | |
|---|---|
| mM | Millimolar |
| Sec | Second |
| Min | Minute |
| H | Hour |
| Rpm | Revolutions per minute |
| FTIR | Fourier-transform infrared spectroscopy |
| $ABTS^{\bullet+}$ | 2,2'-azino-bis(3-ethylbenzothiazoline-6-sufonic acid) |
| MIC | Minimum inhibitory concentration |
| MBC | Minimum bactericidal concentration |
| CFU | Colony forming unit |
| DMEM | Dulbecco's modified eagle medium |
| FBS | Fetal bovine serum |
| SFM | Serum-free medium |
| $IC_{50}$ | 50% inhibitory concentration |
| NHDF | Normal human dermal fibroblast |
| MTT | 3-(4,5-dimethylthiazol-2-yl)-2,5-dipheyltetrazolium bromide |
| DMSO | Dimethylsulfoxide |
| $^{1}H$ NMR | Proton nuclear magnetic resonance |
| ppm | Parts per million |
| DE | The degree of esterification |
| DA | The degree of acetylation |
| DS | The degree of substitution |
| $\eta$ | Viscosity |
| cP | Centipoise |
| PBS | Phosphate buffer solution |
| BSA | Bovine serum albumin |

# ABBREVIATIONS AND SYMBOLS

| | |
|---|---|
| AMF | The actual macromer fraction |
| G’ | Storage modulus |
| G” | Loss modulus |

# CHAPTER 1

# INTRODUCTION

## 1.1 Background and Significant of Research Problem

The wound care market in Thailand is experiencing significant growth, driven by increasing awareness of advanced wound management techniques and the rising prevalence of chronic conditions such as diabetes and obesity. A growing demand for innovative wound care products, including advanced dressing wounds and care devices characterizes the market. Key factors contributing to this growth include an aging population, improved healthcare infrastructure, and heightened healthcare spending. Additionally, enhancing healthcare services and the presence of local and international players in the market propel the industry's expansion. The integration of modern technologies and an emphasis on research and development are also crucial in advancing wound care solutions in Thailand (Statista, 2024).

Full-thickness wounds, which penetrate the dermis and affect deeper tissues such as subcutaneous fat, muscles, and even bones, pose significant challenges in wound care. These wounds can result from severe trauma, surgical procedures, or chronic conditions such as pressure ulcers and diabetic foot ulcers and suffer from a high risk of complications, including infection, delayed healing, and extensive scarring. The healing process is often prolonged due to substantial tissue loss and the need to regenerate multiple skin layers (Metcalfe & Ferguson, 2007; Fui et al., 2019). To overcome these challenges, advanced wound care techniques and products are employed. Using bioengineered skin substitutes (Urciuolo et al., 2019; Halim et al., 2010) and advanced dressing like hydrocolloids and hydrogels (some products that can heal full-thickness wounds) can significantly enhance the healing process. These solutions provide a conducive environment for tissue regeneration, maintain optimal moisture levels, and protect the wound from infections (Sung & Lee, 2016; Jiang et al.,

2016), Ishihara et al., 2002; Abdel-Mohsen et al., 2016; Anjum et al., 2016). Additionally, implementing a multidisciplinary approach that includes regular debridement, infection control, and nutritional support is crucial. Nowadays, the hydrogel dressing has been developed for full-thickness wound healing to obtain faster and more effective wound healing.

Hydrogels are highly effective in treating full-thickness wounds due to their unique properties and ability to create an optimal healing environment. These hydrophilic polymer networks can retain a large amount of water, providing a moist wound environment crucial for promoting cellular activities in wound healing. The moisture maintained by hydrogels helps soften necrotic tissue, facilitating autolytic debridement and reducing the risk of infection. In full-thickness wound healing, hydrogels can significantly enhance the repair process. They can be formulated to deliver bioactive agents such as growth factors, antimicrobial agents, and stem cells directly to the wound site, thereby accelerating tissue regeneration and reducing inflammation (Pan et al., 2017; Wei et al., 2022). Hydrogels also conform closely to the wound bed, which protects the wound from external contaminants and mechanical stress while relieving pain due to their cooling effect.

Injectable hydrogel represents a cutting-edge approach for treating full-thickness wounds, offering several advantages over traditional wound care methods. These hydrogels comprise biocompatible polymers that can be injected in a liquid state and then solidified in situ to form a gel-like structure. This unique characteristic allows them to fill irregularly shaped wounds and adhere closely to the wound site (Gao et al., 2020; Zhang et al., 2020). This adaptability is particularly beneficial for irregularly shaped wounds in difficult-to-access areas. One of the key benefits of injectable hydrogels is their ability to deliver bioactive agents directly to the wound site. This localized delivery system enhances the therapeutic efficacy by maintaining high concentrations of these agents at the injury site, promoting faster and more effective healing. Additionally, the hydrated environment created by the hydrogels supports cell proliferation and migration providing a barrier against infections (Liang et al., 2019). Injectable hydrogel can also be designed to release its therapeutic payload controlled, further optimizing the healing process and reducing the need for frequent dressing changes.

Self-healing hydrogels represent an advancement in treating full-thickness wounds, allowing them to repair themselves after damage, thus maintaining their structural integrity and function over time (Zhu et al., 2022; Toohey et al., 2007). These hydrogels are designed with dynamic cross-linking networks that can autonomously reform after being disrupted, mimicking the natural healing processes of living tissues. This self-healing capability is particularly beneficial for full-thickness wounds, which often undergo significant stress and mechanical strain during healing. The self-healing hydrogel also reduces frequent dressing changes, minimizing disruption to the healing tissue and reducing patient discomfort. Emerging research indicated that injectable and self-healing hydrogels can significantly improve full-thickness wound healing by facilitating the regeneration of skin layers, reducing scar formation, and also enhancing the speed and quality of wound healing (Yang et al., 2020; Zhao et al., 2022). These make injectable self-healing hydrogels a promising solution in advanced wound care and medical applications. The self-healing ability of a hydrogel should be evaluated. This ability depends on the material's capacity to repair itself without external stimuli and to recover its structural integrity to support its intended function quickly. Moreover, injectability and flow properties should also be studied. The material should exhibit shear-thinning behavior for easy injection and retain homogeneity during the injection process. After injection, the material should then recover its original structure.

Natural product extracts have been used and incorporated into the hydrogel to enhance biocompatibility and biological activities. Natural product extracts such as curcumin (CM) and α-magostin (MT) are known for their anti-inflammatory and antibacterial activities. These natural product extracts can promote cell regeneration, reduce infection risk, and accelerate the healing process (de Andrade Neto et al., 2021; Sharahi et al., 2020; Kamar et al., 2019; Zarena et al., 2012; Moongkarndi et al., 2004). However, CM and MT are poorly water-soluble. Then, the inclusion complexation using cyclodextrin has been used to improve the water solubility. Moreover, the hydrophilic nature of hydrogels provides a moist environment crucial for wound healing, while CM and MT display antioxidant, anti-inflammatory, and antibacterial activities for wound healing improvement. Thus, the hydrogels containing drugs improve the healing outcome and protect the wound from the external environment,

making natural product extracts-loaded hydrogels a superior choice for advance wound care.

In this work, CM and MT were separately complexed with β-cyclodextrin (β-CD) and incorporated into the injectable self-healing hydrogel for full-thickness wound treatment. The injectable self-healing hydrogels were prepared by co-injection of two polymer solutions until they formed a gel-state. The modified polymers used to prepare the injectable self-healing hydrogels were quaternized chitosan (QCS) and oxidized pectin (OPEC). The chitosan was modified to obtain QCS, which has amino groups, while pectin was modified to obtain OPEC, which has aldehyde groups. These groups can react to produce a Schiff's base reaction, which has a self-healing ability. QCS and OPEC were examined for their chemical structure using $^{1}$H-NMR. Furthermore, gelation time, self-healing time, gel fraction, swelling, mass loss, and mechanical properties of the injectable self-healing hydrogel were characterized. For the hydrogels loaded with curcumin inclusion complex (CMx) or α-mangostin inclusion complex (MTx) were further determined for their biological activities, including antibacterial activity, antioxidant activity, anti-inflammatory activity, cytotoxicity, and cell migration.

## 1.2 Research Objectives

1.2.1 To investigate the effect of hydrogel composition on its gelling ability, self-healing ability, and mechanical properties.

1.2.2 To establish the effect of the hydrogel composition on its cytotoxicity and wound healing.

1.2.3 To establish the effect of the hydrogel composition on its antibacterial, anti-inflammatory, and antioxidant activities.

1.2.4 To investigate the effect of hydrogel composition and inclusion complexes, on its gel formation, mechanical properties, and biological activities.

## 1.3 Scope of Research

A systematic investigation was conducted in two sequential phases to achieve the research objectives. The first phase focused on developing a self-healing hydrogel by modifying pectin to introduce aldehyde groups, which can interact with amino groups on chitosan. While chitosan was modified to QCS to improve the water solubility and antibacterial activity. After that, the optimization of hydrogel composition was investigated by varying the concentration of OPEC (10 and 15% w/v) and QCS (2, 4, and 6 % w/v). Subsequently, the volume ratios of QCS:OPEC were varied, such as 0.2:0.8, 0.4:0.6, 0.6:0.4, and 0.8:0.2 mL. The physiochemical properties of the hydrogels were characterized, including gelation time, gel formation, self-healing ability, and mechanical properties, alongside biological evaluations of cytotoxicity, antibacterial activity, and wound healing efficacy.

The second phase investigated the incorporation of inclusion complexes into the optimized hydrogel system, beginning with the determination of optimal molar ratios between β-CD and MT or CM (1:1 molar ratio) to produce MTx or CMx, followed by characterization of the water solubility and crystalline structure of drug-β-CD inclusion complexes. The biological activities of the drug-β-CD inclusion complexes were evaluated for their antioxidant, antibacterial, anti-inflammatory activities, and cytotoxicity. After that, the drug-β-CD inclusion complexes were loaded in the hydrogels. The rheological and mechanical properties of the hydrogels containing drug-β-CD inclusion complexes were evaluated by rheometer and texture analyzer. Moreover, antioxidant activity, anti-inflammatory activity, antibacterial activity, cytotoxicity, and wound closure of the hydrogels containing drug-β-CD inclusion complexes were studied to evaluate the potential use of these hydrogels for wound dressing applications.

# CHAPTER 2

# LITERATURE REVIEWS

## 2.1 Wound

A wound, by definition, is a disruption of the normal structure and function of the skin or tissue. The wound can be classified into different types based on their cause, appearance, and depth, including abrasion, laceration, punctures, incisions, and avulsions (Velnar et al., 2009). Each type of wound requires a specific approach to care and treatment. The body's natural response to a wound involves a complex healing process in 4 stages: hemostasis, inflammation, proliferation, and remodeling. Initially, the body works to stop bleeding through clot formation, followed by an inflammatory phase where the immune system activates to remove debris and fight potential infection. During the proliferative phase, new tissue begins to form, and in more severe wounds, collagen is laid down to provide structural support. This is when granulation tissue fills the wound bed, and re-epithelialization occurs as the skin closes. Finally, the remodeling phase strengthens the new tissue, though scars may form as a result of the healing process (Wang & Windbergs, 2017). Wound healing can be affected by numerous factors such as infection, poor circulation, diabetes, malnutrition, and the overall health of the individual. Severe of chronic wounds may need medical treatments like sutures, antibiotics, or advanced therapies to heal properly. Effective wound care is crucial for faster healing and preventing complications like infections or chronic wounds, which can require long-term management. The depth of a wound plays a crucial role in its classification, treatment, and healing process. Superficial wounds affect only the outermost layers of the skin, such as abrasions or minor cuts, which usually heal quickly with minimal scarring. However, deeper wounds penetrate through the dermis into underlying tissues, including muscles, tendons, or even bones. These types of wounds can result from trauma, surgery, or chronic conditions like pressure ulcers. A full-thickness wound is characterized by the destruction of both the epidermis and dermis, extending into the subcutaneous tissue and, in severe cases, involving

muscles, tendons, and bones. These wounds represent a significant disruption of the skin's structural integrity, requiring a more complex healing response compared to partial-thickness wounds (Rivera et al., 2007). The primary mechanisms of full-thickness wound healing include inflammation, tissue proliferation, and remodeling. A longer inflammatory phase as the body heals with significant tissue damage and potential infection risks. Moreover, the slower formation of granulation tissue is due to the depth and complexity of the wound, which may require external support like advanced therapies. Consequently, in full-thickness wounds significantly delay re-epithelialization and scar formation. The final stage, remodeling, is marked by the deposition of type III collagen, which is gradually replaced by the more robust type I collagen, resulting in scar formation. This phase can last from months to years, with the tensile strength of the wound reaching only about 80% of its original integrity.

Given the complexity of full-thickness wounds, therapeutic interventions often involve advanced techniques such as negative pressure wound therapy (NPWT), skin grafts, or bioengineered tissue substitutes to enhance healing (Han & Ceilley, 2017). Understanding the pathophysiology of full-thickness wound healing is crucial for developing effective treatment strategies and improving patient outcomes. Full-thickness wounds are typically more challenging to treat due to the greater risk of infection, delayed healing, and complications such as necrosis or tissue loss. The treatment often involves thorough cleaning, debridement of dead tissue, and the use of advanced dressing or grafting to promote regeneration. The healing of full-thickness wound is a complex process involving inflammation and remodeling influenced by factors like circulation, health conditions, and wound care. Severe wounds may need surgery or long-term care to avoid complications, making it crucial to assess wound depth for effective treatment and to reduce lasting damage.

## 2.2 Wound Dressings

Wound dressings are an essential component in treating and managing wounds, protecting the wound site, promoting healing, and preventing infection (Vowden & Vowden, 2014). They come in various types, each tailored to specific wound

characteristics such as exudate levels, depth, and the presence of infection. The primary function of wound dressing is to maintain a moist environment, which accelerates healing by supporting cell migration and reducing the risk of scar formation (Murakami et al., 2010; Horn, 2012). Different dressings, such as hydrocolloids, foams, hydrogels, and alginates, are designed to manage varying levels of exudate, with some dressings offering additional benefits like antimicrobial properties. The correct selection of a wound dressing is crucial in facilitating autolytic debridement, managing pain, reducing scarring, and preventing complications like maceration or infection. Proper dressing not only enhances the body's natural healing process but also minimizes discomfort for the patient.

**2.2.1 Film Dressings**

Film dressings are thin, transparent, adhesive wound covering made from a polyurethane membrane that allows oxygen and moisture vapor to pass through while providing a protective barrier against bacteria and contaminations. They are primarily used for superficial wounds, minor burn, surgical incisions, and as a secondary dressing to secure other wound care materials. Tanaka et al. prepared gelatin film dressing for superficial or deep partial-thickness wounds in the skin (Tanaka et al., 2005). Moreover, Chin et al. developed the film dressing using alginate-pectin for wound healing (Chin et al., 2018).

**2.2.2 Foam Dressing**

Foam dressings are designed to absorb moderate to heavy amounts of exudate while maintaining a moist wound environment. They are often used for venous ulcers, surgical wounds, and pressure ulcers. The foam dressings have high absorptive capacity, ability to cushion the wound, and flexibility, making them ideal for use on difficult-to-dress areas like heels or elbows. Foam dressings are also non-adhesive, reducing trauma to the wound during dressing changes. Mostly, foam dressings were prepared using polyurethane (Liu et al., 2017; Forni et al., 2018). However, they are not suitable for dry or necrotic wounds. Moreover, they are typically more expensive than the other types and might require frequent changes if saturated.

**2.2.3 Hydrogel Dressing**

Hydrogel dressings are increasingly recognized for their effectiveness in managing full-thickness wounds due to their unique properties that promote a moist

environment, which is critical for optimal healing. These dressings are composed of cross-linked polymer networks that can retain a significant amount of water, typically 70-90% by weight, allowing for hydration of the wound bed while simultaneously absorbing exudates. The ability to maintain moisture is crucial in full-thickness wounds, as it facilitates autolytic debridement, accelerates granulation tissue formation, and enhances epithelial cell migration across the wound surface. Hydrogel dressings also act as a thermal insulator, maintaining the optimal temperature for the enzymatic activity involved in wound repair and protecting the wound from external contamination. Pan et al. developed a soft, flexible, porous, translucent, breathable, non-adhesive hydrogel-based wound dressing for full-thickness skin defect. The hydrogel was prepared by mixing poly(vinyl alcohol) solution, Human-like collagen solution, carboxymethyl chitosan solution, and Tween80 as a pore-forming agent, followed by two freeze-thawing cycles, and finally removing the tween80 by immersing these hydrogels in ultrapure water. The hydrogels showed a suitable moisture vapor transmission rate, outstanding hemostatic performance, and bacterial barrier activity, which are beneficial in promoting the wound healing process. Furthermore, they exhibited excellent mechanical properties, biocompatibility, and histocompatibility. Therefore, these hydrogels promoted full-thickness skin wound healing (Pan et al., 2017). Wei et al. synthesized chitosan/alginate hydrogel dressing crosslinked via hydrogen and covalent bonds. These hydrogels displayed suitable pore size and tunable rheological properties for cell adhesion. Moreover, hemostatic property and antibacterial activity due to the amino groups from chitosan were exhibited. These hydrogels have great potential as multifunctional hydrogel dressing for full-thickness wounds (Wei et al., 2022).

## 2.3 Injectable Hydrogel Dressing

Injectable hydrogel dressings are an advanced class of wound care materials designed to promote healing by providing a versatile, minimally invasive solution for managing a variety of wounds, particularly full-thickness and complex wounds (Qu et al., 2018; Zhao et al., 2017). These hydrogels are composed of biocompatible polymers

that can be injected in a liquid state and subsequently solidify or form a gel in situ, with its superior fluidity allowing it to fill irregular wounds or deep wounds without wrinkling or fluting. This unique feature allows the hydrogel to fill irregular wound cavities, making it especially useful for wounds that are difficult to access or treat with traditional dressing (Li et al., 2015). Injectable hydrogels are typically made from more than one polymer. There are two ways to prepare the injectable hydrogels, co-injection of 2 polymers, the hydrogels are formed after injection of 2 polymers with a proper gelation time. The other way, the injectable hydrogels are designed to respond to environmental stimuli, such as temperature or pH, allowing them to solidify upon injection or change properties in response to the wound's conditions (Alexandae et al., 2013; Lavanya et al., 2020).

The key benefits of injectable hydrogel dressings are their ability to deliver therapeutic agents directly to the wound site. They can be loaded with bioactive molecules, such as growth factors, antimicrobial agents, or stem cells, which are released gradually as the hydrogel degrades over time (Ma et al., 2020; Hu et al., 2020). This localized delivery system helps to promote wound healing, enhancing cell proliferation, reducing infection, and modulating the inflammatory response. Additionally, the physical properties of injectable hydrogels, such as stiffness, porosity, and degradation rate, can be tailored to suit specific wound environments, ensuring optimal support during the different stages of healing. The injectable hydrogel dressings are particularly promising for treating chronic or full-thickness wounds, including pressure ulcers, burns, and diabetic foot ulcers, where traditional wound dressings might fail to provide sufficient coverage or support. The ability to form a protective barrier while also delivering bioactive treatments directly to the wound bed sets injectable hydrogels apart from conventional dressing (Gao et al., 2020; Del Olmo et al., 2022). Du et al. successfully developed a new type of injectable hydrogel through the chemical cross-linking between hydrophobically modified chitosan (hmCS) and oxidized dextran (OD) and the hydrophobic interaction of hydrophobic aliphatic chains. The hmCS/OD solution was injected into a rat's body through the skin to form a gel. It showed remarkable potential in wound healing and other tissue regeneration applications (Du et al., 2019). Moreover, the injectable hydrogel can be prepared from stimuli-responsive polymers. Zhu et al. developed a versatile hydrogel composite with

injectability, thermo-sensitivity, and antibacterial activity for full-thickness and large wounds. Hydroxypropyl chitosan was adopted and reversibly cross-linked with poly(N-isopropylacrylamide) to build a thermosensitive hydrogel. This hydrogel can be injected into the wound site through the syringe due to its thermos-sensitivity. The hydrogel solution turned to a gel state when the temperature changed. Moreover, this hydrogel exhibited antibacterial and anti-inflammatory activities, which possess great promise in clinical application as a wound dressing (Zhu et al., 2022).

## 2.4 Self-Healing Hydrogels

Self-healing hydrogel dressings represent a cutting-edge advancement in wound care, especially for managing full-thickness wounds (Chen et al., 2018; Chen et al., 2022). These hydrogels possess the remarkable ability to autonomously repair themselves after damage or deformation, offering a durable and adaptable solution for the dynamic environment of a wound bed. The self-healing hydrogels are composed of biocompatible polymers that form a network capable of recovering from mechanical disruption (Sharma et al., 2018; Han et al., 2019). This property is particularly beneficial in full-thickness wounds, which often require extended periods of healing and are prone to dressing disruption due to body movement, wound exudate, or external force. The self-healing hydrogels can maintain their structural integrity and continue to function even after experiencing damage, ensuring consistent coverage and wound protection. Moreover, these hydrogels provide a moist environment that promotes faster tissue regeneration and reduces pain in patients with deep or chronic wounds. To achieve self-healing properties, the dynamic covalent bond and the physical non-covalent interaction are incorporated into the hydrogels. Many researchers have developed self-healing hydrogels for wound healing, drug delivery, or medical applications. Moreover, the gelation and healing time are considered, as shown in Table 2.1.

**Table 2.1** The Development of the Self-Healing Hydrogels

| Self-healing mechanism | Gelation time (min) | Healing time (min) | Healing condition | Reference |
|---|---|---|---|---|
| Imine bond | 10-20 | 24 h | 37 °C | Sun et al. (2019) |
| | 30 | 24 h | 37 °C | Xiao et al. (2019) |
| | 2 | 2 h | - | Li et al. (2018) |
| | 1 | 15 min | - | Yuan et al. (2021) |
| Imine bond and hydrogen bond | 0.8 | 20 min | 37 °C | Zhou et al. (2021) |
| hydrogen bond | 1 min | 15 min | 37 °C | Wan et al. (2022) |
| Disulfide bond | 1 min | 10 | - | Chen et al. (2019) |
| Acylhydrazone bones | 120 min | 0.5 h | Room temperature | Chen et al. (2019) |
| Hydrogen bond | 9 min | 5 min | - | He et al. (2021) |

### 2.4.1 Dynamic Covalent Bonds

Dynamic covalent bonds are a type of chemical bonding used extensively in materials developed for biomedical application (Bertsch et al., 2022). This dynamic behavior allows materials to adapt, heal, or reconfigure themselves, making it particularly useful for designing self-healing materials. The bonds such as imine bond (Schiff's base) (Liu et al., 2018), disulfide (Bi et al., 2023), and boronate ester bonds (An et al., 2020) are often used in the systems due to their ability to break and reform under mild conditions. However, the boronate ester bonds can be hydrolyzed in water.

Furthermore, the usefulness is limited to environments with controlled or predictable pH levels. Thus, the use of self-healing boronate ester bonds may not provide much mechanical strength and limit the wound healing application (Kirchner et al., 2024). The disulfide has poor stability in the presence of reducing agents (Bebiano et al., 2024). This bond depends on specific redox conditions for reversibility, which can limit its functionality in environments where these conditions are not easily controlled. The Schiff's base reaction, which involves the formation of an imine bond between an amine and an aldehyde or ketone, offers a significant advantage for full-thickness wound healing due to its dynamic and reversible nature. In the context of wound dressings, Schiff's base chemistry allows the creation of hydrogels that can adapt and self-heal in response to the wound environment. This is particularly beneficial for full-thickness wounds, which often require prolonged healing periods and are subject to mechanical stress from body movement. The Schiff's base-based hydrogels can maintain a moist wound environment, promoting faster tissue regeneration and responding to fluctuations in pH. Additionally, the reversible nature of imine bonds allows for controlled material degradation, ensuring that the dressing gradually disintegrates as the wound heals. This adaptability, combined with the biocompatibility of the Schiff's base reaction, makes it a promising mechanism for developing advanced, responsive wound dressings tailored to the unique needs of full-thickness wounds. Zhang et al. designed a composite hydrogel dressing with antibacterial activity and self-healing ability. These composite hydrogels were prepared based on Schiff's base and thiol-alkynone double cross-links. The amino group of chitosan was reacted with the aldehyde group of oxidized alginate to obtain the Schiff's base reaction. These hydrogels displayed good self-healing, mechanical properties, and good antibacterial activity (Zhang et al., 2022). Moreover, Li et al. prepared self-healing hydrogel based on dynamic Schiff's base reaction. In this work, hyaluronic acid was used to prepare the self-healing hydrogels. Firstly, dialdehyde-modified hyaluronic acid (AHA) was synthesized. Then the AHA/cystamine dihydrochloride (AHA/Cys) hydrogels were formed by blending AHA and Cys at acidic pH levels (Li et al., 2020). Chen et al. produced an injectable self-healing hydrogel that effectively promotes wound healing. In this study, konjac glucomannan was modified to obtain an aldehyde group from oxidized konjac glucomannan. After that, the aldehyde group reacted with the amino

groups of chitosan to form imine bonds or Schiff's base reactions. These hydrogels exhibited good self-healing and injectable properties. Moreover, these developed hydrogels were injectable and significantly shortened wound recovery time in a full-thickness skin defect (Chen et al., 2018).

**2.4.2 Physical Non-Covalent Interactions**

The self-healing hydrogels based on physical non-covalent interactions utilize reversible, weak forces like hydrogen bonding, ionic interactions, van der Waals forces, and hydrophobic interaction to achieve their dynamic and adaptable properties. The key advantage of non-covalent interactions is their ability to break and reform quickly under physiological conditions without external stimuli. This allows the hydrogel to maintain its integrity even under stress or movement, which is particularly beneficial for wounds on joints or frequently disturbed areas. Ye et al. prepared hydrogels by mixing solutions of humic acid (HA) and polyvinylpyrrolidone (PVP), in which the HA worked as a crosslinking agent to form a hydrogel bond with the PVP. These hydrogen bonds are dynamic leading to self-healing properties. These hydrogen bond-crosslinked hydrogels exhibited adhesive properties and rapid hemostasis, which have the potential to be a wound dressing material (Yu et al., 2022). Zhang et al. developed chitosan-based self-healing hydrogels formed through noncovalent interactions. The hydrogels were fabricated using *in situ* free radical polymerization of acrylic acid (AA) and acrylamide (AM) in the presence of chitosan in dilute acetic acid aqueous solution. In this study, multiple noncovalent interactions were formed. These included ionic interactions between the anionic acrylic acid (AA) segments and the positively charged amino groups of chitosan and hydrogen bonds were introduced between AM segments and hydrogen bonding between AM segments and the chitosan backbone. These self-healing hydrogels crosslinked via noncovalent interaction showed rapid network recovery, high stretchability, and efficient self-healing properties at high water content (Zhang et al., 2019).

## 2.5 Chitosan

Chitosan, a biopolymer derived from the deacetylation of chitin found in the exoskeletons of crustaceans, has gained significant attention as a key component in hydrogel wound dressings due to its unique combination of biocompatibility, biodegradability, and inherent bioactivity. Chitosan-based hydrogels are particularly attractive for wound healing applications because they not only provide a moist environment that accelerates healing but also exhibit antimicrobial properties, which reduce the risk of infection (Raafat et al., 2008). Chitosan is a cationic polymer, meaning it has a positive charge, which allows it to interact electrostatically with the negatively charged cell membranes and extracellular matrix components. Moreover, this interaction can promote cell adhesion, migration, and proliferation, which are crucial for regenerating damaged tissues in full-thickness wounds. Additionally, chitosan can act as a hemostatic agent by promoting blood clotting, which is beneficial for controlling bleeding in acute wounds (Ahmed et al., 2016; Kozen et al., 2008). It has been used as a hydrogel dressing that can provide self-healing properties because amino groups of chitosan can react with aldehyde groups to produce imine bonds, the Schiff's base reaction. Qu et al. used the benzaldehyde-terminated amphiphilic segment Pluronic F127 to form micelles reacting with chitosan to prepare the self-healing hydrogel (Qu et al., 2018). However, there are some challenges associated with the use of chitosan in hydrogel wound dressing. One limitation is that pure chitosan is not soluble at neutral or alkaline pH levels, restricting its use in certain physiological conditions. This limitation makes it necessary to modify chitosan to improve its performance.

Quaternized chitosan (QCS) is a chemical-modified form of chitosan in which quaternary ammonium groups are introduced to enhance its properties, making it more suitable for hydrogel dressings. This modification significantly improves the solubility of chitosan across a wider pH range, especially in neutral and alkaline environments. Moreover, quaternization boosts the antimicrobial activity of chitosan as the positively charged quaternary ammonium groups more effectively disrupt the negatively charged bacterial cell membranes (Zhang et al., 2015). Wang et al. prepared an antimicrobial

hydrogel dressing using hyaluronic acid and QCS for wound treatment. In this work, chitosan was used to improve water solubility and antimicrobial activities (Wang et al., 2019). Xue et al. synthesized QCS to prepare hydrogels as wound dressing materials. In this work, QCS was used to improve the antibacterial and adhesive properties. These hydrogels were developed for applying to a full-thickness skin defect model and evaluated for their effect on wound repair (Xue et al., 2019). Additionally, QCS does not prevent the Schiff's base reaction between the amino groups of chitosan and the aldehyde groups. Zhao et al. synthesized QCS-g-polyaniline and benzaldehyde groups functionalized poly(ethylene glycol)-co-poly(glycerol sebacate) to prepare injectable conductive self-healing hydrogel through a Schiff's base reaction for wound healing. In this study, the amino group in quaternized chitosan reacted with the aldehyde groups from benzaldehyde. These hydrogels displayed a self-healing time of 2 hours after damage (Zhao et al., 2017).

## 2.6 Pectin

Pectin, a natural polysaccharide primarily derived from the cell walls of fruits, has emerged as a promising material for hydrogel wound dressing preparation due to its excellent biocompatibility, biodegradability, and ability to form a hydrogel. Therefore, pectin has been used as a gelling agent (Sriamornsak, 2003). As a plant-based polymer, pectin is composed mainly of galacturonic acid units, allowing it to form gels in the presence of divalent cations like calcium ions. This characteristic makes it highly adaptable for hydrogel wound dressing, where a moist, stable environment is essential for accelerating the healing process. One of the key advantages of pectin-based hydrogels for wound healing is their ability to interact with the extracellular matrix and skin cells, promoting tissue regeneration. Pectin has been shown to support fibroblast proliferation, which is crucial for the production of collagen and the reconstruction of the dermal layer in full-thickness wounds. Rezvanian et al. prepared hydrogel through ionic crosslinking of alginate and pectin for wound dressing application (Rezvanian et al., 2017). Giusto et al. developed a new, easy-to-make pectin-honey hydrogel as a wound healing membrane. In this research, the pectin-honey hydrogel had optimal

characteristics for wound healing (Giusto et al., 2017). Moreover, Gupta et al. prepared hydrogels that consisted of pectin and gelatin. The pectin was oxidized to obtain the aldehyde group (-CHO). The crosslinking reaction occurred through the formation of a Schiff's based reaction between the aldehyde group of oxidized pectin and the amino group of gelatin (Gupta et al., 2014). However, no research report oxidized pectin reacted with quaternized chitosan to prepare the injectable self-healing hydrogel through a Schiff's base reaction.

## 2.7 Natural Product Extracts

Natural product extracts contain bioactive compounds which have the potential to heal the wound. Recently, natural product extracts have increased attention in biomaterial fabrication due to their properties such as antioxidant activity, antimicrobial activity, anti-inflammatory activity, anticancer activity, and anti-tyrosinase activity (Talib, 2011; Rahmani et al., 2015; Rao et al., 2016; Anand et al., 2008; Ghasemzadeh et al., 2018). Curcumin (CM) is a polyphenol compound, which is the main compound of the medical plant turmeric (Trigo-Gutierrez et al., 2021). CM has various pharmacological effects, including anti-inflammatory, antioxidant, and antibacterial activities. Shefa et al. prepared hydrogels loaded with CM by a freeze-thaw method for wound dressing. The cell viability analysis of the hydrogels using MTT assay indicated they were non-toxic. Moreover, the wound closure was studied using full-thickness excision wounds in a rat model, which showed a better % wound closure of the CM-loaded hydrogels when compared to the control (Shefa et al., 2020). Jing et al. fabricated composite hydrogels as wound dressing materials. CM-containing nanoparticles were loaded into silk fibroin and sodium alginate hydrogels. The composite hydrogel exhibited excellent biocompatibility and antibacterial properties against Gram-negative (*E. coli*) and Gram-positive (*S. aureus*) bacteria. In addition, the obtained composite hydrogels improved the closure of bacterial-infected wounds (Jing et al., 2023). Gupta et al. prepared CM-loaded cellulose hydrogels for wound treatment. The antioxidant activity of the hydrogels was evaluated using a DPPH assay, and the results showed that these hydrogels decreased oxidative stress at the wound site.

Moreover, the hydrogels displayed hemocompatibility, cytocompatibility, and antioxidant properties, supporting the potential use in hydrogel dressings (Gupta et al., 2019). Mangosteen (*Garcinia mangostana* Linn) has gained much attention in medical applications. The mangosteen peels contain phenolic compounds such as xanthones and mangostin, which display antibacterial, anti-inflammatory, anti-cancer, antioxidant, and wound healing properties. Xanthones are effective for wound-healing agents due to stimulating fibroblast cell proliferation (Yang et al., 2017; Obolskiy et al., 2019). Moreover, the mangostin comprises α- mangostin, β-mangostin and γ-mangostin (Mahabusarakam et al., 1987). Many studies have reported the biological activity of mangosteen (Moongkarndi et al., 2014; Chavan et al., 2021). Ghasemzadeh et al. reported the antioxidant and antimicrobial activities of the α-mangostin (MT). The antioxidant activity was evaluated using DPPH assay and exhibited good antioxidant activity. In addition, MT exhibited antibacterial activity against Gram-positive bacteria (Ghasemzadeh et al., 2018).

## 2.8 Cyclodextrin Inclusion Complex

Cyclodextrins (CDs) are considered valuable compounds that can be applied in different industrial fields, such as for food or pharmaceutical applications (Cravotto et al., 2006; Jug et al., 2008; Loftsson et al., 2010; Li et al., 2014). CDs are a group of cyclic oligosaccharides composed of glucose units linked by α-1,4-glycosidic bonds, with three main types: α-cyclodextrin (6 glucose units), β-cyclodextrin (7 glucose units), and γ-cyclodextrin (8 glucose units), each having progressively larger internal cavities. The hydrophilic outer surface of CDs enables them to dissolve in water, while their hydrophobic inner cavity can trap non-polar guest molecules, such as poorly soluble drugs (Szejtli, 1998). This unique structural feature makes CDs highly valuable in pharmaceutical formulations for enhancing drug solubility, bioavailability, and stability. The encapsulation of a guest molecule within the CD cavity occurs through non-covalent forces, including van der Waal interactions, hydrogen bonding, and hydrophobic forces. This inclusion process can protect sensitive molecules from degradation caused by environmental factors such as oxidation, heat, and light,

prolonging the shelf-life of the encapsulated compounds. CDs are non-toxic ingredients, and the three CDs, β-CD is the most widely used because its cavity fits expected guests with molecular weight between 200 and 800 g/mol and also because of its ready availability and reasonable price (Szente & Szejtli, 2004). Various methods are employed to form CD inclusion complexes, such as kneading, co-precipitation, freeze-drying, and spray drying (Cid-Samamed et al., 2022).

**2.8.1 Kneading**

The kneading method (the paste method) is moderately simple for poorly water-soluble guests. This method involves dissolving CD in DI water in a mortar, and then the guest is added to obtain the paste. After the paste solid is obtained, the free particles will be removed with a small amount of solvent. This method is highly efficient and scalable. However, this method might achieve incomplete complexation due to uneven solvent distribution or insufficient mixing. Thus, the complex may require additional processing to ensure complete encapsulation (da Silva Junior et al., 2017; Wadhwa et al., 2017).

**2.8.2 Co-Precipitation**

The co-precipitation method is useful for non-water-soluble guests. The guest is dissolved in ethanol, and the appropriate amount of CD in DI water is added to the guest solution with agitation. After that, the solution is cooled, and formation of complex crystals occur (Jiang et al., 2019). Moreover, different organic solvents such as diethyl ether or benzene can also be used to dissolve the guest when using this method. The co-precipitation is one of the most used methods due to its simplicity and efficiency.

**2.8.3 Freeze-Drying**

The freeze-drying method, also known as lyophilization, is widely used for forming inclusion complexes with CDs. This method involves dissolving the guest molecule and CD in a suitable solvent, typically water or a water-alcohol mixture. The resulting solution is then frozen to convert the solvent into a solid state, after which the solvent is removed by sublimation under reduced pressure, leaving behind a dry powder containing the inclusion complex (Mohan et al., 2012). Freeze-drying offers several advantages, including producing highly stable and pure complexes and preserving the integrity of thermolabile (heat-sensitive) compounds since the process avoids high

temperatures. This makes it especially suitable for pharmaceuticals where drug stability is crucial. Furthermore, the freeze-dried complexes often exhibit enhanced solubility and bioavailability compared to their unprocessed counterparts.

### 2.8.4 Spray Drying

The spray drying method is widely used for forming inclusion complexes with CDs, especially in industrial applications, due to its scalability and efficiency. The host and CD are first dissolved in a suitable solvent to create a homogeneous solution. This solution is then atomized into fine droplets and rapidly dried using hot air, forming a fine powder containing the inclusion complex. The high surface area of the atomized droplets allows for quick solvent evaporation, which facilitates the encapsulation of the guest molecule within the cyclodextrin cavity (Shan-Yang & Yun-Horng, 1989; Hay et al., 2017). The spray drying method offers several advantages, including its rapid processing time and suitability for continuous large-scale production. Additionally, it enhances the solubility and bioavailability of poorly soluble drugs, making it a preferred method for pharmaceutical formulations on an industrial scale.

## 2.9 Cyclodextrin Inclusion Complex with Natural Product Extracts

The natural products have poor water solubility, reducing their absorption and effectiveness in the body. Moreover, natural products are sensitive to environmental factors, which might degrade before reaching the target. These factors restrict the application of CM and MT in pharmaceutical formulation. Thus, improvement in the stability and solubility of curcumin is important. Cyclodextrin inclusion can protect the active ingredients from degradation, extending their shelf life and maintaining their potency (Parameta et al.,2011; Khan & Singh, 2016). Many researchers have reported CM-CD inclusion complex (CMx), Celebioglu and Uyar prepared CMx-loaded nanofibrous via electrospinning to improve water soluble and antioxidant activity (Celebioglu & Uyar., 2020). Zhang et al. synthesized CMx for cancer therapy. This study encapsulated CM into CD to improve CM delivery (Zhang et al., 2016). CMx and MT-CD inclusion complex (MTx) have also been prepared and incorporated into hydrogels. Gupta et al. prepared CMx loaded into a hydrogel for wound dressing (Gupta

et al., 2020). Kiti et al. prepared CMx and incorporated it into a bilayer wound dressing (Kiti et al., 2020). Wathoni et al. prepared MTx in hydrogel formulation to improve wound healing properties (Wathoni et al., 2020).

However, no study has explored the use of MTx and CMx incorporated into injectable self-healing hydrogels for wound dressing applications. Building upon prior research on QCS/OPEC-based self-healing injectable hydrogels. This study aims to enhance the biological activity of these materials by incorporating MTx and CMx as bioactive compounds. In particular, the inclusion of these natural products is expected to enhance the antioxidant and anti-inflammatory activity of the hydrogels.

In this research, MTx and CMx were prepared and incorporated into the QCS/OPEC injectable self-healing hydrogels for wound dressing applications. Firstly, the QCS/OPEC hydrogel was investigated for use as a wound dressing. Additionally, these hydrogels have self-healing ability, which prolongs the shelf-life of the hydrogel, leading to reduced dressing replacement. Subsequently, MTx and CMx were incorporated into the hydrogel. Moreover, the biological activated such as anti-inflammatory, cytotoxicity, and wound closure effects were further evaluated.

# CHAPTER 3

# RESEARCH METHODOLOGY

## 3.1 Materials

| | |
|---|---|
| Chitosan (CS, degree of deacetylation > 90%, Mw: 500-700 kDa) | Bio 21 Co., Ltd, |
| Pectin from citrus peel (Galacturonic acid ≥ 74.0 %) | Sigma-Aldrich, USA |
| Glycidyl trimethylammonium chloride (GTMAC) | Sigma-Aldrich, USA |
| Sodium periodate (≥ 99.8%) | Sigma-Aldrich, USA |
| Curcumin (CM) | Aktin Chemicals, Inc., |
| α-Mangostin (MT) | Sigma-Aldrich, USA |
| (2-hydroxypropyl)-β-Cyclodextrin (β-CD, average Mw: ~1380) | Sigma-Aldrich, USA |
| 2,2'-azino-bis(3-ethylbenzothiazoline-6-sulfonic acid) diammonium salt (ABTS) | Sigma-Aldrich, USA |
| Ethylene glycol (≥ 99%) | Sigma-Aldrich, USA |
| 3-(4,5-dimethylthiazol-2yl)-2,5-diphenyltetrazolium bromide (MTT) | Thermo Fisher Scientific |
| Dulbecco's Modified Eagle Medium (DMEM) | Thermo Fisher Scientific |
| Fetal bovine serum (FBS) | Thermo Fisher Scientific |

## 3.2 Methodology

### 3.2.1 Preparation of Quaternized Chitosan (QCS)

The chitosan was modified by dissolving 1 g of chitosan in acetic acid (1% v/v, 70 mL) overnight. Following this, 10 mL of GTMAC was added to the chitosan solution under continuous stirring, and the resulting solution was refluxed at 60 ºC for 6 h. The

resulting QCS solution was dialyzed against distilled water using a snakeskin membrane for 3 days with the exchange of water every day and lyophilized to form the solid QCS product.

**3.2.2 Preparation of Oxidized Pectin (OPEC)**

The OPEC was prepared by dissolving 2 g of pectin in ethanol/water solution (20 mL ethanol/80 mL water). After that, 0.32 g of sodium periodate in 3 mL of distilled water was added to pectin solution. The resulting solution was stirred for 2 h in the dark. Following this, 5 mL of ethylene glycol was added and stirred for 2 h. The OPEC solution was dialyzed against distilled water using a snakeskin membrane for 3 days with the exchange of water every day and lyophilized to form the solid OPEC product.

**3.2.3 Characterization of QCS and OPEC Polymers**

$^1$H NMR and 1D DOSY NMR spectroscopy were run on a Bruker 500 MHz spectrometer. All samples were run in $D_2O$ at approximately 10 g/L at room temperature. 1D DOSY spectra were collected with the following acquisition parameters; $\Delta$ = 100 ms, $\delta$ = 2 ms, gradient strength = 95 %, number of scans = 128. All data were analyzed with Bruker Topspin software.

The degree of esterification, DE, in pectin was calculated from standard $^1$H NMR spectra using equation 3.1.

$$\text{DE}\ (\%) = \frac{\frac{\int \text{CH}_3+\text{H}(\text{C}_2)-\int \text{H}(\text{C}_3)}{3}}{\int \text{H}(\text{C}_3)} \times 100\% \qquad (3.1)$$

Where $\int CH_3$+H(C2) represents the integral of protons on the methoxy group as well as the proton on C2 as these overlap (3.5-3.8 ppm), and $\int$H(C3) is the integral of the proton on C3 (3.9 ppm).

The degree of acetylation, DA, of chitosan was calculated using equation 3.2.

$$\text{DA}\ (\%) = \frac{\frac{\int \text{CH}_3}{3}}{\frac{\int \text{H}(\text{C2}-\text{C6})}{6}} \times\ 100\% \qquad (3.2)$$

Where $\int$H(C2-C6) represents the integral of protons on C2-C6 on both monomer units (2.9 – 4.0 ppm) and $\int CH_3$ represents the three methyl protons of the N-acetyl-D-glucosamine unit of chitosan (1.96 ppm).

The degree of substitution, DS, to quantify the degree of quaternization of QCS was calculated using the integrals of the peak corresponding to the methylene (2.7 ppm) of the introduced functionality and methyl protons of the N-acetyl-D-glucosamine unit of chitosan (1.96 ppm) using equation 3.3.

$$\mathrm{DS}\ (\%) = \frac{\frac{\int \mathbf{CH_2}}{\mathbf{2}}}{\frac{\int \mathbf{CH_3}}{\mathbf{3}}} \times\ \mathrm{DA}\ (\%) \tag{3.3}$$

**3.2.4 Viscosity**

Viscosity values for pectin, OPEC, and the OPEC solution used to prepare the hydrogels were determined using Ubbelohde at 27 ºC by comparing the runoff time of each solution with water at the same temperature. Aqueous polymer solutions of 0.05 %w/v were evaluated with reference to ultrapure water. The viscosity was calculated using equation 3.4 with the viscosity of water at 27 °C as 0.8025 cP.

$$\eta_s = \eta_w \frac{d_s t_s}{d_w t_w} \tag{3.4}$$

where η is the viscosity, d is the measured density, and t is the runoff time. Subscript s denotes the tested solution and w represents water.

**3.2.5 Fourier-Transform Infrared Spectroscopy (FTIR)**

FTIR spectra were collected using a Perkin Elmer Spectrum Two FTIR Spectrometer. Perkin Elmer Spectrum software was used to collect transmission data from 4,000-450 $cm^{-1}$ with a resolution of 4 $cm^{-1}$ and an accumulation of 4 scans. The instrument was equipped with an ATR Imaging Accessory using a diamond crystal window.

**3.2.6 X-Ray Photoelectron Spectroscopy (XPS)**

XPS data were acquired using a Kratos AXIS SUPRA+ X-ray photoelectron spectrometer. The incident radiation was monochromatic Al Kα X-rays (1,486.6 eV) operated at 10 mA emission current and 12 kV anode potential. The electron collection spot size was ~700 × 300 $\mu m^2$. Survey scans were taken at an analyzer pass energy of 160 eV and high-resolution scans at 20 eV. Survey scans were carried out over 1,200 - 0 eV binding energy range with 1.0 eV steps. High-resolution scans were run with 0.1 eV steps. Base pressure in the analysis chamber was $10^{-9}$ Torr and during sample

analysis $10^{-8}$ Torr. Spectra were converted into VAMAS format for further analysis (CasaXPS version 2.3.24 PR1.0). Peak fitting was done with a Shirley baseline with Kratos library Relative Sensitivity Factors. All spectra were charge corrected to the C-C peak at 285.0 eV. For high-resolution peak fitting the following constraints were used: C 1s FWHM 0.9-1.1, O 1s FWHM 1.1-1.5.

**3.2.7 Cytotoxicity of QCS and OPEC Polymers**

First, the OPEC and QCS polymers were characterized by indirect cytotoxicity using Normal Human Dermal Fibroblast cell line (NHDF). The NHDF cells were cultured in 10% DMEM at 37 °C in a humidified atmosphere of 95% air and 5% $CO_2$. The NHDF cells were seeded in a 96-well plate at 8,000 cells/well. The cells were cultured in 10% DMEM and incubated at 37 ℃ for 24 h to allow cell attachment. After that, the culture medium in each well was replaced with different sample solutions. Meanwhile, the OPEC and QCS were dissolved in water with heating to mimic solutions prepared for hydrogel fabrication. The OPEC (7.5 %w/v) and QCS (2%w/v) were prepared. Subsequently, cells were re-incubated for 24 h after replacing with sample solutions. The percentage of cell viability was determined by an MTT assay. Briefly, the culture medium was removed and replaced with 100 µL of 0.5 mg/mL MTT solution. After 3 h incubation, the MTT solution was removed, and 100 µL of dimethyl sulfoxide was added to dissolve the formazan crystals. The absorbance of the solution was measured at 570 nm using a microplate reader (BioTek Instruments, USA). The viability of the cells cultured with the fresh medium was used as a control.

An MTT assay was used to quantify the viability of the cells cultured by each extraction medium as per standard procedures.

**3.2.8 Preparation of QCS/OPEC Hydrogels**

First, OPEC (1.5 g) and QCS (0.4 g) were separately prepared by adding 10 mL of water to the polymers. After that, the solution was stirred at 60 °C followed by stirring at 37 °C for 2 h. The ratio of QCS to OPEC was optimized first. The gelation and hydrogel formation were evaluated visually after co-injecting the OPEC and QCS solutions. The gel formation of the hydrogel occurred within 1 min and was given a score of according to the following: (0) no gel formation; (1) partial gel formation with excess solution present; (2) near complete gel formation with small amount of solution present.

15 % w/v of OPEC solution and 4 %w/v of QCS solution were used by co-injecting into a 24-well plate and stirring with a spatula. One type prepared from 0.6 mL QCS and 0.4 mL OPEC (named HG_0.6:0.4) and one type prepared from 0.8 mL QCS and 0.2 mL OPEC (named HG_0.8:0.2).

**3.2.9 Gel Fraction**

The gel fraction was measured by the dry mass of freeze-dried as-prepared hydrogel samples, obtaining the initial dry mass ($W_{i,d}$). Subsequently, the dried samples were immersed in water at 37 ºC for 6 and 24 h to swell the samples and remove soluble components. The remaining gel was wiped thoroughly with tissue paper and weight ($w_{s,w}$). Then, the dry weight of the swollen sample after freeze-drying was recorded ($W_{s:water,d}$). The gel fraction (%) was calculated using equation 3.5. Moreover, the water swelling ratio, $Q_w$, was calculated using equation 3.6.

$$Gel\ fraction\ (\%) = \frac{W_{s:water,d}}{W_{i,d}} \times 100\% \quad (3.5)$$

$$Q_w = \frac{W_{s,w} - W_{s:water,d}}{W_{s:water,d}} \quad (3.6)$$

**3.2.10 Rheological Analysis of Hydrogels**

The rheological analysis of the HG_0.6:0.4 and HG_0.8:0.2 samples was measured using ARES-G2 rheometer (TA Instrument Ltd., USA) accompanied by 40 mm diameter parallel geometry. The solutions of QCS with or without inclusion complex and OPEC were co-injected into a vial and mixed for 1 min before being placed in the 1 mm gap. The rheological properties of the hydrogels were measured during the gelation process with a temperature of 37 ºC at a fixed frequency of 1 Hz and a 1 %strain. The storage modulus (G') and loss modulus (G") were recorded. Moreover, the self-healing behavior of the hydrogels was determined by a rheometer. An alternate strain sweep was performed at a fixed angular frequency of 1 Hz, switching the amplitude oscillation strain from low strain (y = 1 %, 100 s for each interval) to high strain (y = 2000 and 100 s for each interval).

### 3.2.11 Self-Healing Properties of Hydrogels

The macroscopic self-healing behavior of the HG_0.6:0.4 and HG_0.8:0.2 samples was characterized by preparing one undyed hydrogel and one dyed hydrogel with red food dye. Both hydrogels were cut in half and placed each half in contact. After that, the self-healing of hydrogel was observed for over 30 min.

### 3.2.12 Mechanical Test and Adhesiveness of Hydrogels

The compressibility and hardness of the HG_0.6:0.4 and HG_0.8:0.2 samples were measured using the texture analyzer (TA.XTplus) in TPA mode. Each disc-shaped hydrogel (diameter of 16 mm and a thickness of 5 mm) sample was compressed at a rate of 5 mm/s until the samples were deformed 75% from their original height by a tubular probe. The compression was applied twice with a 15 s delay between them. The force-time plots from the TPA mode were analyzed to obtain the hardness and compressibility values of the hydrogels. The hardness was taken from the maximum force of the first positive curve on the force-time plots. The compressibility was taken from the area under the first positive curve on the force-time plots.

Furthermore, the adhesion performance of the HG_0.6:0.4 and HG_0.8:0.2 samples was evaluated using the texture analyzer (TA.XTplus) with a load cell capacity and a test speed of 5 kg and 2 mm/sec, respectively. Porcine skin (2.0 × 2.0 cm2) soaked in PBS for 30 min was used as the model tissue and attached to the probe using double-sided adhesive. To measure the adhesiveness of the hydrogels, the probe was lowered to the surface of the sample loaded in a plastic petri dish and held for 30 s at 0.02 N. The probe was then moved upwards at 5 mm/s. The adhesiveness of each sample was recorded as the maximum force on the force-time plots produced via detachment of the pig skin from the surface of the sample.

### 3.2.13 Cytotoxicity of Hydrogels

Each hydrogel sample (1 g wet weight) was sterilized under UV radiation for 30 min on each side. The sterilized sample was immersed in a culture medium (2 mL) for 24 h to obtain the extraction medium. After that, the extraction medium was diluted with culture medium to produce various hydrogel concentrations of 50, 10, 5, and 0.5 mg/mL. The cytotoxicity was studied using NHDF cells, and the cell viability was determined using an MTT assay, as previously mentioned in section 3.2.7.

### 3.2.14 *In Vitro* Wound Healing Assay

The scratch wound healing assay was used to investigate wound closure or cell migration. The NCTC clone 929 cells ($2\times10^5$ cells/well) were cultured in a 24-well tissue culture polystyrene plate for 24 h. The L929 monolayer cell was scratched using a SPLScar$^{TM}$ scratcher (tip width: 0.5 mm; SPL Life Sciences, Korea) and gently washed with PBS to eliminate cell fragments. The hydrogels (100 mg wet weight) were immersed in 2 mL of 10% DMEM at 37 °C for 24 h and diluted with 10% DMEM to produce the extraction medium at concentration of 10 mg/mL which is equivalent to 1 mg/mL solid. This extraction medium was added to the cells and incubated at 37 °C for 48 h. SFM was used as the control. Photographs of the scratched area were recorded at 0 and 48 h. The percentage of reduction (wound closure) of the scratched witdth was calculated following the equation 3.7

$$Wound\ closure\ (\%) = \frac{(A-B)}{A} \times 100 \qquad (3.7)$$

Where A is the width of the initial scratch wound measured immediately after scratching and B is the width of scratch wound after scratching for 48 h.

### 3.2.15 Antibacterial Activity of QCS, OPEC Polymer, and Hydrogels

Antibacterial activity of the polymers and hydrogels was evaluated against the gram-positive bacterial (*S. aureus*) as well as the gram-negative bacteria (*E. coli*). The OPEC and QCS polymers were dissolved in water with heating to mimic solutions prepared for hydrogel fabrication. Meanwhile, the hydrogel (1.0 g) was immersed in PBS (1.0 mL) at 37 ºC for 24 h. For all solutions, a volume of 100 µL was pipetted into the first row of the 96-well plate and used as a stock concentration. The sample solutions were serially diluted twofold using Nutrient Broth (NB) medium to obtain various concentrations. Subsequently, the standardized bacterial suspension was diluted to give a final bacteria concentration of $10^5$ CFU/mL. A volume of 50 µL of the bacterial suspension was added to all wells. An additional well containing NB medium only was used as a negative control. Amoxicillin and ampicillin were used as positive control for gram-positive and gram-negative bacteria, respectively. The well plates were incubated at 37 °C for 24 h. After incubation, the optical density (OD) at 625 nm of the well plates was measured. The lowest concentration of a sample that retained its inhibitory effect,

resulting in 50% inhibition of bacteria growth (OD value half of bacteria only control) was considered as the  value. The MBC value was determined by sub-culturing the broth used for $MIC_{50}$ determination onto fresh agar plates. After incubation (24 h), the plates were examined for the growth of bacteria to determine the concentration of the sample for which 99.9% bacterial isolated was killed. These experiments were done in triplicate (n = 3).

**3.2.16 Preparation of α-Mangostin Inclusion Complex (MTx)**

There are 3 methods used to prepare the mangostin inclusion complex. The first method, MTx was prepared using MT and β-CD in a 1:1 mole ratio via three different methods. For the first method, 1.62 g of β-CD was dissolved in 10 mL of distilled water. This β-CD solution was then slowly added to a solution of 0.5 g of MT dissolved in 10 mL of methanol. The resulting mixture was sonicated at room temperature for 15 min and subsequently stirred at 120 rpm using a magnetic stirrer at room temperature for 48 h. The mixture was then filtered through a 0.45 µm cellulose acetate syringe filter and evaporated using a rotary evaporator at 65 rpm and 70 °C. The concentrated mixture was dried in an oven at 50 °C for 12 h, yielding a light yellow MTx powder.

In the second method, 1.62 g of β-CD in 10 mL of distilled water. Then, 0.5 g of MT was added to the β-CD solution. The mixture was stirred in a sealed beaker at room temperature for 24 h. The resulting solution was filtered through a 0.45 µm cellulose acetate syringe filter and then freeze-dried to obtain the solid MTx-DI compound.

For the third method, 1.62 g of β-CD was dissolved in 10 mL of distilled water, and 0.5 g of MT was dissolved in 10 mL of methanol. The MT solution was then slowly added to the β-CD solution. The mixture was stirred at room temperature for 48 h. Subsequently, the solution was filtered through a 0.45 µm cellulose acetate syringe filter and evaporated using a rotary evaporator (65 rpm, 70 °C) to remove the methanol. The concentrated mixture was then freeze-dried to obtain the solid MTx-NS compound.

**3.2.17 Preparation of Curcumin Inclusion Complex (CMx)**

The CMx was prepared using CM and β-CD in a mole ratio of 1:1. β-CD (3.75 g) was dissolved in distilled water (20 mL). Then, 1 g of CM was added to the β-CD solution and stirred at room temperature for 24 h. The mixture was filtrated through a

0.45 μm cellulose acetate syringe filter and lyophilized using a freeze-dryer to obtain CMx powder.

**3.2.18 Characterization of Drug-β-CD Inclusion Complexes**

The crystalline or amorphous nature of β-CD, CM, MT, CMx, MTx, physical mixture of MT and β-CD (MTpm), and physical mixture of CM and β-CD (CMpm) were investigated by X-ray diffraction (XRD). The sample was scanned between 2 theta (2θ) of 5 - 30° with a step size of 0.013° and a scan speen of 0.012°/min using an X' pert-pro MPD diffractrometer (Malvern Panalytical, UK) equipped with Cu Kα radiation (1.540 Å) at 30 mA and 40 kV.

**3.2.19 Antioxidant Activity of Drug-β-CD Inclusion Complexes**

The antioxidant activity of MT, CM, and drug-β-CD inclusion complexes (MTx, MTx-DI, MT-NS, and CMx) was characterized using ABTS assay. The samples were dissolved in methanol with varying concentrations and treated with 100 μM of DPPH solution (1:1 volume ratio). After that, the sample solution was kept in the dark for 30 min at room temperature. The antioxidant activity of samples was measured by using microplate reader at wavelength of 517 nm. The %antioxidant activity was calculated by following equation (3.8).

$$\text{Antioxidant activity (\%)} = \frac{A_{control} - (A_{sample} - A_{control\ of\ sample})}{A_{control}} \times 100 \quad (3.8)$$

$ABTS^{\bullet+}$ was generated by mixing an equal volume of ABTS solution (7 mM) and potassium persulfate solution (2.45 mM). The mixture was kept in the dark for 16-18 h. After that, the obtained $ABTS^{\bullet+}$ solution was diluted with distilled water to obtain a working $ABTS^{\bullet+}$ solution (absorbance of 0.70±0.10 at 734 nm). A control was prepared by mixing 100 μL of distilled water. The sample solutions were prepared as a description above. Then, 100 μL of each sample solution was mixed with 100 μL of working $ABTS^{\bullet+}$ solution. After that, the mixture was kept in the dark at room temperature for 30 min. The antioxidant activity of the sample against $ABTS^{\bullet+}$ radicals was determined by measuring the absorbance at 734 nm using a microplate reader. The antioxidant activity (%) was calculated according to equation (3.9)

$$\text{Antioxidant activity (\%)} = \frac{A_{control} - (A_{sample} - A_{control\ of\ sample})}{A_{control}} \times 100 \quad (3.9)$$

**3.2.20 Antibacterial Activity of Drug-β-CD Inclusion Complexes**

The antibacterial activity was determined against the gram-positive bacteria, the gram-negative bacteria. The broth dilution was prepared the same as previously mentioned in section 3.2.15 to determine MIC and MBC of MTx and CMx (100 mg/mL) samples. The sample solution (50 µL) was added to 96-well plates. Subsequently, 50 µL of bacterial suspension ($10^5$ CFU/mL) was added to each well and incubated at 37 °C for 24 h. The turbidity of the solution was measured as an indication of the growth of bacteria. The turbidity of the samples was compared to the control sample, which contained only sample solution in the same concentration and nutrient broth medium to determine MIC. After the MIC determination of the sample, 10 µL of the cultures, which showed no visible bacterial growth, was added to a fresh agar plate and incubated at 37 °C for 24 h. The lowest concentration of the sample that killed 99.9% of bacteria was defined as MBC. The nutrient broth medium was used as a negative control. The MIC and MBC were evaluated in triplicate (n = 3).

**3.2.21 Anti-Inflammatory Activity of Drug-β-CD Inclusion Complexes**

The MTx and CMx samples were separately dissolved in 10% DMEM and diluted with 10% DMEM to produce various concentrations (2.5, 1.25, 0.62, and 0.31 mg/mL). The anti-inflammatory activity was conducted on the mouse macrophage-like cell line RAW 264.7. The cells were cultured in DMEM with 10% FBS, 100 units per mL penicillin/streptomycin, and L-glutamine at 37 °C in a humidified atmosphere of 95% and 5% $CO_2$. The cells were seeded in a 96-well plate at $1\times10^5$ cells/well and cultured for 24 h. The cells were pretreated with the inclusion complex solutions for 1 h. Then, the inflammatory induction with lipopolysaccharide was performed at °C for 24 h. A solution of 0.1% v/v dimethyl sulfoxide in DMEM was used as the untreated group. The Griess assay was used to monitor nitric oxide (NO) production from cells. Briefly, the culture medium was mixed with distilled water and the Griess reagent. After 15 min, the optical density was measured at 540 nm using a microplate reader. The NO level is expressed based on the nitrite calibration curve and the relative NO was calculated using equation (3.9)

$$\text{NO inhibition}(\%) = \left[\frac{(A_{control} - A_{sample}) - (A_{sample} - A_{background})}{(A_{control} - A_{blank})}\right] \times 100\% \qquad (3.9)$$

Where $A_{control}$ is the absorbance of the control (cells, media and LPS but no sample), $A_{sample}$ is the absorbance of the sample (cells, media, LPS, and sample), $A_{background}$ is the absorbance of the background (sample and media), and $A_{blank}$ is the absorbance of cells and media. The $IC_{50}$ value was obtained as the concentration of the sample that inhibits NO secretion by 50%, as determined by the dose-response curve using non-linear regression. The NO inhibition of the sample was evaluated in triplicate (n = 3).

**3.2.22 Cytotoxicity of Drug-β-CD Inclusion Complexes**

Each inclusion complex sample (50 mg) was dissolved in 10% DMEM (1 mL) and diluted with 10% DMEM to produce various sample concentrations (50, 25, 12.5, and 6.25 mg/mL for MTx and 10, 5, 2.5, and 1.25 mg/mL for CMx).

The cytotoxicity was studied using the Normal Human Dermal Fibroblast cell line (NHDF), as previously described in section 3.2.7. The percentage of cell viability was determined by an MTT assay. The viability of the cells cultured with the fresh medium was used as a control.

**3.2.23 Preparation of QCS/OPEC Hydrogels Containing Drug-β-CD Inclusion Complexes**

The solutions of OPEC (15% w/v) and QCS (4% w/v) were prepared by dissolving in distilled water as description above. To prepare hydrogels containing drug-β-CD inclusion complexes, CMx, MTx, or MTx/CMx were dissolved in the QCS solution to obtain the total inclusion complex concentration at 4 mg/mL in the final hydrogel, before mixing with OPEC solution. The resulting mixture was stirred with a spatula to obtain the hydrogels containing the inclusion complexes. Three hydrogel compositions were prepared in this study: a hydrogel sample named HG, and two hydrogels containing MTx, CMx, or MTx/CMx to obtain HG_MTx, HG_CMx, and HG_MTx/CMx, respectively.

**3.2.24 Gel Fraction of Hydrogels**

The gel fraction was done as previously mentioned in section 3.2.9 by measuring the dry mass hydrogel samples, obtaining the initial dry mass ($W_{i,d}$). Subsequently, the dried samples were immersed in water at 37 ºC for 24 h to swell the

samples and remove soluble components and weight ($w_{s,w}$). Then, the dry weight of the swollen sample after freeze-drying was recorded ($W_{s:water,d}$). The gel fraction (%) was calculated using equation 3.5.

**3.2.25 Water Swelling and Mass Loss of Hydrogels**

The swelling and mass loss were evaluated for the freshly as-prepared hydrogel samples. The initial wet weight of each sample ($W_{i,w}$) was recorded before placing them on an inert polymer mesh, which was inserted into a falcon tube containing 10 mL of phosphate buffer solution (PBS) with 2% of bovine serum albumin (BSA) and 0.05% w/v sodium azide for 1, 2, 4, and 6 days. At each point, the sample was collected and the swollen weight ($W_{s,w}$) was rescored. The swollen hydrogel was dried using freeze-drying and the dry weight ($W_{s,d}$) was recorded. To determine the mass loss of the hydrogels, the prepared wet hydrogels were weighed ($W_{i,w}$) and then freeze-dried using lyophilization technique. The dried weight of hydrogels was measured ($W_{i,d}$). Then, the actual macromer fraction (AMF) using equation (3.10). The initial weight of a sample in the dry state was evaluated following equation (3.11). Subsequently, the swelling and mass loss of the samples were calculated using equations (3.12) and (3.13), respectively.

$$AMF = \frac{W_{i,d}}{W_{i,w}} \tag{3.10}$$

$$W_{i,d} = W_{i,w} \times AMF \tag{3.11}$$

$$Water\ swelling\ ratio = \frac{W_{s,w}}{W_{s,d}} \tag{3.12}$$

$$Mass\ loss\ (\%) = \frac{W_{i,d} - W_{s,d}}{W_{i,d}} \times 100\% \tag{3.13}$$

**3.2.26 Rheological Analysis of Hydrogels**

The rheological analysis of the HG, HG_MTx, and HG_CMx samples was measured using ARES-G2 rheometer (TA Instrument Ltd., USA) accompanied by 40 mm diameter parallel geometry as previously described in section 3.2.10. The solutions of QCS with MTx or CMx and OPEC were co-injected into a vial and mixed for 1 min before being placed in the 1 mm gap. The storage modulus (G') and loss modulus (G") were recorded. Moreover, the self-healing behavior of the hydrogels was determined by a rheometer. An alternate strain sweep was performed at a fixed angular frequency

of 1 Hz, switching the amplitude oscillation strain from low strain (y = 1 %, 100 s for each interval) to high strain (y = 3000 %, 100 s for each interval).

**3.2.27 Self-Healing Properties of Hydrogels**

The macroscopic self-healing behavior of hydrogel samples was characterized as previously mentioned in section 3.2.11.

**3.2.28 Mechanical Test and Adhesiveness of Hydrogels**

The compressive strength, hardness, and compressive strength of the HG, HG_MTx, and HG_CMx samples were evaluated using the texture analyzer (TA.XTplus) in a compression mode. Each disc-shaped hydrogel sample was compressed at a rate of 5 mm/s until the samples were deformed 90% from their original height by a tubular probe (diameter of 12.5 mm). The compression was applied once. The force-time plots from the compression mode were analyzed to obtain the hardness and compressibility values of the hydrogels. The hardness was obtained from the maximum force of the force-time plots. The compressibility was obtained from the area under the force-time plots. The compressive strength was obtained from the maximum stress. After the samples were deformed by pressing with a tubular probe, the hydrogels were allowed to recover for 24 h before the compressibility, hardness, and compressive strength were analyzed.

The adhesiveness of the samples was evaluated using the texture analyzer (TA.XTplus) with a load cell capacity of 50 kg and a test speed of 2 mm/sec. Porcine skin ($2.0 \times 2.0$ $cm^2$) soaked in PBS for 30 min was used as the model tissue and attached to the probe using double-sided adhesive. The probe was lowered to the surface of the samples, and the force was held at 0.02 N for 30 sec. The probe was the moved upward at 5 mm/s. The adhesiveness of the samples was recorded as the maximum force on the force-time plots produced via detachment of the porcine skin from the surface of the sample.

**3.2.29 Cytotoxicity of Hydrogels**

Each hydrogel sample (1 g wet weight) was sterilized under UV radiation for 30 min on each side. The sterilized sample was immersed in a culture medium (2 mL) for 24 h to obtain the extraction medium. After that, the extraction medium was diluted with culture medium to produce various hydrogel concentrations of 50, 10, 5, and 0.5

mg/mL (this is equivalent to solid concentrations of 5, 1, 0.5, and 0.05 mg/mL based on the AMF value).

The cytotoxicity was studied using NHDF cells. The NHDF cells were cultured in 10% DMEM at 37 °C in a humidified atmosphere of 95% air and 5% $CO_2$. The NHDF cells were seeded in a 96-well plate at 8,000 cells/well. The cells were cultured in 10% DMEM and incubated at 37 °C for 24 h to allow cell attachment. After that, the culture medium in each well was replaced with different sample solutions (see description above) and incubated at 37 °C for 24 h. The percentage of cell viability was determined by an MTT assay. Briefly, the culture medium was removed and replaced with 100 µL of 0.5 mg/mL MTT solution. After 3 h incubation, the MTT solution was removed, and 100 µL of dimethyl sulfoxide was added to dissolve the formazan crystals. The absorbance of the solution was measured at 570 nm using a microplate reader (BioTek Instruments, USA). The viability of the cells cultured with the fresh medium was used as a control

**3.2.30 Antioxidant Activity of Hydrogels**

Each hydrogel sample (1 g wet weight) was immersed in PBS (2 mL) for 24 h to obtain the extraction medium. After that, the extraction medium was diluted with PBS to produce various hydrogel concentrations of 500, 250, 125, and 62.5 mg/mL (this is equivalent to solid concentrations of 50, 25, 12.5, and 6.25 mg/mL based on the AMF values).

The antioxidant activity was evaluated by an ABTS assay. $ABTS^{\bullet+}$ was generated by mixing an equal volume of ABTS solution (7 mM) and potassium persulfate solution (2.45 mM). The mixture was kept in the dark for 16-18 h. After that, the obtained $ABTS^{\bullet+}$ solution was diluted with distilled water to obtain a working $ABTS^{\bullet+}$ solution (absorbance of 0.70±0.10 at 734 nm). A control was prepared by mixing 100 µL of working $ABTS^{\bullet+}$ solution and 100 µL of distilled water. The sample solutions were prepared (as a description above). Then, 100 µL of each sample solution was mixed with 100 µL of working $ABTS^{\bullet+}$ solution. After that, the mixture was kept in the dark at room temperature for 30 min. The antioxidant activity of the sample against $ABTS^{\bullet+}$ radicals was determined by measuring the absorbance at 734 nm using a microplate reader. The antioxidant activity (%) was calculated using equation (3.1).

### 3.2.31 Antibacterial Activity of Hydrogels

The antibacterial activity of the hydrogel samples was determined by colony counting. A 1,000 mg hydrogel sample was sterilized under UV radiation for 30 min each side and placed in the falcon tube. A bacterial suspension (1 mL, $10^5$ CFU/mL) was added to the sample and incubated at 37 °C for 24 h. After that, 5 mL of distilled water was added and mixed for 5 min using a vortex mixer. The sample suspension was serially diluted with 0.1% peptone, and 100 µL of the diluted sample was spread on a nutrient agar plate. The nutrient agar plate was further incubated at 37 °C for 24 h. Finally, the viable bacteria were counted, and the bacterial reduction (%) was calculated using equation 3.14.

$$\text{Bacterial reduction (\%)} = \frac{(B - A)}{B} \times 100\% \qquad (3.14)$$

Where A is the number of bacteria recovered from the sample after incubation at 37 °C for 24 h, and B is the number of bacteria recovered from control (bacterial suspension at the same concentration) at 37 °C for 24 h.

### 3.2.32 Anti-Inflammatory Activity of Hydrogels

The extraction medium was prepared by immersing the hydrogel samples (1 g wet weight) in PBS (2 mL). The extraction medium was diluted with 10% DMEM to produce various concentrations of 62.5, 31.2, 15.6, 7.81, and 3.91 mg/mL (this is equivalent to solid concentrations of 6.25, 3.12, 1.56, 0.78, and 0.39 mg/mL based on the AMF value).

The anti-inflammatory activity was conducted on the mouse macrophage-like cell line RAW 264.7. The cells were cultured in DMEM supplemented with 10% FBS, 100 units per mL penicillin/streptomycin, and L-glutamine at 37 °C in a humidified atmosphere of 95% and 5% $CO_2$. The cells were seeded in a 96-well plate at $1\times10^5$ cells/well and cultured for 24 h. The cells were pretreated with hydrogel extraction media (see description above) for 1 h. Then, the inflammatory induction with lipopolysaccharide was performed at 37 °C for 24 h. A solution of 0.1% v/v dimethyl sulfoxide in DMEM was used as the untreated group. The Griess assay was used to monitor NO production from the cells. Briefly, the culture medium was mixed with distilled water and the Griess reagent. After 15 min, the optical density was measured at 540 nm using a microplate reader. The NO level is expressed based on the nitrite

calibration curve ($r^2 > 0.990$) and the relative NO inhibition (%) was calculated using equation (3.9).

**3.2.33 *In Vitro* Wound Healing Assay**

The scratch wound healing assay was used to investigate wound closure or cell migration of the injectable self-healing hydrogel including MTx or CMx. In this evaluation was done as previously described in section 3.2.14. The NHDF cells ($2\times10^5$ cells/well) was used to evaluate the wound healing. The NHDF monolayer cell was scratched using a SPLScar$^{TM}$ scratcher (tip width: 0.5 mm; SPL Life Sciences, Korea). The hydrogels (100 mg wet weight) were immersed in 2 mL of 10% DMEM at 37 °C for 24 h and diluted with 10% DMEM to produce the extraction medium at concentration of 10 mg/mL which is equivalent to 1 mg/mL solid. This extraction medium was added to the cells and incubated at 37 °C for 24 h. SFM was used as the control. Photographs of the scratched area were recorded at 0 and 24 h. The percentage of reduction (wound closure) of the scratched area was calculated following the equation 3.15.

$$Wound\ closure\ (\%) = \frac{(A-B)}{A} \times 100 \qquad (3.15)$$

Where A is the area of the initial scratch wound measured immediately after scratching, and B is the area after scratching for 24 h. The area of gap was calculated using ImageJ.

**3.2.34 Statistical Analysis**

Data are presented as means ± standard error of means. Student's t-test was used for two independent data groups and one-way analysis of variance (ANOVA) with Tukey's post hoc test in SPSS (IBM SPSS< USA) was used for multiple data groups. The statistical significance was accepted at $p < 0.05$.

# CHAPTER 4

# RESULTS AND DISCUSSION

## 4.1 Characterization of QCS and OPEC Polymers

The QCS polymer was synthesized from the reaction of chitosan with GTMAC, while OPEC was synthesized from the periodate oxidation of pectin. The FTIR spectra of chitosan and QCS (Figure 4.1A) display the characteristic bands as reported (Lawrie et al., 2007). A new prominent band appeared at 1479 $cm^{-1}$ due to the C-H bending of the methyl substituent of the quaternary ammonium groups compared to the chitosan spectrum (Kaolaor et al., 2019). Additionally, the peak intensity due to the O-H stretching at 3287 $cm^{-1}$ and that of the methyl C-H stretching at 2918 $cm^{-1}$ has increased in QCS, verifying the conjugation of GTMAC to chitosan. The FTIR spectrum of pectin (Figure 4.1B) displays the characteristic bands at 1732 $cm^{-1}$ and 1606 $cm^{-1}$ from the ester and carboxylate groups, respectively (Gupta et al., 2013). The spectrum of OPEC (Figure 4.1B) is very similar, the only difference being the relative intensity of these two bands, however, the interpretation of this change is complicated by the overlapping vibrational mode for water at 1635 $cm^{-1}$. This lack of significant change in the spectra of the polymer and its oxidized analogue has previously been observed in the literature for similar systems (Kim et al., 2022; Aston et al., 2015).

The 1D DOSY spectra of chitosan and QCS are displayed in Figure 4.3A. The spectrum of chitosan is in accordance with published work (Fernandez-Megia et al., 2005). This includes a resonance at 1.9 ppm corresponding to methyl protons of the *N*-acetylglucosamine unit and the resonance at 3.1 ppm corresponding to the proton on C2 of the glucosamine unit. The resonance in 3.5-4 ppm region correspond to the protons on C3 to C6 as well as the proton on C2 for the *N*-acetylglucosamine unit, while the resonance at 4.8 ppm is due to the proton on C1. Based on the $^{1}H$ NMR data, a degree of acetylation (DA%) of 10% was determined in agreement with the supplier information. The spectrum of QCS was likewise in accordance with published work (Channasano et al., 2005). This includes resonances at 2.6 ppm corresponding to the

methylene protons, at 4.4 ppm corresponding to the methine proton and at 3.1 ppm from the methyl protons of the quaternary ammonium groups.

To quantify the degree of substitution (DS%) in QCS, $^{1}$H NMR was used with a DS value of 44% obtained. XPS analysis confirmed the presence of chloride in the QCS sample (Figure 4.4) and using the N 1s atom % and Cl 1s atom %, a degree of substitution could be estimated to be approximately 40% in agreement with the NMR analysis. Overall, this polymer can be described as a terpolymer containing 10% N-acetylglucosamine units, 46% glucosamine units and 44% quaternized glucosamine units.

The 1D DOSY and $^{1}$H NMR spectra of pectin and OPEC are provided in Figures 4.2B and 4.3B). The signal from the neutral sugar L-rhamnose at 1.26 ppm was observed as previously reported (Grasdalen et al., 2007) but at a very low percentage. The degree of esterification, DE(%), of pectin was determined from $^{1}$H NMR spectra and a value of 82% was obtained. This DE(%) matches the spectral features of the anomeric region previously reported for pectin with similar composition (Grasdalen et al., 2007). The XPS spectra of the pectin sample as well as the OPEC sample are shown in Figure 4.4B. It was found that sodium was present in the narrow scan of both samples indicating that the carboxylate exists as the sodium salt. Using the O 1s atom % and Na 1s atom %, the amount of carboxylic acid-containing monomer units could be estimated to be approximately 13% in agreement with the NMR analysis. Overall, the pectin polymer can be described as constituting mainly 82% ester and 13% acid form accounting for some neutral sugars. There are no discerning features in the $^{1}$H NMR spectrum or XPS data that can assist in quantifying the degree of oxidation of OPEC. Previous works on evaluation of the degree of oxidation of polysaccharides have shown that the periodate oxidation reaction goes to near completion (Aston et al., 2015; Channasano et al., 2005). We therefore estimate that the OPEC of the current study has a degree of oxidation of 14% (e.g. 14% of the monomer units have been oxidized).

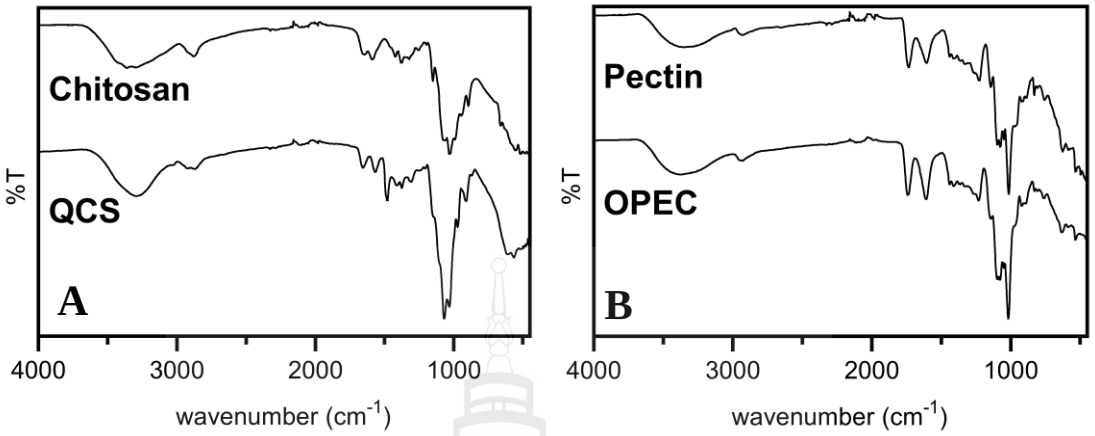


**Figure 4.1** FTIR Spectra of (A) Chitosan and QCS (B) Pectin and OPEC

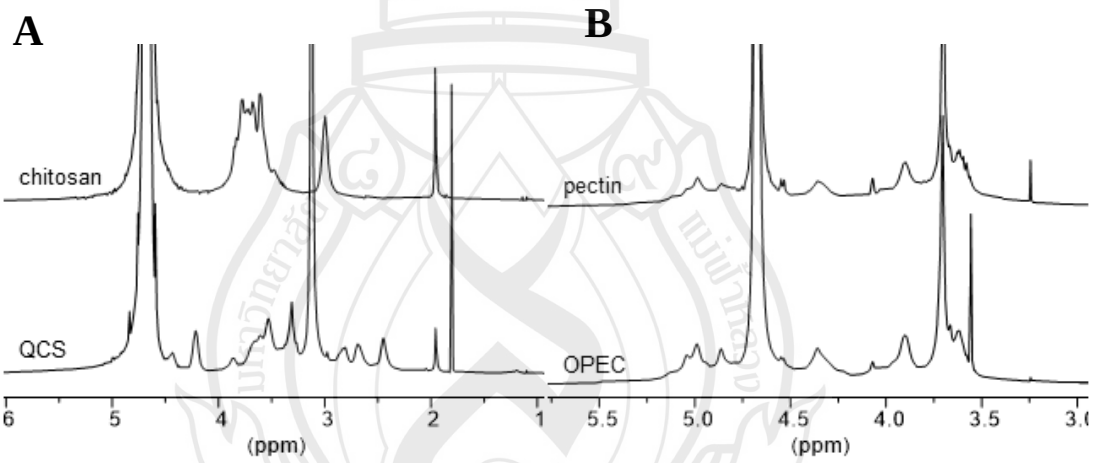


**Figure 4.2** $^{1}$H NMR Spectra of (A) Chitosan and QCS (B) Pectin and OPEC

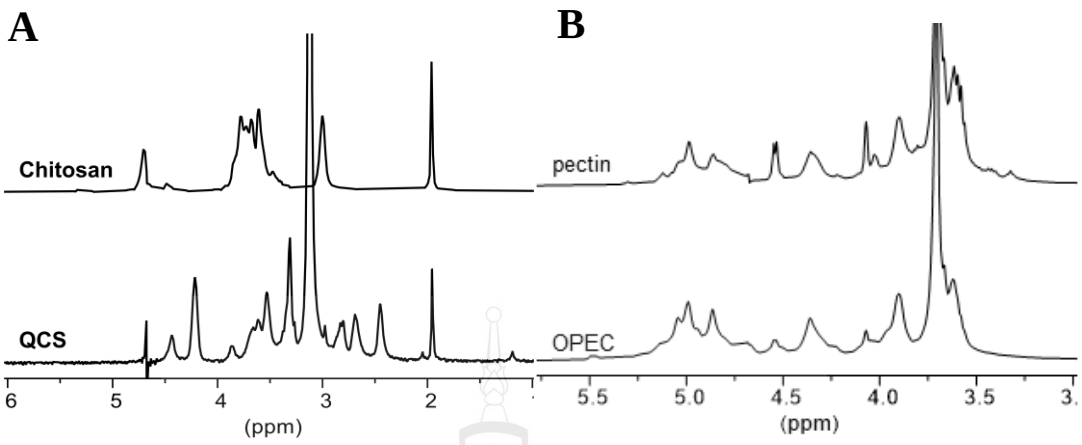


**Figure 4.3** 1D DOSY NMR Spectra of (A) Chitosan and QCS and (B) Pectin and OPEC

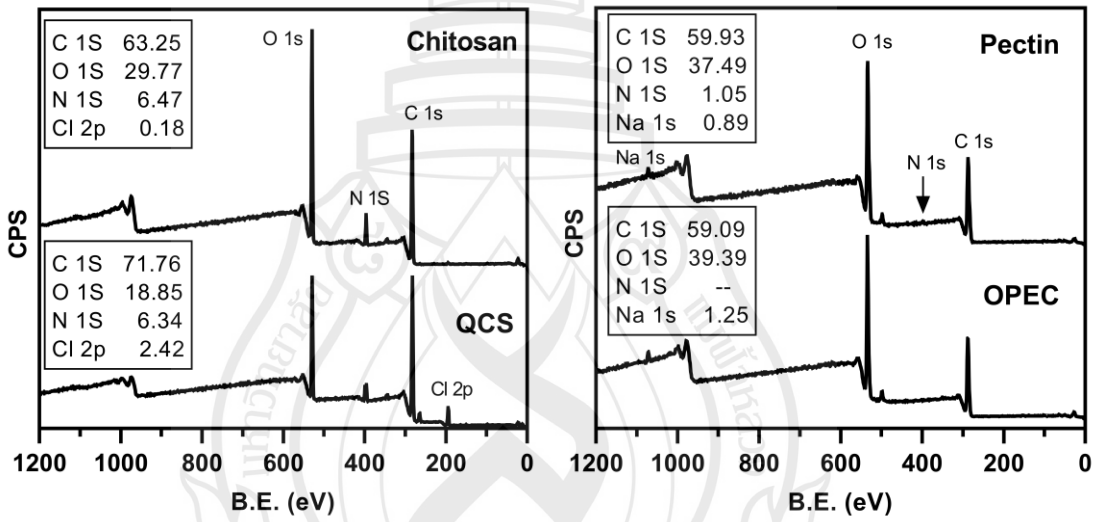


**Figure 4.4** XPS Survey Spectra of (A) Chitosan and QCS; (B) Pectin and OPEC. Trace Amounts (< 0.7% of Other Elements Such as Ca and Si were Also Observed)

## 4.2 Fabrication of QCS/OPEC Hydrogels

First, each polymer solution was prepared by heating at 60 ºC until no solids could be seen, followed by stirring at 37 ºC for an additional 2 h. This was done to ensure full dissolution of the polymers and in addition to lower the molecular weight of OPEC as it is known that polysaccharides oxidized using periodate are hydrolytically unstable (Gupta et al., 2013). Hydrogels were prepared by co-injection of a QCS and

OPEC solution. To optimize the mass ratio of QCS and OPEC. Using different OPEC and QCS concentrations and varying the volume ratios, gelation was evaluated visually. It was found that combining a 10 %w/v OPEC solution with either a 2 %w/v or 4% w/v of QCS solution only resulted in partial gel formation. A series of experiments using a combination of a 4 %w/v QCS solution and a 15 %w/v OPEC solution were therefore investigated and the resulting data are shown in Table 4.1. It was found that an equal or higher volume of the QCS solution was required to form a gel. These volume ratios are equivalent to QCS to OPEC mass ratios of 1:3.8 to 1:0.94.

**Table 4.1** Gel Formation Ability of Mixtures of QCS and OPEC

| **QCS 4% w/v (mL)** | **OPEC 15 %v/v (mL)** | **QCS:OPEC Mass ratio** | **Gel formation[1]** | **Gel fraction[2] (%)** | **$Q_w$[2] (%)** |
|---|---|---|---|---|---|
| 0.2 | 0.8 | 1:15 | 0 | NA | NA |
| 0.4 | 0.6 | 1:5.6 | 0 | NA | NA |
| 0.5 | 0.5 | 1:3.8 | 2 | NT | NT |
| 0.6 | 0.4 | 1:2.5 | 2 | 76 ± 1 | 34 ± 9 |
| 0.8 | 0.2 | 1.0.94 | 2 | 74 ± 2 | 70 ± 7 |

**Note** 1: Scoring system (0) no gel formation; (1) partial gel formation with excess solution present; (2) near complete gel formation with small amount of solution present. 2: determined after 6 h, n = 3. NA = not applicable, NT = not tested.

## 4.3 Characterization of QCS/OPEC Hydrogels

The injectable self-healing OPEC/QCS hydrogels were successfully prepared by co-injectable OPEC and QCS solutions (specific amounts and concentrations are detailed in Table 4.1. Solutions of OPEC and QCS were prepared by adding water to the dry polymers and then stirring at 60 ºC until they were dissolved, followed by stirring at 37 ºC for 2 h. The initial study evaluating various OPEC and QCS concentrations found the optimal 4 %w/v QCS and 15 %w/v OPEC. To optimize the QCS to OPEC ratio, gelation was evaluated visually after co-injecting the OPEC (15 % w/v) solution and QCS (4 %w/v) solution in a vial and stirring with a spatula. The

hydrogels (HG_0.8:0.2 and HG_0.6:0.4) demonstrated good injectability and a rapid gelation time, as evidenced by their ability to be picked up with tweezers within just 1 minute of formation (Figure 4.5).

The gel fraction at 6 h of these hydrogels (Table 4.1) was found to be 76 and 74 % with no significant difference between the two. However, the water content after 6 h of immersion was significantly different between the two hydrogels with values of 34 and 70 %. The higher water content of HG_0.8:0.2 compared to HG_0.6:0.4 indicates that HG_0.6:0.4 has a higher crosslinking density, which correlates with the closer mol ratio of functional groups. Overall, it can be concluded that the self-healing properties are likely due to a combination of two possible interactions occurring between QCS and OPEC: Schiff's base reaction and electrostatic interactions. The HG-0.6:0.4 sample has a mole ratio of the functional groups suited to optimize these interactions, resulting in a hydrogel network of greater integrity (compared to HG_0.8:0.2).

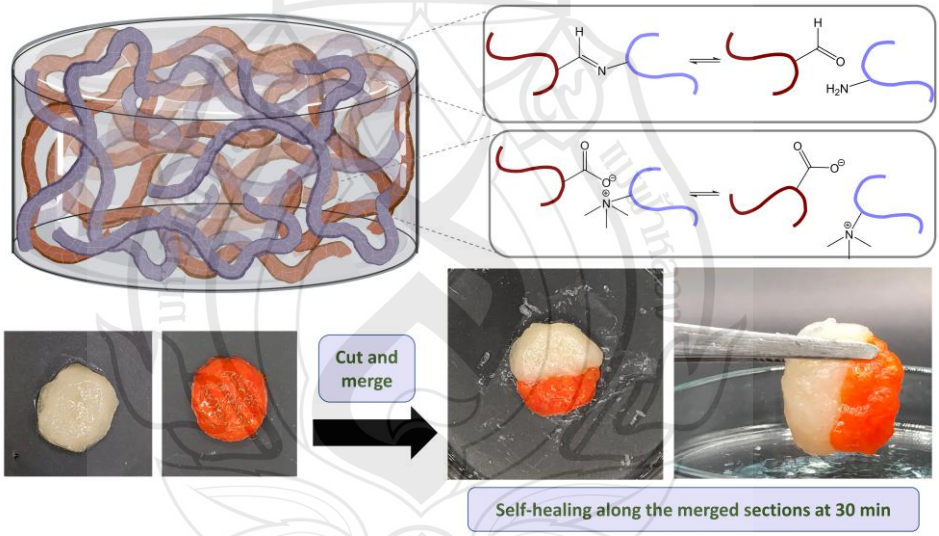


**Figure 4.5** Schematic Representation of Potential Intra and Intermolecular Interactions Between QCS and OPEC. Visual Observation of the Self-Healing Behavior of the Injectable Hydrogel HG_0.6:0.4. Part of Diagram with BioRender.com

## 4.4 Rheological Analysis of QCS/OPEC Hydrogels

Due to the aim of producing an antibacterial hydrogel, the two hydrogel systems with the highest QCS content, HG_0.6:0.4 and HG_0.8:0.2, were evaluated further. To confirm the QCS/OPEC hydrogel formation, the rheological analysis of the hydrogel compositions QCS:OPEC of 0.6:0.4 and 0.8:0.2 was run in triplicate and one example is displayed in Figure 4.6. The gelation process was monitored by measuring the storage modulus G' and loss modulus G'' over a period of 400 sec (Figure 4.6A). The storage modulus G' was found to be above the loss modulus G'' from the first timepoint of 6 sec, corresponding to less than one min after the precursor solutions were combined. The storage modulus remained above the loss modulus over the entire measurement of 400 sec. At all time points, the storage modulus for the HG_0.6:0.4 sample was found to be more than twice that of the HG_0.8:0.2 sample, with the values measured at 406 sec of 394 ± 93 Pa and 177 ± 89 Pa, respectively. For the HG_0.8:0.2 sample, both the storage and loss modulus seemed to be reaching a plateau, while for the HG_0.6:0.4 sample, a continued increase in the measured values was apparent. As highlighted in previous work (Zhang et al., 2011), this indicates slow gelation in the rheometer potentially due to limited mixing or loss of water during the experiment.

The elastic response of the hydrogels was analyzed through a strain sweep (Figure 4.6B) to assess when the storage modulus G' became lower than the loss modulus G'' indicating that the hydrogels collapsed. Both hydrogel samples showed a gradual decrease in the storage modulus G' from a strain of approximately 30%, indicating gradual collapse of the hydrogel network. For the HG_0.6:0.4 sample, G' became smaller than G'' at 1660 ± 580% strain, while for the HG_0.8:0.2 sample, this occurred at 390 ± 130% strain, indicating that the HG_0.6:0.4 sample has a hydrogel network of greater integrity.

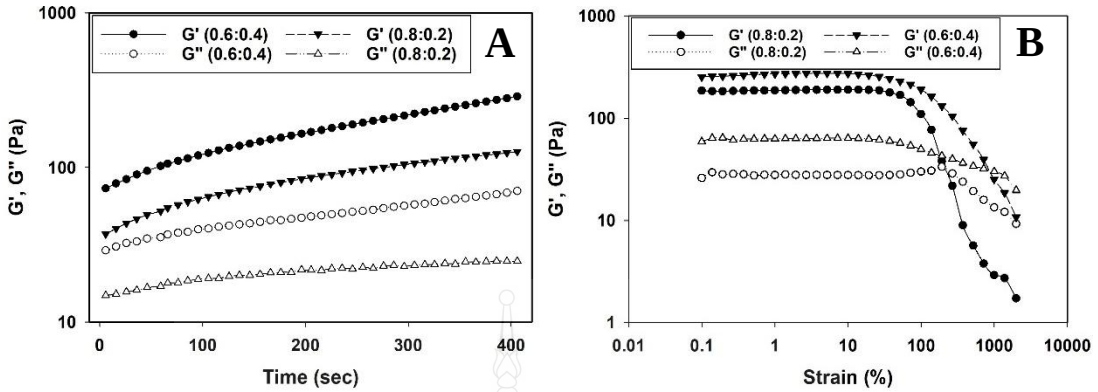


**Figure 4.6** The Rheological Analysis of the HG_0.6:0.4 and HG_0.8:0.2 Samples (A) Storage Modulus G' and Loss Modulus G" Analysis During the Gelation Process (37 ºC, Frequency 1.0 Hz, Strain 1%); (B) G' and G" Strain Sweep (37 ºC, Frequency 1.0 Hz, Strain 1%)

## 4.5 Self-Healing Properties of QCS/OPEC Hydrogels

When a hydrogel is placed into a wound site, the hydrogel will be subjected to external mechanical force, which may cause the hydrogel to disintegrate (Li et al., 2015). In order to overcome this issue, the use of self-healing properties can be employed since such hydrogels can heal or re-form after fracture therefore reducing the frequency of dressing replacement.

The macroscopic evaluation of the self-healing properties of the HG_0.6:0.4 sample after curing in an oven is illustrated in Figure 4.5. One disc-shaped hydrogel was dyed with red food dye, and one was left as prepared. Each was cut in half and one half of each type was then put in close proximity touching each other. After 30 min, the hydrogel had healed as can be seen when it is being picked up by forceps. Studies in the literature using chitosan-based polymers in combination with oxidized polymers (Li et al., 2021; Yu et al., 2022; Li et al., 2020), report the time for self-healing from a few min, 30 min, and 3 h. The faster gelation times similar to that of the current study are observed for hydrogel systems where in addition to the Schiff's base mechanism, electrostatic interactions can also contribute to self-healing.

Based on the data obtained from the rheological analysis of the hydrogels (Figure 4.6C), the self-healing properties were evaluated from G' and G'' in continuous

step strain measurements switching from a strain of 1 % and 2000% with intervals of 100 sec. The experiment was run in duplicate and one example is displayed in Figure 4.7. For HG_0.8:0.2, gel disassembly and reassembly were seen to be rapid with continuous gelation during the low high strain sweep. For HG_0.6:0.4, gel disassembly and reassembly were likewise observed, however, during the high strain sweeps a much more pronounced gelation process was observed. For this gel, full recovery was only observed after the first high strain – low strain cycle. These results support the self-healing properties of the gel samples and are similar to what have previously been reported for similar systems (Du et al., 2019; Yu et al., 2022; Li et al., 2020; Kim et al., 2022).

As illustrated in Figure 4.5, there are two possible interactions that can occur between QCS and OPEC. One is based on Schiff's base reaction between an amine of QCS and an aldehyde of OPEC, forming an imine. The other is electrostatic interactions between the negatively charged carboxylate group of OPEC and the positively charged quaternary ammonium group of QCS. However, there is no simple way of evaluating their relative contribution to hydrogel (Aston et al., 2015). A control experiment mixing QCS and pectin at a mass ratio of 1:2.5 produced a gel which confirms that electrostatic intermolecular interactions form part of the crosslinking mechanism. Considering the relative abundance of these functional groups, it is likely that both reactions take place. Thus, QCS has near equal proportion of amine (46%) and quaternary ammonium (44%) groups and OPEC has near equal proportion of carboxylate groups (13%) and saccharide units undergone oxidation (14%). Importantly, the proportion of aldehydes and carboxylate groups in OPEC is much less than the proportion of amine and quaternary ammonium groups in QCS so it would be estimated that a closer molar ratio of amines and aldehydes as well as quaternary ammonium and carboxylate groups would be present in HG_0.6:0.4 compared to HG_0.8:0.2.

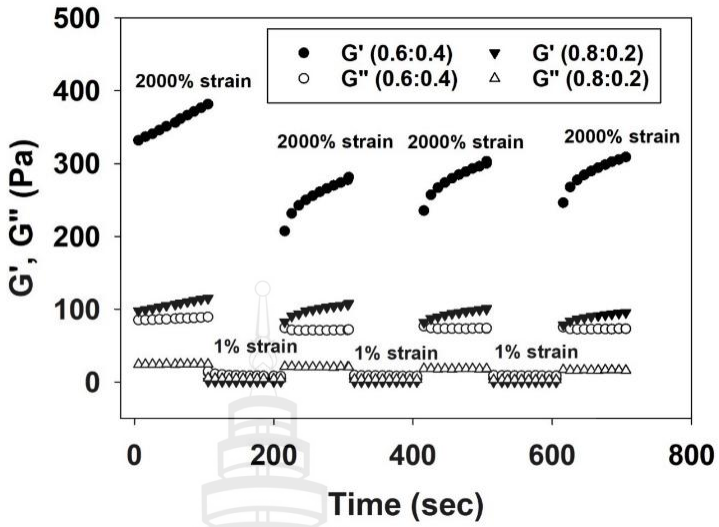


**Figure 4.7** Continuous Step Strain Analysis of the HG_0.6:0.4 and HG_0.8:0.2 Sample. Low Strain of 1% and High Strain of 2000% were Applied with 100 s Intervals

## 4.6 Mechanical Properties of QCS/OPEC Hydrogels

To apply a hydrogel to a wound site, the hydrogel should have mechanical performance that allows it to withstand the physiological force caused by the movement of tissue, yet be pliable so as to adapt to the wound site. Thus, the texture profile analysis (TPA) mode was used to evaluate the compressibility and hardness of the hydrogels with values given in Table 4.2. It was found that the compressibility of the hydrogels was not significantly different with values of 162 and 117 mN s for HG_0.6:0.4 and HG_0.8:02, respectively. However, HG_0.6:0.4 showed a significantly higher hardness than HG_0.8:02 (700 versus 320 mN), making the HG_0.6:0.4 a better candidate for the application.

A hydrogel used in wound healing should adhere to the wound site during the healing process and should be easy to apply and remove without inducing trauma. To evaluate the adhesive properties of the hydrogels, the adhesive mode of the texture analyzer was used. Porcine skin soaked in PBS for 30 min was used as the model tissue because its mechanical and biological properties are similar to those of human skin (Debeer et al., 2913; Ranamukhaarachchi et al., 2016). The adhesiveness of the

HG_0.8:0.2 was significantly higher than that of the HG_0.6:0.4 (Table 4.2). Generally, in chronic wound management, adhesive wound dressings may cause pain and injury to the wound during dressing changes (Klode et al., 2011). Kolde et al. reported the adhesion of commercial wound dressings on healthy skin. The required energy to remove the wound dressings from human skin ranges between 0.70 to 2.25 N (Klode et al., 2011). From the results, the adhesiveness of these hydrogel films showed low adherence to the skin, which was lower than that of the gold standard, commercial fibrin glue (15 ± 3 kPa) (Mehdzadeh et al., 2012) and commercial hydrogel formulations (0.51-3.56 kPa) (Murphy et al., 2012). Therefore, the results obtained in the current study confirmed that these hydrogels would be easy to remove after use.

**Table 4.2** Compressibility, Hardness, and Adhesiveness of HG_0.6:0.4 and HG_0.8:0.2

| Sample name | Compressibility (mN s) | Hardness (mN) | Adhesiveness (Pa) |
|---|---|---|---|
| **HG_0.6:0.4** | 162 ± 58 [1] | 700 ± 320 [1] | 133 ± 14 [2] |
| **HG_0.8:0.2** | 117 ± 50 [1] | 320 ± 150 [1]* | 190 ± 15 [2]* |

**Note** 1: n = 5; 2: n = 4; *$p < 0.05$ compared between two samples.

## 4.7 *In Vitro* Cytotoxicity of OPEC, QCS, and Hydrogels

The indirect cytotoxicity of all hydrogels must be evaluated to confirm their biocompatibility. The ISO 10993–5 standard states that "reduction of cell viability by more than 30% is considered a cytotoxic effect". Figure 4.8 displays the viability of cells cultured with the extraction media from the QCS, OPEC, and hydrogels. It was found that the viability of cells was greater than 70% after treatment for 24 h, except for HG_0.8:0.2 at concentrations of 10 and 50 mg/mL. It can therefore be concluded that HG_0.8:0.2 showed higher toxicity than HG_0.6:0.4 (Figure 4.8C). The indirect cytotoxicity of the polymers QCS and OPEC were likewise evaluated. It was found that QCS was cytotoxic to values as low as 0.004 %w/v (Figure 4.8A and 4.8B).

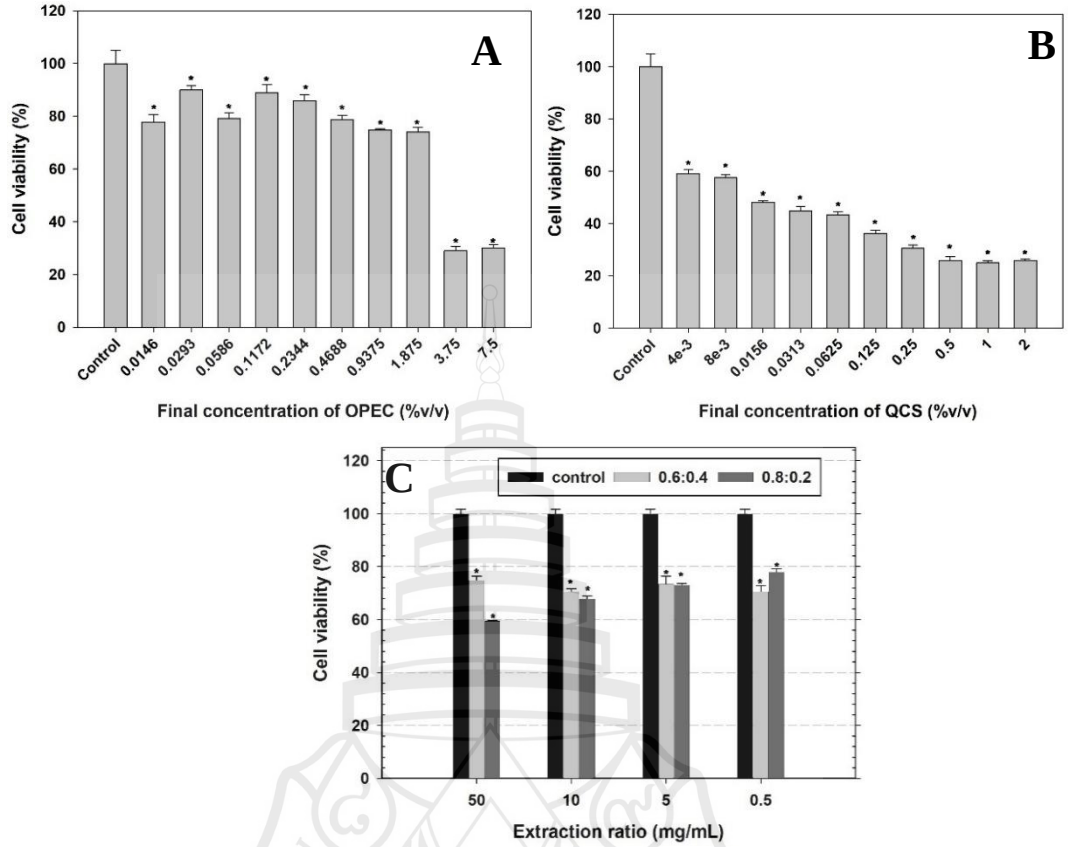


**Figure 4.8** Indirect Cytotoxicity of (A) OPEC, (B) QCS, and (C) HG_0.6:0.4 and HG_0.8:0.2 Hydrogels (n = 3). $^{*}p < 0.05$ Compared with the Control at Any Given Extraction Ratio

## 4.8 *In Vitro* Cell Migration

Cell migration is a requirement for successful wound closure and healing. In this study, the scratch wound healing assay was employed to investigate this cell behavior. The cell migration into the scratch area was observed after treatment with extraction media for 48 h. It was observed that the cells treated with extraction media of HG_0.6:0.4 and HG_0.8:0.2 migrated into the scratch area during the 48-h period. Compared to control (wound closure of 22 ± 1 %), there was no significant difference for HG_0.8:0.2 (wound closure of 24 ± 1 %) (Figure 4.9). However, compared to both control and HG_0.8:0.2, HG_0.6:0.4 displayed a significantly higher value (wound closure of 31 ± 3 %), making this hydrogel a good candidate for application in wound management.

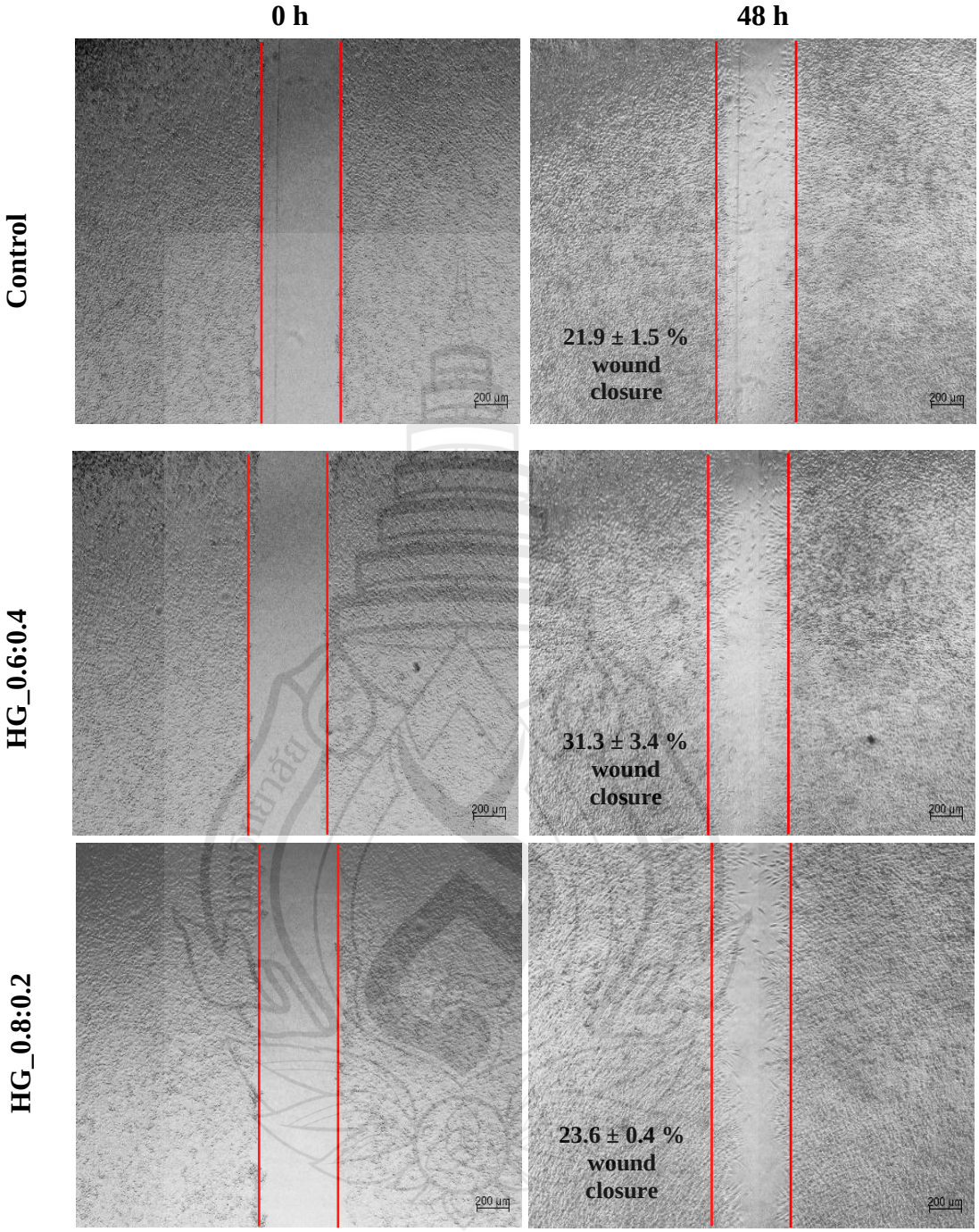


**Figure 4.9** Examples of Images Taken of Scratch Assay to Evaluate the Wound Closure of the Extraction Media for the Two Hydrogels

## 4.9 Antibacterial Activity of QCS, OPEC, and Hydrogels

Wounds are easily infected by the environment. Therefore, the antibacterial activity is important to investigate. The antibacterial activity of the polymers and the HG_0.6:0.4 and HG_0.8:0.2 samples was evaluated against E. coli TISTR 527 and S. aureus TISTR 746 by a broth dilution technique. The influence on bacterial growth was studied in order to determine the $MIC_{50}$ and MBC. The $MIC_{50}$ was determined as the minimal concentration that suppresses bacterial growth by 50% after 24 h of incubation with an initial loading of 105 CFU/mL. The MBC was the minimum amount required to inhibit 99.9% of bacterial growth on agar plates after 24 h of incubation. From Table 4.3 and Figure 4.10, the QCS showed higher antibacterial activity than OPEC against both E. coli TISTR 527 and S. aureus TISTR 746. The permanent positive charge of the quaternary ammonium groups of QCS could interact with the negatively charged sites on a bacterial cell wall leading to cell lysis and death. The quaternary ammonium groups of QCS also cause the denaturation of proteins, by deforming the permeability of the cell wall and reducing the normal flow of critical nutrients into the cell which leads to cell death (Cheah et al., 2019; Daels et al., 2011). The similar values of $MIC_{50}$ and MBC for the extraction solutions from the HG_0.6:0.4 and HG_0.8:0.2 samples were higher than 500 mg/mL against both E. coli TISTR 527 and S. aureus TISTR 746 indicating low antibacterial activity of the hydrogels. In addition, the similar values of the $MIC_{50}$ and MBC for the ampicillin and amoxicillin used as positive controls were 0.26 mg/mL and 0.064 mg/mL, respectively, confirming the inhibition of bacterial growth as the reference.

**Table 4.3** Minimum Inhibition Concentration (MIC) and Minimum Bactericidal Concentration (MBC) Values[1] Against *E. coli* TISTR 527 and *S. aureus* TISTR 746

| Sample | *E. coli* TISTR 527 | | *S. aureus* TISTR 746 | |
|---|---|---|---|---|
| | **$MIC_{50}$ (mg/mL)** | **MBC (mg/mL)** | **$MIC_{50}$ (mg/mL)** | **MBC (mg/mL)** |
| OPEC | 37.5 | 37.5 | 37.5 | 37.5 |
| QCS | 0.04 | > 10 | 0.04 | 10 |
| HG_0.6:0.4 [2] | >500 | > 500 | >500 | >500 |
| HG_0.8:0.2 [2] | >500 | > 500 | >500 | >500 |
| Ampicillin | 0.26 | 0.26 | NT | NT |
| Amoxicillin | NT | NT | 0.064 | 0.064 |

**Note** 1: $MIC_{50}$ was defined as the sample concentrations that inhibited growth of 50%, MBC was defined as the sample concentrations that inhibited growth of 99.9%; 2: extract from hydrogel, concentration refers to maximum if the hydrogel had completely dissolved. NA = not applicable, NT = not tested.

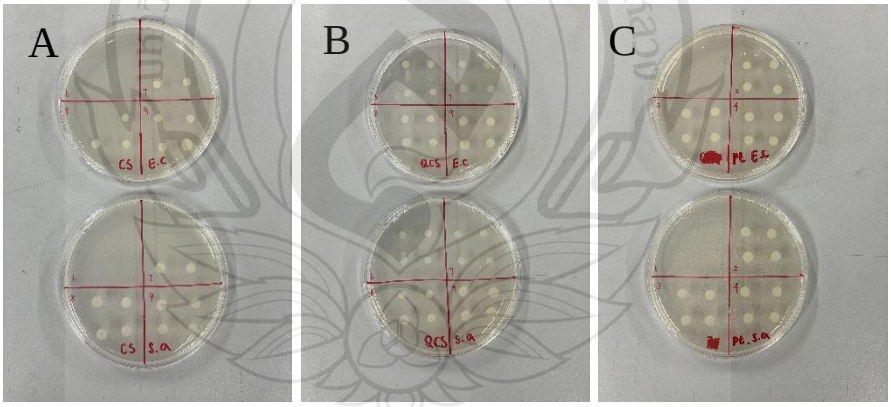


**Figure 4.10** Selected Images of Minimal Bacterial Concentration (MBC) Against *E. coli* TISTR 527 and *S. aureus* TISTR 746 of (A) Chitosan, (B) QCS, (C) Pectin, (D) OPEC, (E) HG_0.6:0.4, and (F) HG_0.8:0.2

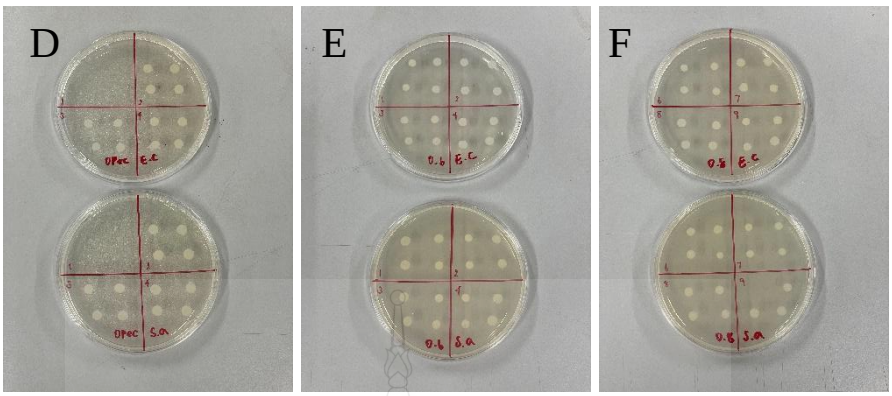


**Figure 4.10** (Continued)

## 4.10 Characterization of MTx and CMx

To enhance the aqueous solubility and stability of MT and CM, these natural product extracts were encapsulated within β-CD, forming inclusion complexes. In this study, the MTx prepared using methanol as a solvent provided the best antioxidant activity and gained better MT solubility than when distilled water was used as a solvent (MTx-DI). The results showed that MTx, MTx-DI, and MTx-NS had IC50 of 3.23, 7.98, and 8.75 mg/mL, respectively. Thus, the MTx preparation method was used in this study. In addition, the successful formation of these inclusion complexes was confirmed through XRD analysis and their ability to dissolve in water. Both MT and CM are crystalline solids with XRD spectra that are consistent with those reported in the literature (Wathoni et al., 2020; Lai et al., 2021), as shown in Figure 4.11. The mixtures of these natural products with β-CD (MTpm and CMpm) displayed XRD patterns, which were a weighted average of the individual components and clearly displayed high intensity peaks of the solid crystalline phases of the pure MT and CM. In agreement with this, the physical mixing technique resulted in materials that were insoluble in water similar to the pure natural products at the same concentration (Figure 4.12). In contrast, the XRD patterns of the inclusion complexes (MTx and CMx) exhibited the absence of crystalline peaks, showing only broad peaks in the 2θ ranges of 10-15° and 15-20°, which are characteristic of pure β-CD. This change in the XRD pattern confirmed the successful formation of the inclusion complexes (Chen et al., 2018). Additionally, MTx and CMx displayed distinct physicochemical properties

compared to the pure natural products and their physical mixtures, being fully soluble in water at concentrations of 10 mg/mL (Figure 4.12). These findings are consistent with previous studies that demonstrated the ability of β-CD to enhance the aqueous solubility of hydrophobic drugs by forming inclusion complexes, thereby significantly altering their solubility and stability profiles (Manholim et al., 2014; Muchtaridi et al., 2023; Wathoni et al., 2020; Yuan et al., 2022).

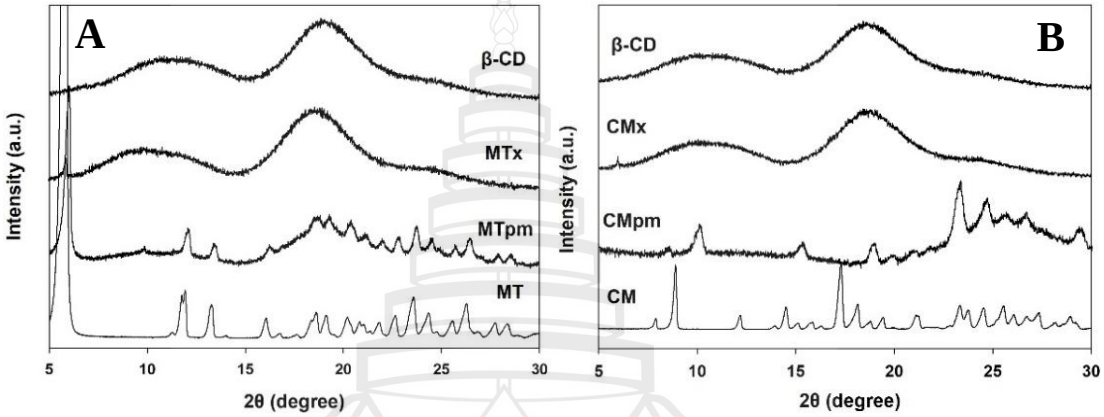


**Figure 4.11** XRD Patterns of (A) MT, MTpm, MTx, and β-CD and (B) CM, CMpm, CMx, and β-CD

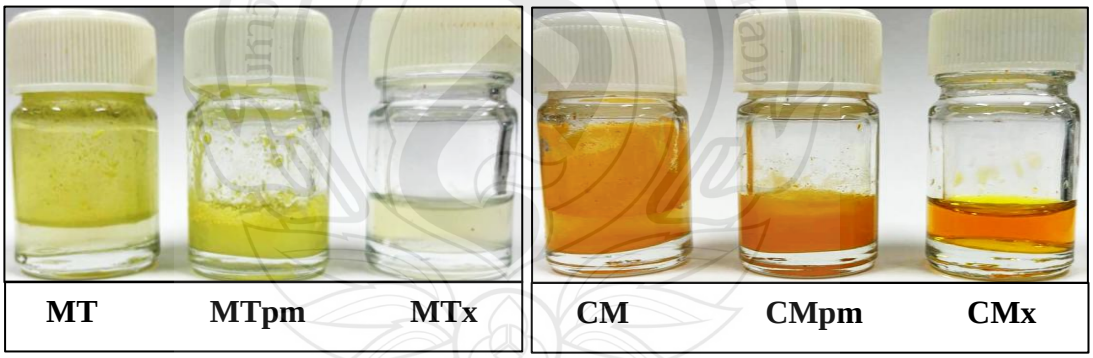


**Figure 4.12** The Solution of MT, MTpm, MTx, CM, CMpm, and CMx in Water at the Concentration of 10 mg/mL

## 4.11 Fabrication of QCS/OPEC Hydrogels Containing Drug-β-CD Inclusion Complexes

To incorporate the inclusion complexes in the hydrogels, they were first dissolved in the QCS solution before the gel formation process, while maintaining the original hydrogel composition. The maximum achievable loading was 4 mg of inclusion complex per 84 mg of dry polymer mass in the resulting hydrogel (Chanmontri et al., 2023). The gel fraction of all hydrogel samples was assessed, with results presented in Table 4.4, indicating that the gel fraction ranged between 81% and 85%. Notably, the incorporation of CMx into the hydrogel significantly improved the gel fraction of the HG, highlighting the impact of the inclusion complex on the hydrogel's properties.

**Table 4.4** Compositions, Gel fraction, Adhesiveness of Injectable Self-healing QCS/OPEC Hydrogels Containing Drug-β-CD Inclusion Complexes

| Sample name | QCS[1] (mL) | OPEC[2] (mL) | MTx (mg) | CMx (mg) | Gel fraction[3] (%) | Adhesiveness[3] (kPa) |
|---|---|---|---|---|---|---|
| HG | 0.6 | 0.4 | - | - | 80.5 ± 1.9 | 16.0 ± 1.2 |
| HG_MTx | 0.6 | 0.4 | 4.00 | - | 81.9 ± 0.9 | 20.3 ± 2.4* |
| HG_CMx | 0.6 | 0.4 | - | 4.00 | 85.2 ± 0.6* | 21.3 ± 0.3* |
| HG_MTx/ CMx | 0.6 | 0.4 | 2.00 | 2.00 | 83.2 ± 1.0 | 23.4± 1.2* |

**Note** * $p < 0.005$ compared with HG; 1. Concentration of QCS is 40 mg/mL; 2. Concentration of OPEC is 150 mg/mL; 3. n = 3.

## 4.12 Swelling and Mass Loss of Hydrogels Containing Drug-β-CD Inclusion Complexes

Swelling ratio and mass loss of the hydrogel samples were investigated by immersing the samples in PBS containing BSA, and the results are shown in Figure 4.13. The initial water content (equivalent to 1/AMF) of the hydrogels was in the range of 9.4 to 10.1. The swelling ratio was 11 after 1 and 2 days of immersion, which

represents a very modest increase, and after this time point, remained relatively constant after 4 and 6 days with some samples showing significant increased (Figure 4.13A). However, this was not in a regular pattern. Specifically, the swelling ratio of HG_CMx increased to 13 after 4 days of immersion (but had decreased by 6 days), and after 6 days of immersion, the swelling ratio of HG_MTx increased to 12. While HG_MTx/CMx showed not significant change. The mass loss of the hydrogels was likewise evaluated in PBS containing BSA, and the results are shown in Figure 4.11B. It can be seen that an increase in immersion time caused an increase in the mass loss of the hydrogels with significant increases for all hydrogels after 2 days. After 6 days, the mass loss was approximately 39% for all the hydrogel samples. It thus appears that the addition of the inclusion complexes has only minor effects, if at all, on gel fraction, swelling ratio, and mass loss of these hydrogels. All hydrogels will release a significant proportion of their components over 6 days, which is valuable as both QCS and OPEC have significant beneficial biological properties to support wound healing (Li et al., 2022).

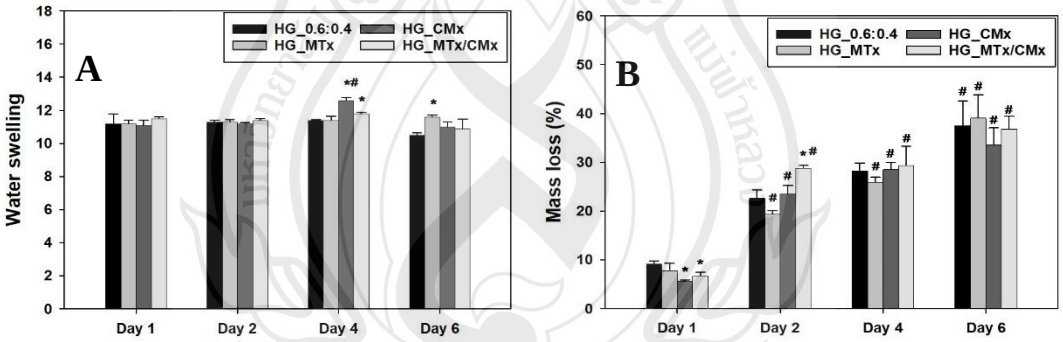


**Figure 4.13** A) Swelling Ratio and (B) Mass Loss of HG, HG_MTx, HG_CMx and HG_MTx/CMx (n = 3). $^{*}p < 0.05$ Compared with HG at Any Given Day (n = 3). $^{\#}p < 0.05$ Compared with Day 1 at Any Given Sample Type (n = 3)

## 4.13 Rheological Analysis of Hydrogels Containing Drug-β-CD Inclusion Complexes

The rheological analysis, conducted in duplicate, was used to confirm the formation of the hydrogels, with data from one run of each sample shown in Fig 4.14. The results indicated that the storage modulus (G') of all samples was higher than the loss modulus (G'') from the first timepoint, which occurred less than one minute after combining the precursor solutions, confirming that the gelation time for these hydrogels was under one minute. Throughout the entire measurement period of 400 seconds, the storage modulus remained consistently above the loss modulus, confirming the solid-like nature of the hydrogels. At 406 seconds, the storage moduli (G') for HG, HG_MTx, HG_CMx, and HG_MTx/CMx were measured at 360 ± 60, 430 ± 120, 440 ± 120, and 399 ± 106 Pa, respectively, with no significant differences between the samples based on measurement variability. The strain sweep analysis further evaluated the elastic response of the hydrogels under increasing oscillatory strain at a constant frequency, with the results also displayed in Figure 4.14. As the strain increased, the storage and loss modulus decreased until the crossover point (e.g. G' lower than G'') was reached and gel-sol transformation occurred. Subsequently, the hydrogels started to behave like fluids. From the results, the crossover points of HG, HG_MTx, HG_CMx, and HG_MTx/CMx were reached at 1410, 1520, 1507, and 1384% strain, respectively. These values are not considered significantly different, indicating a high integrity of the hydrogel networks (Kaolaor et al., 2019; Li et al., 2021).

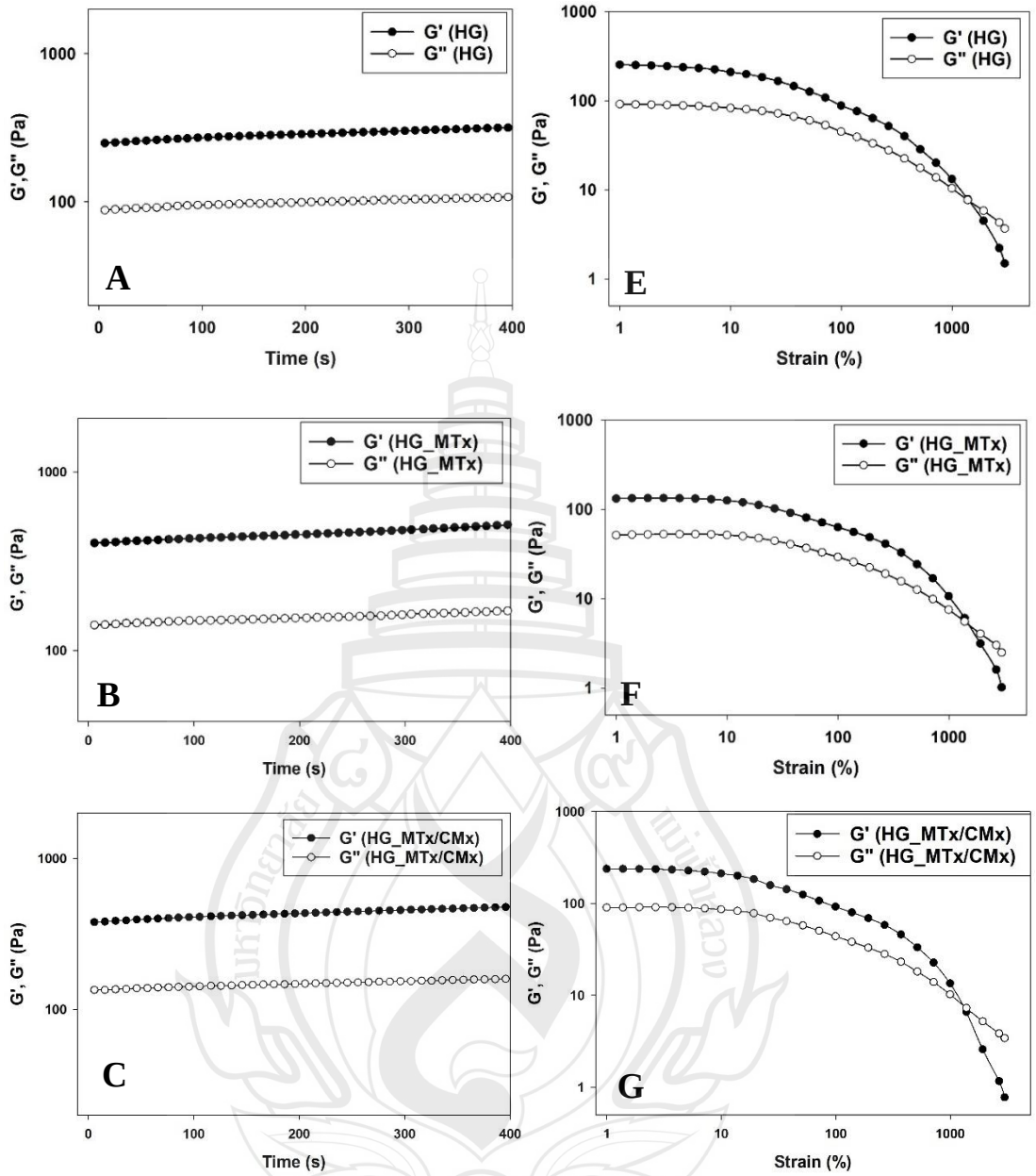


**Figure 4.14** Representative Data for Rheological Analysis of the HG (A and E), HG_MTx (B and F), HG_CMx (C and G), and HG_MTx/CMx (D and H) Samples. (A - D) Storage Modulus G’ and Loss Modulus G” Analysis During the Gelation Process (37 °C, Frequency 1.0 Hz, Strain: 1 %); (E - H) G’ and G” Strain Sweep (37 °C, Frequency 1.0 Hz)

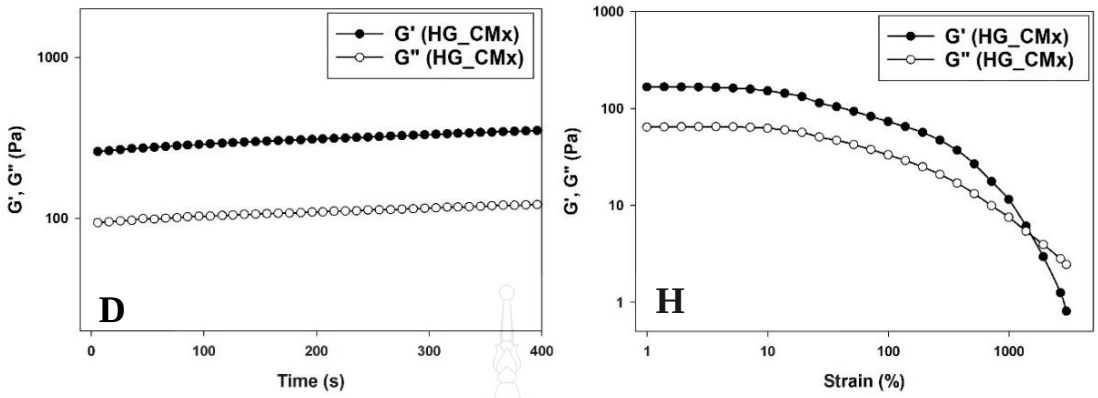


**Figure 4.14** (Continued)

## 4.14 Self-healing Analysis of Hydrogels Drug-β-CD Inclusion Complexes

For effective wound healing, a hydrogel should be capable of self-reforming after deformation caused by external mechanical forces. To assess the self-healing properties of hydrogels containing the inclusion complexes MTx and CMx on a macroscopic scale, the samples were evaluated as shown in Figure 4.15. Two disc-shaped hydrogels were prepared: one dyed and one undyed. Both were cut in half, and the halves were placed in contact with each other to observe self-healing. The self-healing time, defined as the duration required before the hydrogel could be picked up with forceps, was approximately 10 minutes for the control HG sample. In contrast, hydrogels containing inclusion complexes exhibited a self-healing time of around 20 minutes. Attempts to increase the loading of the inclusion complexes resulted in a significantly prolonged self-healing time, leading to the decision to limit the study to the compositions. The increased self-healing time of the hydrogels containing inclusion complexes indicates that their presence restricts the Schiff's base reaction and electrostatic interaction of OPEC and QCS and can be attributed to space occupied by the inclusion complexes hindering the polymer strands to diffuse rapidly into close proximity (Martinotti et al., 2020; Groult et al., 2021).

Based on the data obtained from the rheological analysis of the hydrogels (Figure 4.16), the self-healing properties were evaluated from G' and G" in continuous step strain measurements switching from a strain of 1 % and 3000 % with intervals of

100 s. When the first 1% strain was applied, G’ was higher than G”, indicating the gel stage of the hydrogels. When 3,000% strain was subsequently applied, the loss modulus G” became higher than the storage modulus G’, indicating hydrogel disassembly or collapse. Gel recovery after applying 1% strain was observed to occur over a period of time and was very similar for all hydrogel samples. Full recovery to the original values of the as-prepared hydrogels was, however, not observed.

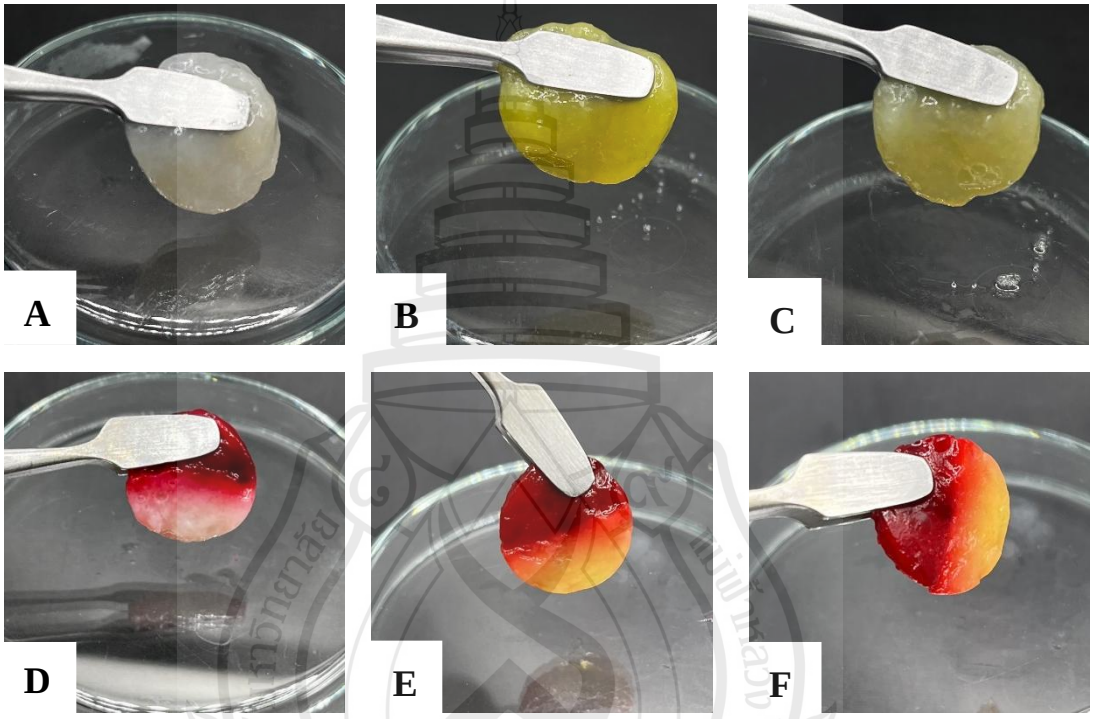


**Figure 4.15** Photographs of (A and D) HG_MTx, (B and E) HG_CMx, and (C and F) HG_MTx/CMx Before (Upper) and After (Lower) Self-Healing

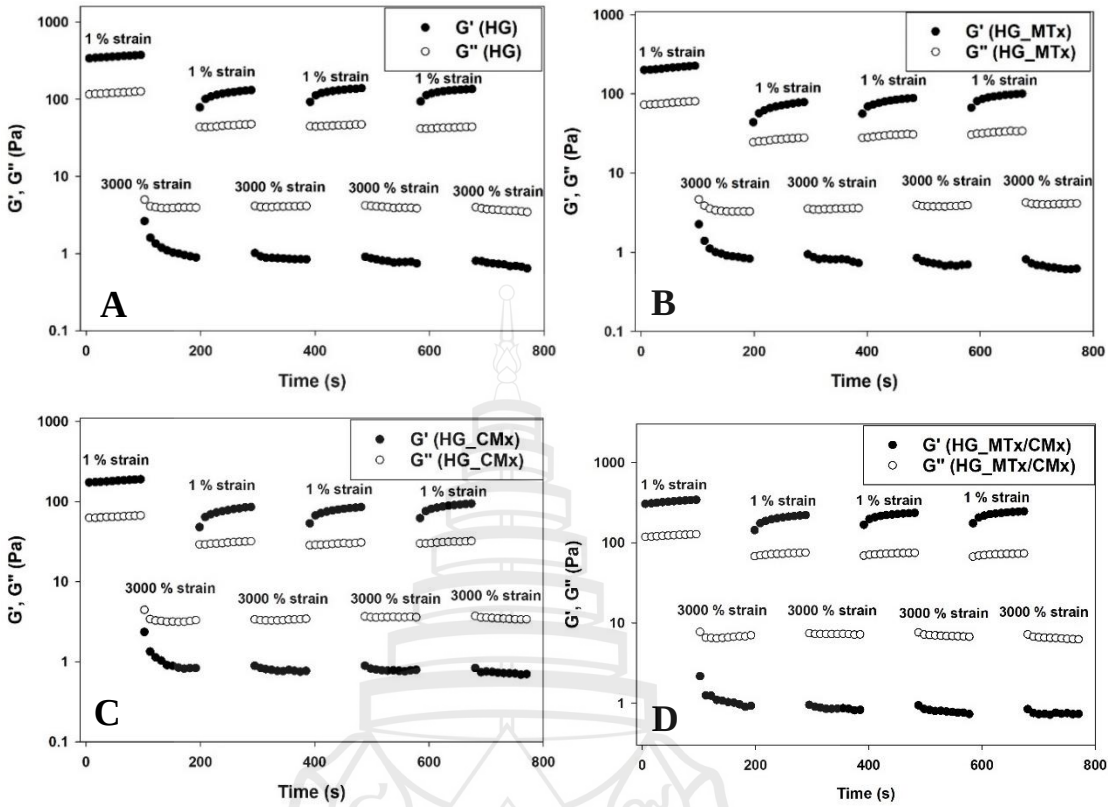


**Figure 4.16** Representative Data for Continuous Step Strain Analysis of (A) HG, (B) HG_MTx, (C) HG_CMx, and (D) HG_MTx/CMx. Low Strain of 1% and High Strain of 3000% were Applied with 100 s Intervals

## 4.15 Mechanical Properties and Adhesiveness of Hydrogels Containing Drug-β-CD Inclusion Complexes

Hydrogels used for wound dressing applications should have mechanical performance that allows them to withstand the physiological force caused by tissue movement. Therefore, the texture profile analysis in compression mode was used to evaluate the compressive strength, compressibility, and hardness of the hydrogels before and after healing, and the data are shown in Figure 4.17. For the as-prepared hydrogel samples, there was no significant change in compressibility upon addition of the inclusion complexes. However, a significant increase in the compressive strength and hardness of the HG_MTx sample was observed compared to the HG sample, while the HG_CMx and HG_MTx/CMx samples displayed higher values that were not

significantly different from the HG sample. This can be attributed to the higher solid content. After the samples were deformed by pressing with a tubular probe during analysis, the hydrogels were allowed to recover for 24 h before the compressibility, hardness, and compressive strength were measured as an indication of retainment of these properties after self-healing. It was found that the mechanical properties of all hydrogel samples decreased after self-healing, and in most cases, this was statistically significant. This phenomenon can be attributed to the formation of fewer reversible dynamic bonds after the self-healing process, leading to decreased mechanical strength (Lawrie et al., 2007) and this is in agreement with the observation made in the continuous step strain measurements (Figure 4.16). From these results, it can be concluded that the mechanical properties of the hydrogels were improved by adding the inclusion complexes. Inclusion complexes could act as a filler that physically reinforces the hydrogel matrix, improving its compressive strength (de Oliveira et al., 2021; May et al., 2023). While values decreased after self-healing, they were similar to that of the as-prepared HG sample.

Hydrogels used in wound healing should adhere to the wound site during the healing process and be easy to apply and remove without inducing trauma. The adhesiveness of the hydrogel samples was therefore studied using porcine skin as a model of mammalian skin. From the gold standard, the adhesiveness of commercial fibrin glue is 15 ± 3 kPa (Kim et al., 2022), and that of commercial hydrogel formations is 0.51 – 3.56 kPa (Aston et al., 2015). As skin is composed of collagen and elastin, the aldehyde groups of OPEC in the hydrogels may contribute to the adhesiveness through the Schiff's base reactions (Fernandez-Megia et al., 2005). From Table 4.2 the hydrogels showed adhesiveness values in the range of 16 to 23 kPa, indicating the ability to adhere to the skin. These hydrogels are designed to have good adhesion and flexibility, which are suitable properties for injectable self-healing hydrogels in wound dressing applications.

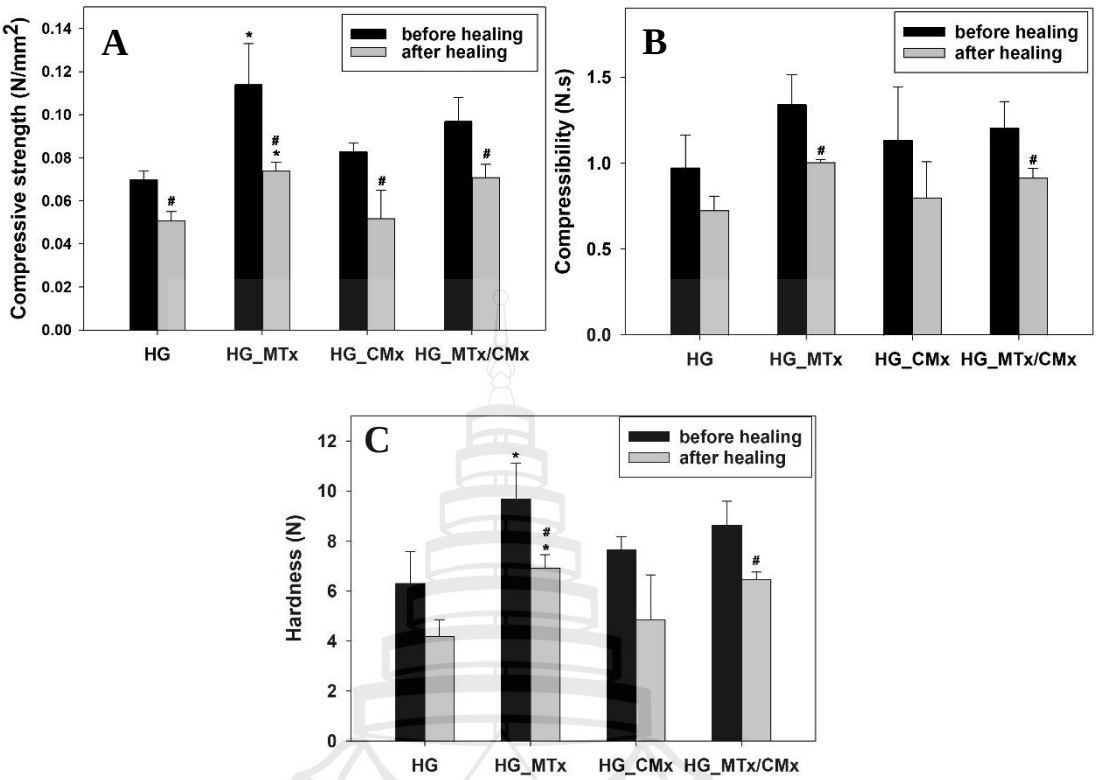


**Figure 4.17** (A) Compressive Strength, (B) Compressibility, and (C) Hardness of Hydrogel Samples Before and After Self-Healing (n = 3). $^{*}p < 0.05$ Compared with HG Before or After Healing. $^{\#}p < 0.05$ Compared with the Hydrogels Before Healing at Any Given Sample Type

## 4.16 Cytotoxicity

The cytotoxicity of MTx and CMx was assessed using MTT assay, with the results displayed in Figures 4.18A and B. It was found that the cell viability of MTx at 50 mg/mL and CMx at 2.5 mg/mL was higher than 70 %. Therefore, MTx and CMx were non-toxic to the cells at these concentrations, although it is noted that CMx showed 20 times higher toxicity than MTx. The indirect cytotoxicity of the HG, HG_MTx, HG_CMx, and HG_MTx/CMx samples was likewise evaluated by MTT assay, as shown in Figure 4.18C. From the results, these hydrogels showed more than 70% of cell viability, indicating they are non-toxic to NHDF cells.

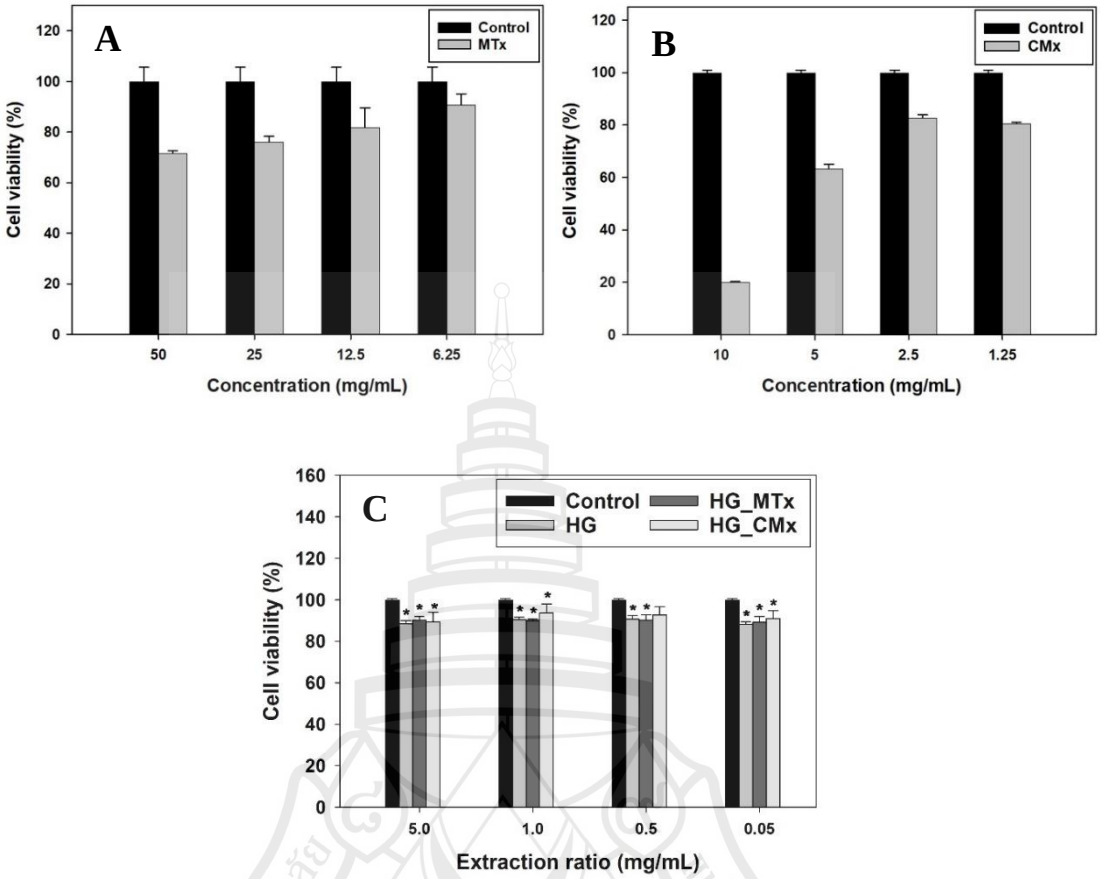


**Figure 4.18** Indirect Cytotoxicity of MTx (A), CMx (B), and HG, HG_MTx, and HG_CMx (C) (n=3). $^{*}p < 0.05$ Compared with HG at Any Given Extraction Ratio

## 4.17 Anti-Inflammatory Activity

In order to evaluate the amount of the inclusion complexes released at 24 h, relevant to the anti-inflammatory assay, UV-vis spectroscopy was used. Figure 4.19 shows the absorbance of the released solution from the HG, HG_MTx, HG_CMx, HG_MTx/CMx samples. It is clear that some OPEC and/or QCS were released into the solution when the absorbance spectrum resulting from the HG sample was compared to those of the pure OPEC and QCS solutions which were similar (see Figure 4.19C). It was therefore necessary to correct for this polymer absorbance when determining the amount of inclusion complexes released. It was found that the released amount of MTx and CMx from HG_MTx and HG_CMx was 12% and 9% (based on the actual amount

of inclusion complex in the hydrogels), respectively. Moreover, it was found that the released amount of MTx and CMx from HG_MTx/CMx was 0% and 0.82% (based on the actual amount of inclusion complex in the hydrogels), respectively.

Wound repair comprises an intricate series of overlapping phases, including inflammation, proliferation, and scar production/remodeling (Channasanon et al., 2007). The invasion of pathogens and tissue injury activates immune cells that produce inflammation mediators such as NO (Grasdalen et al., 1988). An excess level of NO subsequently results in delayed healing. The inclusion complexes were investigated for their anti-inflammatory activity, as shown in Table 4.5. The results demonstrated that $IC_{50}$ values for inhibiting NO production of MTx, CMx, and MTx/CMx were 0.7, 0.4, and 0.5 mg/mL, respectively, demonstrating better performance by CMx. Both inclusion complexes displayed $IC_{50}$ values well below their cytotoxicity levels. As a result, the inclusion complexes have a potential to be incorporated in the injectable self-healing hydrogels to support wound healing. In terms of the percent inhibition of NO production by the inclusion complexes, it can be seen from Figure 4.20A that at a concentration of 1.25 mg/mL, full inhibition was achieved. For lower concentrations, it was clear that CMx had a stronger inhibitory effect than MTx.

The anti-inflammatory activity of the hydrogels was also studied to confirm their efficiency in supporting wound healing. From Figure 4.20B, the results demonstrated at the highest extraction ratio (equivalent to 6.25 mg/mL dry mass), near complete inhibition of NO production could be achieved for the hydrogels containing the inclusion complexes, while the value for the HG sample was significantly lower. At some extraction ratios, there was, however, no significant difference. The $IC_{50}$ value for inhibition of NO production from the hydrogel extraction medium was in the range of 1.6 – 1.8 mg/mL dry mass equivalent. Considering the $IC_{50}$ values for both the inclusion complexes and the hydrogel samples, it can be seen that the components of the hydrogel itself have good inhibition of NO production with added benefit from the incorporation of the inclusion complexes.

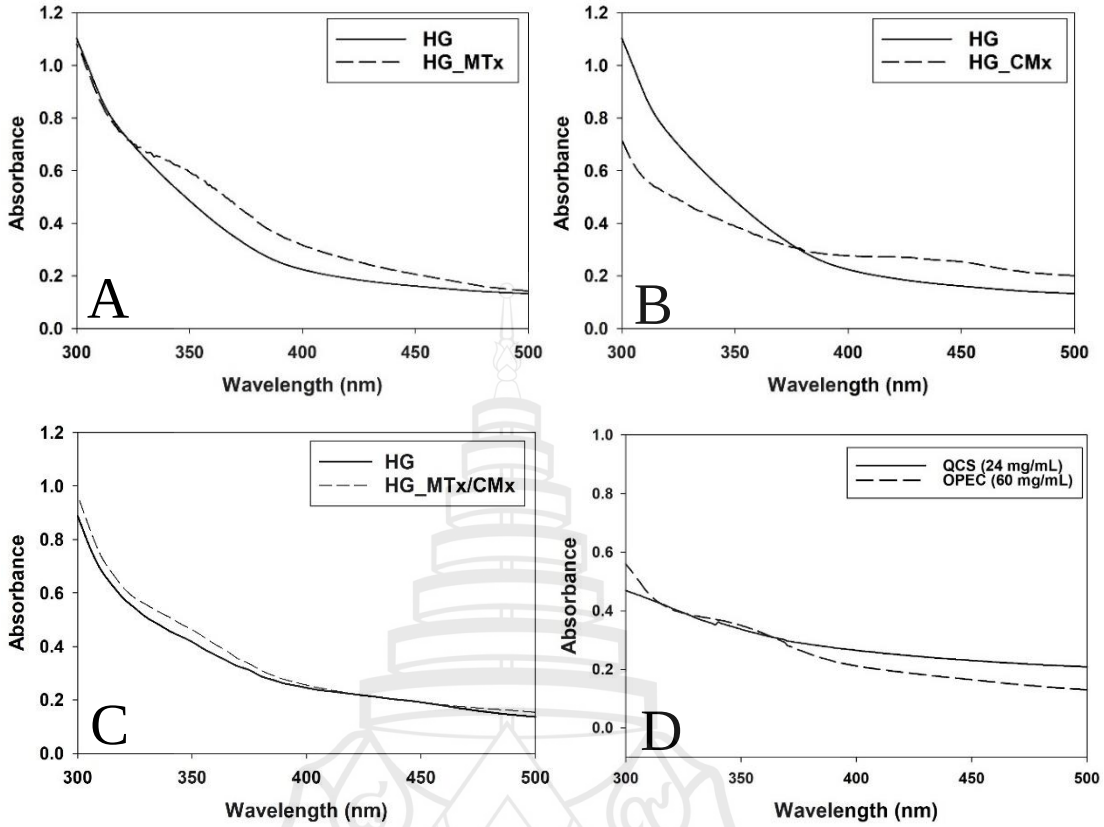


**Figure 4.19** UV Spectra of Extraction Media From HG, HG_MTx (A), HG_CMx (B), and HG_MTx/CMx. Extraction Media (500 mg/mL) of Hydrogels were Prepared in PBS for 24 h. (C) UV Spectra of QCS and OPEC Solutions

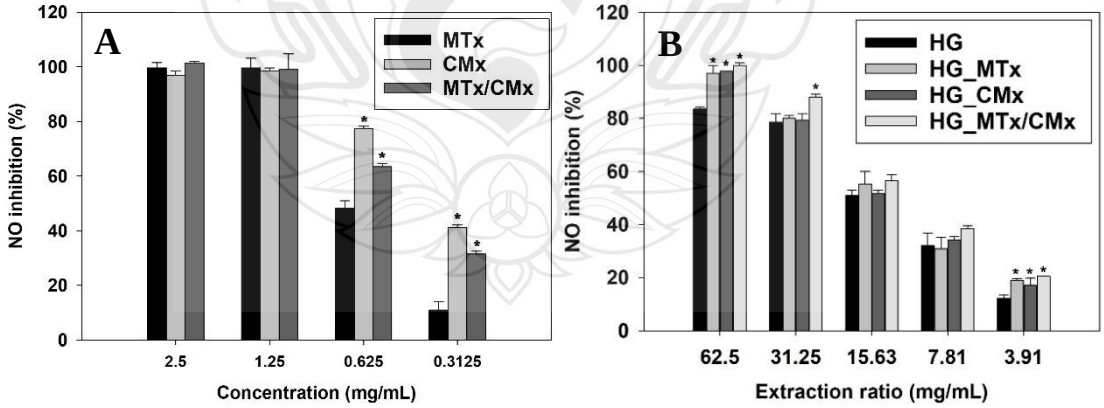


**Figure 4.20** (A) Anti-Inflammatory Activity of MTx, CMx, and MTx/CMx (n=3). $^{*}p < 0.05$ Compared with MTx at Any Given Concentration. (B) Anti-Inflammatory Activity of HG, HG_MTx, HG_CMx, and HG_MTx/CMx (n=3). $^{*}p < 0.05$ Compared with HG at Any Given Extraction Ratio

**Table 4.5** Antioxidant and Anti-Inflammatory Activities of MTx, CMx, and MTx/CMx (n=3).

| Sample | $IC_{50}$ (mg/mL) | |
|---|---|---|
| | **Antioxidant activity** | **Anti-inflammatory activity** |
| MTx | 3.794 ± 0.020 | 0.694 ± 0.019 |
| CMx | 2.482 ± 0.067 | 0.390 ± 0.004 |
| MTx/CMx | 3.143 ± 0.019 | 0.531 ± 0.014 |

## 4.18 Antioxidant Activity

Reactive oxygen species (ROS), including free radicals, are the key to oxidative stress, leading to cell damage and an inflammatory status (Balakrishnan et al., 2005). The excessive production of ROS prevents the transition from the inflammatory stage to the proliferative stage during wound healing, and as such, high levels of ROS delay wound healing (Nypelö et al., 2021)). Therefore, the inhibition of free radicals produced during oxidative stress in cells can accelerate the process of wound healing. This can be achieved by free radical inhibition by bioactive agents.

The antioxidant activity of MTx, CMx, MTx/CMx was evaluated using an $ABTS^{\bullet+}$ assay (Table 4.5). The $IC_{50}$ values were found to be 3.8, 2.5, and 3.14 mg/mL for MTx, CMx, and MTx/CMx, respectively. The antioxidant activity of the natural products MT and CM is attributed to the radical scavenging ability of the phenol groups in their structures that can donate a hydrogen atom with the resulting radical being resonance stabilized (Li et al., 2015). As such, they can neutralize endogenous radicals and prevent them from causing cellular damage. Previous studies have likewise found these natural products to have radical scavenging properties (Debeer et al., 2013; Ranamukhaarachchi et al., 2016). In terms of the percentage of antioxidant activity by the inclusion complexes, it can be seen from Figure 4.21A that at a high concentration of 10 mg/mL, high inhibition was achieved for CMx, while the effect from MTx and MTx/CMx was significantly lower, and a difference between the two types of inclusion complexes was also observed for lower concentrations.

The antioxidant activity of the hydrogel samples is shown in Figure 4.21B, represented as % activity. At the highest extraction ratio (50 mg/mL dry mass), near complete quenching of the $ABTS^{\bullet+}$ radicals were achieved by the hydrogels containing the inclusion complexes, which was significantly higher than the HG sample. At lower extraction ratios, only HG_CMx showed significantly higher antioxidant activity than the HG sample. These results were in agreement with that observed for the inclusion complexes (Table 4.5), where a higher activity was observed for CMx. As was observed for the study on inhibition of NO production in Section 3.7, it is clear that both components of the hydrogel and the inclusion complexes have the ability to quench $ABTS^{\bullet+}$ radicals.

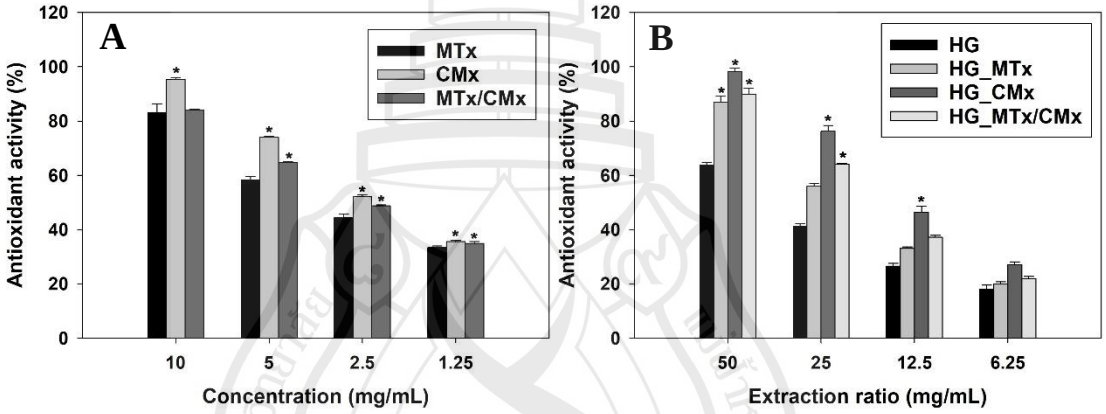


**Figure 4.21** (A) Antioxidant Activity of MTx, CMx, and MTx/CMx (n=3). $^{*}p < 0.05$ Compared with MTx at Any Given Concentration. (B) Antioxidant Activity of HG, HG_MTx, HG_CMx, and HG_MTx/CMx (n=3). $^{*}p < 0.05$ Compared with HG at Any Given Extraction Ratio

## 4.19 Antibacterial Activity

The duration of the wound healing process is directly related to the risk of bacterial infection, with longer healing times increasing the likelihood of infection. Previously, we assessed the antibacterial properties of the polymers QCS and OPEC, as well as the extraction media from the HG sample, against *E. coli* and *S. aureus* using a broth dilution assay. While QCS demonstrated good antibacterial activity, the HG sample alone did not show significant antibacterial effects. To enhance the antibacterial properties of the hydrogel samples, we investigated the potential of the inclusion

complexes MTx, CMx, and MTx/CMx to inhibit bacterial growth against *E. coli* and *S. aureus* using the same assay, with results summarized in Table 4.6. The minimum inhibitory concentration ($MIC_{50}$) values for MTx, CMx, MTx/CMx against *E. coli* were 12 mg/mL, 3 mg/mL, and greater than 100, respectively, although their minimum bactericidal concentration (MBC) values were both greater than 100 mg/mL. Against *S. aureus*, the $MIC_{50}$ values were 0.2 mg/mL for MTx, 50 mg/mL for CMx, and 1.5 mg/mL for MTx/CMx with MBC values of 3 mg/mL for MTx, greater than 100 mg/mL for CMx, and 3 mg/mL for MTx/CMx. These results indicate that while CMx exhibited slightly better antibacterial activity against the Gram-negative *E. coli*, MTx and MTx/CMx showed significantly higher activity against the Gram-positive *S. aureus*. Our previous findings demonstrated that QCS, in particular, possesses strong antibacterial effects against both bacterial strains. Therefore, incorporating both the inclusion complexes and QCS into the hydrogel formulations is expected to enhance their antibacterial efficacy, supporting better wound healing outcomes by reducing bacterial growth.

Antibacterial dressings are crucial in wound care as they limit bacterial colonization and prevent infections that can disrupt the healing process. These dressings act as barriers to block bacteria from entering the wound while preventing bacterial growth within the wound site. To evaluate the antibacterial efficacy of the hydrogel samples, we employed a colony counting method, which allows direct contact between the bacteria and the hydrogel, offering, a more accurate assessment compared to broth dilution assays that only test the extraction media from the hydrogel. The antibacterial activity of the hydrogels samples against *E. coli* (Gram-negative) and *S. aureus* (Gram-positive) was assessed using this method, and the percentage reduction in bacterial growth is shown in Figure 4.122. Against *E. coli*, bacterial reduction rates were 94%, 77%, 86%, and 83% for HG, HG_MTx, HG_CMx, and HG_MTx/CMx, respectively, with the HG sample showing significantly better bacterial inhibition. Gram-negative bacteria, like *E. coli*, have a negatively charged surface, allowing the quaternary ammonium groups of QCS to interact strongly, disrupt cell permeability, and ultimately cause bacterial cell death. This mechanism likely accounts for the high efficacy of the HG sample in reducing *E. coli* growth.

In contrast, against *S. aureus*, the bacterial reduction rates for HG, HG_MTx, HG_CMx, and HG_MTx/CMx were 76%, 88%, 86%, and 93%, respectively, demonstrating that the inclusion complexes significantly enhanced antibacterial activity compared to the HG alone. The enhanced effect against *S. aureus* can be attributed to the phenolic compounds MT and CM, which have been shown to inhibit bacterial growth by targeting the peptidoglycan layer of Gram-positive bacteria and penetrating bacterial cells. Overall, the injectable self-healing hydrogels containing drug-β-CD inclusion complexes can reduce bacterial growth of both *E. coli* and *S. aureus* by up to 80%, due to the complementary antibacterial properties of QCS and the inclusion complexes.

**Table 4.6** Antibacterial Activity of MTx, CMx, and MTx/CMx and Amoxicillin Against *E. coli* TISTR 527 and *S. aureus* TISTR 746 (n=3)

| **Sample** | ***E. coli* TISTR 527** | | ***S. aureus* TISTR 746** | |
|---|---|---|---|---|
| | **$MIC_{50}$ (mg/mL)** | **MBC (mg/mL)** | **$MIC_{50}$ (mg/mL)** | **MBC (mg/mL)** |
| MTx | 12.5 | > 100 | 0.20 | 3.13 |
| CMx | 3.13 | > 100 | 50 | > 100 |
| MTx/CMx | > 100 | > 100 | 1.56 | 3.13 |
| Amoxicillin | 0.004 | 0.015 | 0.001 | 0.390 |

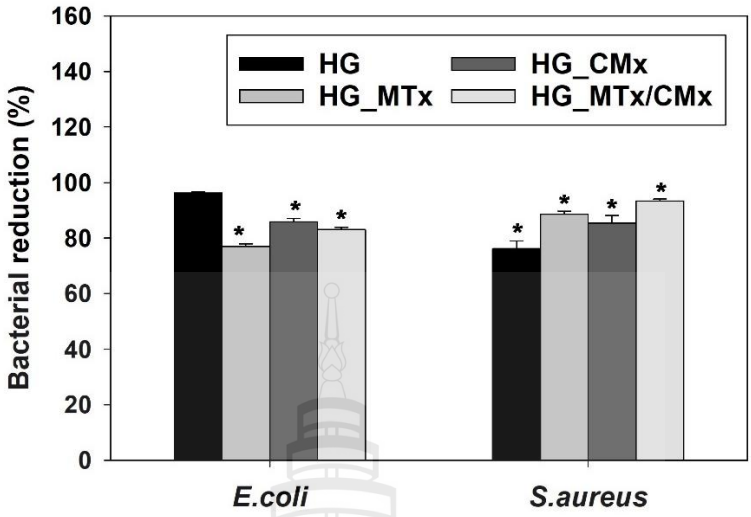


**Figure 4.22** Antibacterial Activity of HG, HG_MTx, HG_CMx, and HG_MTx/CMx (n=3). $^{*}p < 0.05$ Compared with HG at Any Given Extraction Ratio

## 4.20 *In Vitro* Wound Healing of Hydrogels Containing Drug-β-CD Inclusion Complexes

Wound healing in response to the extraction media from the HG, HG_MTx, and HG_CMx samples was conducted on NHDF cells. The cell migration was assessed using an *in vitro* scratch assay that relates to the healing process of the cells. The images of cells at the beginning and after 24 h are illustrated in Figure 4.23. The areas remaining after 24 h were evaluated to determine the percentage of wound closure. From the results, the wound closure of the HG, HG_MTx, HG_CMx, and HG_MTx/CMx samples was 82, 63, 51, and 41%, respectively, relative to the control sample that displayed a value of 47%. Adding MTx CMx, and MTx/CMx decreased cell migration compared to the hydrogel alone. Although the potential use of these drug-loaded hydrogels was reduced, the hydrogels could support wound healing better than the control.

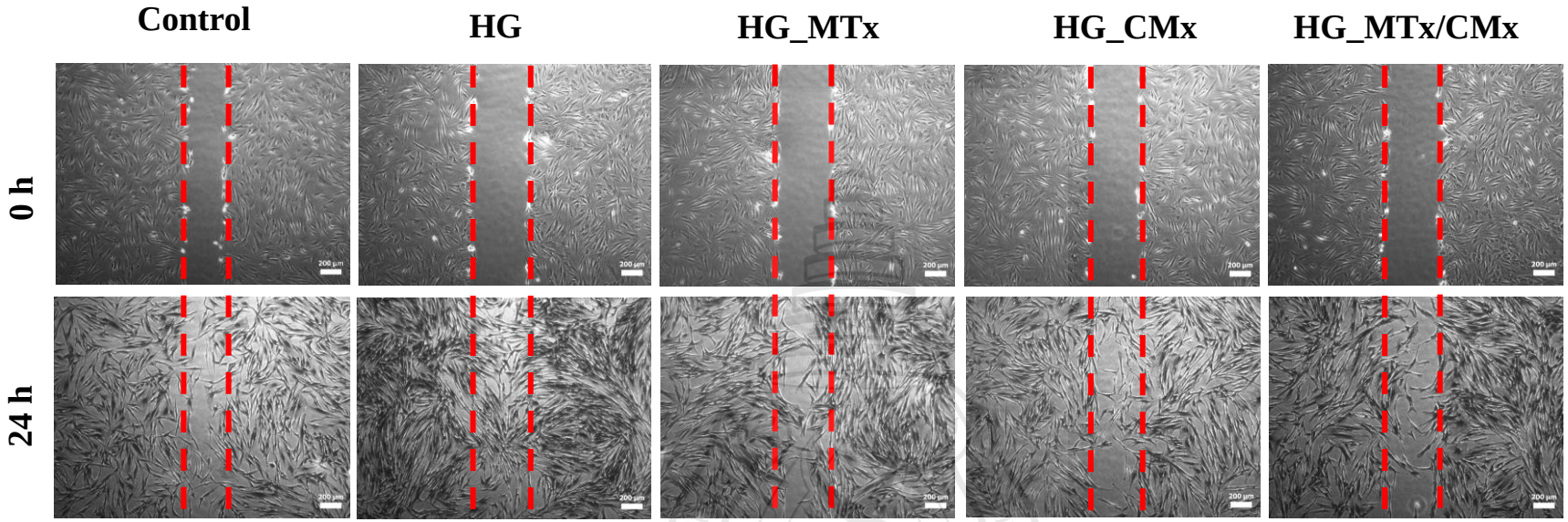


**Figure 4.23** Representative Light Microscope Images of *In Vitro* Scratch Wound Healing Assay at 0 and 24 h Using NHDF Cells (n=2)

# CHAPTER 5

# CONCLUSION

In this study, the chemical analysis of the polymers QCS and OPEC allowed for the evaluation of different functional group proportions, leading to the development of self-healing hydrogels through the co-injection of polymer solutions at specific concentrations and reagent ratios. Optimizing the QCS and OPEC ratios enhanced both Schiff's base reactions and ionic interactions, contributing to the self-healing properties. The hydrogel with a mole ratio of amino to aldehydes and quaternary ammonium to carboxylate groups closest to optimal (HG) exhibited promising mechanical properties, adhesiveness, solution stability, cytocompatibility, and wound closure capabilities. While QCS demonstrated antibacterial properties, it also had higher cytotoxicity than OPEC, necessitating careful balancing of polymer ratios for stability, achieved on the hydrogel formulation. Additionally, the MT- and CM-β-CD inclusion complexes (MTx and CMx) were successfully prepared to enhance the water solubility of these natural products. Their incorporation into the hydrogel increased macroscopic self-healing time without altering rheological properties. While the gel fraction significantly increased for HG_CMx, other properties, such as swelling ratio and mass loss remained consistent across samples. Some mechanical properties, including compressive strength and hardness, improved with inclusion complexes, although they maintained similar order magnitudes. In terms of biological activities, while CMx exhibited higher cytotoxicity, it also demonstrated better antioxidant and anti-inflammatory activities compared to MTx and MTx/CMx. Moreover, MTx/CMx showed higher antioxidant and anti-inflammatory activities than MTx due to the addition of CMx. In addition, HG_ MTx/CMx showed better anti-inflammatory compared with HG_MTx and HG_CMx. The inclusion complexes enhanced various biological activities of the hydrogels, supporting cell migration and promoting wound healing. Given the higher toxicity of CMx, the injectable self-healing hydrogel containing the MTx inclusion complex emerges as the most suitable candidate for wound dressing applications. In the future, studies on injectable self-healing hydrogel for wound healing should focus on comprehensive *in vivo* evaluation to validate their

therapeutic potential and safety, while the *in vitro* biological activities have demonstrated promising results, including antioxidant, anti-inflammatory, and antibacterial activities and cell migration. Moreover, long-term studies should evaluate the hydrogel's stability, degradation products, and potential immunogenicity to ensure its suitability for clinical application. On the other hand, scaling up the production of injectable self-healing hydrogel for wound healing is challenging. One of the key steps to ensure the transition from laboratory to commercial scale is process optimization to ensure a reproducible batch process and optimize reaction times, temperatures, and other parameters to maintain hydrogel properties at a large scale. Moreover, a suitable packaging design for the product should be considered to maintain the product's integrity during storage and transport.

# REFFERENCES

Abdel-Mohsen, A. M., Jancar, J., Massoud, D., Fohlerova, Z., Elhadidy, H., Spotz, Z., & Hebeish, A. (2016). Novel chitin/chitosan-glucan wound dressing: Isolation, characterization, antibacterial activity and wound healing properties. *International Journal of Pharmaceutics*, *510*(1), 86-99.

Ahmed, S., & Ikram, S. (2016). Chitosan based scaffolds and their applications in wound healing. *Achievements in the Life Scienc*es, *10*(1), 27–37. https://doi.org/ 10.1016/j.als.2016.04.001

Alexander, A., Khan, J., Saraf, S., & Saraf, S. (2013). Poly (ethylene glycol)–poly (lactic-co-glycolic acid) based thermosensitive injectable hydrogels for biomedical applications. *Journal of Controlled Release*, *172*(3), 715-729.

An, H., Bo, Y., Chen, D., Wang, Y., Wang, H., He, Y., & Qin, J. (2020). Cellulose-based self-healing hydrogel through boronic ester bonds with excellent biocompatibility and conductivity. *RSC Advances*, *10*(19), 11300-11310.

Anand, P., Thomas, S. G., Kunnumakkara, A. B., Sundaram, C., Harikumar, K. B., Sung, B., Aggarwal, B. B. (2008). Biological activities of curcumin and its analogues (Congeners) made by man and Mother Nature. *Biochemical Pharmacology*, *76*(11), 1590-1611.

Anjum, S., Arora, A., Alam, M. S., & Gupta, B. (2016). Development of antimicrobial and scar preventive chitosan hydrogel wound dressings. *International Journal of Pharmaceutics*, *508*(1-2), 92-101.

Aston, R., Wimalaratne, M., Brock, A., Lawrie, G., & Grøndahl, L. (2015). Interactions between chitosan and alginate dialdehyde biopolymers and their layer-by-layer assemblies. *Biomacromolecules*, *16*(6), 1807-1817.

Balakrishnan, B., Lesieur, S., Labarre, D., & Jayakrishnan, A. (2005). Periodate oxidation of sodium alginate in water and in ethanol–water mixture: a comparative study. *Carbohydrate Research*, *340*(7), 1425-1429.

Bebiano, L. B., Lourenço, B. N., Granja, P. L., & Pereira, R. F. (2024). Hydrogels as dynamic covalent networks for skin repair. *Hydrogels for Tissue Engineering and Regenerative Medicine* (pp. 605-624). Academic Press.

Bertsch, P., Diba, M., Mooney, D. J., & Leeuwenburgh, S. C. (2022). Self-healing injectable hydrogels for tissue regeneration. *Chemical Reviews*, *123*(2), 834-873.

Bi, H., Zhang, X., Wang, Q., Yong, Q., Xu, W., Xu, M., & Wang, X. (2023). Dynamic reversible disulfide bonds hydrogel of thiolated galactoglucomannan/cellulose nanofibril with self-healing property for protein release. *Industrial Crops and Products*, *206*, 117615.

Celebioglu, A., & Uyar, T. (2020). Fast-dissolving antioxidant curcumin/cyclodextrin inclusion complex electrospun nanofibrous webs. *Food Chemistry, 317*, 126397.

Chavan, T., & Muth, A. (2021). The diverse bioactivity of α-mangostin and its therapeutic implications. *Future Medicinal Chemistry, 13*(19), 1679-1694.

Chen, H., Cheng, J., Ran, L., Yu, K., Lu, B., Lan, G., & Lu, F. (2018). An injectable self-healing hydrogel with adhesive and antibacterial properties effectively promotes wound healing. *Carbohydrate Polymers, 201*, 522-531.

Chen, H., Cheng, R., Zhao, X., Zhang, Y., Tam, A., Yan, Y., & Deng, L. (2019). An injectable self-healing coordinative hydrogel with antibacterial and angiogenic properties for diabetic skin wound repair. *NPG Asia Materials, 11*(1), 3.

Chen, J., He, J., Yang, Y., Qiao, L., Hu, J., Zhang, J., & Guo, B. (2022). Antibacterial adhesive self-healing hydrogels to promote diabetic wound healing. *Acta Biomaterialia, 146*, 119-130.

Chen, M., Tian, J., Liu, Y., Cao, H., Li, R., Wang, J., & Zhang, Q. (2019). Dynamic covalent constructed self-healing hydrogel for sequential delivery of antibacterial agent and growth factor in wound healing. *Chemical Engineering Journal, 373*, 413-424.

Chin, C. Y., Jalil, J., Ng, P. Y., & Ng, S. F. (2018). Development and formulation of Moringa oleifera standardised leaf extract film dressing for wound healing application. *Journal of Ethnopharmacology, 212*, 188-199.

Cid-Samamed, A., Rakmai, J., Mejuto, J. C., Simal-Gandara, J., & Astray, G. (2022). Cyclodextrins inclusion complex: Preparation methods, analytical techniques and food industry applications. *Food Chemistry, 384*, 132467.

Cravotto, G., Binello, A., Baranelli, E., Carraro, P., & Trotta, F. (2006). Cyclodextrins as food additives and in food processing. *Current Nutrition & Food Science, 2*(4), 343-350.

de Andrade Neto, J. B., de Farias Cabral, V. P., Nogueira, L. F. B., da Silva, C. R., Sa, L. G. D. A. V., da Silva, A. R., & Júnior, H. V. N. (2021). Anti-MRSA activity of curcumin in planktonic cells and biofilms and determination of possible action mechanisms. *Microbial Pathogenesis, 155*, 104892.

de Oliveira, A. C., de Lima, G. R., Klein, R. S., Souza, P. R., Vilsinski, B. H., Garcia, F. P., & Martins, A. F. (2021). Thermo-and pH-responsive chitosan/gellan gum hydrogels incorporated with the β-cyclodextrin/curcumin inclusion complex for efficient curcumin delivery. *Reactive and Functional Polymers, 165*, 104955.

Debeer, S., Le Luduec, J. B., Kaiserlian, D., Laurent, P., Nicolas, J. F., Dubois, B., & Kanitakis, J. (2013). Comparative histology and immunohistochemistry of porcine versus human skin. *European Journal of Dermatology*, *23*(4), 456-466.

Del Olmo, J. A., Alonso, J. M., Sáez-Martínez, V., Benito-Cid, S., Moreno-Benítez, I., Bengoa-Larrauri, M., & Pérez-Álvarez, L. (2022). Self-healing, antibacterial and anti-inflammatory chitosan-PEG hydrogels for ulcerated skin wound healing and drug delivery. *Biomaterials Advances*, *139*, 212992.

Du, X., Liu, Y., Wang, X., Yan, H., Wang, L., Qu, L., & Wang, L. (2019). Injectable hydrogel composed of hydrophobically modified chitosan/oxidized-dextran for wound healing. *Materials Science and Engineering: C, 104*, 109930.

Fernandez-Megia, E., Novoa-Carballal, R., Quiñoá, E., & Riguera, R. (2005). Optimal routine conditions for the determination of the degree of acetylation of chitosan by 1H-NMR. *Carbohydrate Polymers*, *61*(2), 155-161.

Forni, C., D'Alessandro, F., Gallerani, P., Genco, R., Bolzon, A., Bombino, C., & Taddia, P. (2018). Effectiveness of using a new polyurethane foam multi-layer dressing in the sacral area to prevent the onset of pressure ulcer in the elderly with hip fractures: a pragmatic randomized controlled trial. *International Wound Journal, 15*(3), 383-390

Fui, L. W., Lok, M. P. W., Govindasamy, V., Yong, T. K., Lek, T. K., & Das, A. K. (2019). Understanding the multifaceted mechanisms of diabetic wound healing and therapeutic application of stem cells conditioned medium in the healing process. *Journal of Tissue Engineering and Regenerative Medicine, 13*(12), 2218-2233.

Wadhwa, G., Kumar, S., Chhabra, L., Mahant, S., & Rao, R. (2017) Essential oil–cyclodextrin complexes: An updated review. *Journal of Inclusion Phenomena and Macrocyclic Chemistry, 89*(1–2),3-58.

Gao, Y., Li, Z., Huang, J., Zhao, M., & Wu, J. (2020). In situ formation of injectable hydrogels for chronic wound healing. *Journal of Materials Chemistry B, 8*(38), 8768-8780.

Ghasemzadeh, A., Jaafar, H. Z., Baghdadi, A., & Tayebi-Meigooni, A. (2018). Alpha-mangostin-rich extracts from mangosteen pericarp: optimization of green extraction protocol and evaluation of biological activity. *Molecules, 23*(8), 1852.

Giusto, G., Vercelli, C., Comino, F., Caramello, V., Tursi, M., & Gandini, M. (2017). A new, easy-to-make pectin-honey hydrogel enhances wound healing in rats. *BMC Complementary and Alternative Medicine, 17*(1), 1-7.

Grasdalen, H., Bakøy, O. E., & Larsen, B. (1988). Determination of the degree of esterification and the distribution of methylated and free carboxyl groups in pectins by 1H-NMR spectroscopy. *Carbohydrate Research, 184*, 183-191.

Groult, S., Buwalda, S., & Budtova, T. (2021). Pectin hydrogels, aerogels, cryogels and xerogels: Influence of drying on structural and release properties. *European Polymer Journal, 149*, 110386.

Gupta, A., Briffa, S. M., Swingler, S., Gibson, H., Kannappan, V., Adamus, G., & Radecka, I. (2020). Synthesis of silver nanoparticles using curcumin-cyclodextrins loaded into bacterial cellulose-based hydrogels for wound dressing applications. *Biomacromolecules, 21*(5), 1802-1811.

Gupta, A., Keddie, D.J., Kannappan, V., Gibson, H., Khalil, I.R., Kowalczuk, M., & Radecka, I. (2019). Production and characterisation of bacterial cellulose hydrogels loaded with curcumin encapsulated in cyclodextrins as wound dressings. *Eur. Polym. J,118*, 437–450.

Gupta, B., Tummalapalli, M., Deopura, B. L., & Alam, M. S. (2014). Preparation and characterization of in-situ crosslinked pectin–gelatin hydrogels. *Carbohydrate polymers, 106*, 312-318.

Halim, A. S., Khoo, T. L., & Yussof, S. J. M. (2010). Biologic and synthetic skin substitutes: an overview. *Indian Journal of Plastic Surgery, 43*(S 01), S23-S28.

Han, G., & Ceilley, R. (2017). Chronic wound healing: a review of current management and treatments. *Advances in Therapy, 34*, 599-610.

Han, J., Ding, Q., Mei, C., Wu, Q., Yue, Y., & Xu, X. (2019). An intrinsically self-healing and biocompatible electroconductive hydrogel based on nanostructured nanocellulose-polyaniline complexes embedded in a viscoelastic polymer network towards flexible conductors and electrodes. *Electrochimica Acta, 318*, 660-672.

Hay, W. T., Behle, R. W., Fanta, G. F., Felker, F. C., Peterson, S. C., & Selling, G. W. (2017). Effect of spray drying on the properties of amylose-hexadecylammonium chloride inclusion complexes. *Carbohydrate Polymers, 157*, 1050-1056.

He, J., Zhang, Z., Yang, Y., Ren, F., Li, J., Zhu, S., & Chu, D. (2021). Injectable self-healing adhesive pH-responsive hydrogels accelerate gastric hemostasis and wound healing. *Nano-micro Letters, 13*, 1-17.

Horn, T. (2012). Wound dressings: Overview and classification. *Der Unfallchirurg, 115*, 774-782.

Hu, C., Zhang, F., Long, L., Kong, Q., Luo, R., & Wang, Y. (2020). Dual-responsive injectable hydrogels encapsulating drug-loaded micelles for on-demand antimicrobial activity and accelerated wound healing. *Journal of Controlled Release, 324*, 204-217.

Ishihara, M., Nakanishi, K., Ono, K., Sato, M., Kikuchi, M., Saito, Y., & Kurita, A. (2002). Photocrosslinkable chitosan as a dressing for wound occlusion and accelerator in healing process. *Biomaterials, 23*(3), 833-840.

Jiang, L., Yang, J., Wang, Q., Ren, L., & Zhou, J. (2019). Physicochemical properties of catechin/β-cyclodextrin inclusion complex obtained via co-precipitation. *CyTA-Journal of Food, 17*(1), 544-551.

Jiang, Q., Wang, J., Tang, R., Zhang, D., & Wang, X. (2016). Hypromellose succinate-crosslinked chitosan hydrogel films for potential wound dressing. *International Journal of Biological Macromolecules, 91*, 85-91.

Jing, Y., Ruan, L., Jiang, G., Nie, L., Shavandi, A., Sun, Y., & Zhu, J. (2023). Regenerated silk fibroin and alginate composite hydrogel dressings loaded with curcumin nanoparticles for bacterial-infected wound closure. *Biomaterials Advances, 149,* 213405.

Jug, M., Bećirević-Laćan, M., & Beæireviæ-laæan, M. (2008). Cyclodextrin-based pharmaceuticals. *Rad Hrvatske akademije znanosti i umjetnosti: Medicinske znanosti,* 9-26.

Kamar, S. S., Abdel-Kader, D. H., & Rashed, L. A. (2019). Beneficial effect of Curcumin Nanoparticles-Hydrogel on excisional skin wound healing in type-I diabetic rat: Histological and immunohistochemical studies. *Annals of Anatomy-Anatomischer Anzeiger, 222,* 94-102.

Kaolaor, A., Phunpee, S., Ruktanonchai, U. R., & Suwantong, O. (2019). Effects of β-cyclodextrin complexation of curcumin and quaternization of chitosan on the properties of the blend films for use as wound dressings. *Journal of Polymer Research, 26,* 1-12.

Kim, Y., Hu, Y., Jeong, J. P., & Jung, S. (2022). Injectable, self-healable and adhesive hydrogels using oxidized Succinoglycan/chitosan for pH-responsive drug delivery. *Carbohydrate Polymers, 284,* 119195.

Kirchner, P. H., Schramm, L., Ivanova, S., Shoyama, K., Würthner, F., & Beuerle, F. (2024). A water-stable boronate ester cage. *Journal of the American Chemical Society, 146*(8), 5305-5315.

Kiti, K., & Suwantong, O. (2020). Bilayer wound dressing based on sodium alginate incorporated with curcumin-β-cyclodextrin inclusion complex/chitosan hydrogel. *International Journal of Biological Macromolecules, 164,* 4113-4124.

Kloss, S., Zehetner, F., Dellantonio, A., Hamid, R., Ottner, F., Liedtke, V., Soja, G. (2012). Characterization of slow pyrolysis biochars: Effects of feedstocks and pyrolysis temperature on biochar properties. *Journal of Environmental Quality, 41*(4), 990-1000.

Kozen, B. G., Kircher, S. J., Henao, J., Godinez, F. S., & Johnson, A. S. (2008). An alternative hemostatic dressing: Comparison of CELOX, HemCon, and QuikClot. *Academic Emergency Medicine, 15*(1), 74–81. https://doi.org/10.1111/j.1553-2712.2007.00009.x

Lavanya, K., Chandran, S. V., Balagangadharan, K., & Selvamurugan, N. J. M. S. (2020). Temperature-and pH-responsive chitosan-based injectable hydrogels for bone tissue engineering. *Materials Science and Engineering: C, 111*, 110862.

Lawrie, G., Keen, I., Drew, B., Chandler-Temple, A., Rintoul, L., Fredericks, P., & Grøndahl, L. (2007). Interactions between alginate and chitosan biopolymers characterized using FTIR and XPS. *Biomacromolecules, 8*(8), 2533-2541.

Li, D. Q., Li, J., Dong, H. L., Li, X., Zhang, J. Q., Ramaswamy, S., & Xu, F. (2021). Pectin in biomedical and drug delivery applications: A review. *International journal of biological macromolecules, 185*, 49-65.

Li, H., Cheng, F., Wei, X., Yi, X., Tang, S., Wang, Z., & Huang, Y. (2021). Injectable, self-healing, antibacterial, and hemostatic N, O-carboxymethyl chitosan/oxidized chondroitin sulfate composite hydrogel for wound dressing. *Materials Science and Engineering: C, 118*, 111324.

Li, L., Yan, B., Yang, J., Chen, L., & Zeng, H. (2015). Novel mussel-inspired injectable self-healing hydrogel with anti-biofouling property. *Advanced Materials (Deerfield Beach, Fla.), 27*(7), 1294-1299.

Li, S., Pei, M., Wan, T., Yang, H., Gu, S., Tao, Y., & Xiao, P. (2020). Self-healing hyaluronic acid hydrogels based on dynamic Schiff base linkages as biomaterials. *Carbohydrate Polymers, 250*, 116922.

Li, X., Fan, R., Tong, A., Yang, M., Deng, J., Zhou, L., & Guo, G. (2015). In situ gel-forming AP-57 peptide delivery system for cutaneous wound healing. *International Journal of Pharmaceutics, 495*(1), 560-571.

Li, Y., Wang, X., Fu, Y. N., Wei, Y., Zhao, L., & Tao, L. (2018). Self-adapting hydrogel to improve the therapeutic effect in wound-healing. *ACS Applied Materials & Interfaces, 10*(31), 26046-26055.

Li, Z., Chen, S., Gu, Z., Chen, J., & Wu, J. (2014). Alpha-cyclodextrin: Enzymatic production and food applications. *Trends in Food Science & Technology, 35*(2), 151-160.

Liang, Y., Zhao, X., Hu, T., Chen, B., Yin, Z., Ma, P. X., & Guo, B. (2019). Adhesive hemostatic conducting injectable composite hydrogels with sustained drug release and photothermal antibacterial activity to promote full-thickness skin regeneration during wound healing. *Small, 15*(12), 1900046.

Liu, X., Niu, Y., Chen, K. C., & Chen, S. (2017). Rapid hemostatic and mild polyurethane-urea foam wound dressing for promoting wound healing. *Materials Science and Engineering: C, 71*, 289-297.

Liu, Y., & Hsu, S. H. (2018). Synthesis and biomedical applications of self-healing hydrogels. *Frontiers in Chemistry, 6*, 449.

Loftsson, T., & Brewster, M. E. (2010). Pharmaceutical applications of cyclodextrins: basic science and product development. *Journal of Pharmacy and Pharmacology, 62*(11), 1607-1621.

Ma, Z., Song, W., He, Y., & Li, H. (2020). Multilayer injectable hydrogel system sequentially delivers bioactive substances for each wound healing stage. *ACS Applied Materials & Interfaces, 12*(26), 29787-29806.

Mahabusarakam, W., Wiriyachitra, P., & Taylor, W. C. (1987). Chemical constituents of Garcinia mangostana. *Journal of Natural Products, 50*(3), 474-478.

Martinotti, S., & Ranzato, E. (2020). Scratch wound healing assay. *Epidermal Cells: Methods and Protocols* (pp. 225-229). https://doi.org/10.1007/7651_2019_259

May, M. N., Sugawara, A., Asoh, T. A., Takashima, Y., Harada, A., & Uyama, H. (2023). Composite hydrogels with host–guest interaction using cellulose nanocrystal as supramolecular filler. *Polymer, 277*, 125979.

Metcalfe, A. D., & Ferguson, M. W. (2007). Tissue engineering of replacement skin: the crossroads of biomaterials, wound healing, embryonic development, stem cells and regeneration. *Journal of the Royal Society Interface, 4*(14), 413-437.

Mohan, P. K., Sreelakshmi, G., Muraleedharan, C. V., & Joseph, R. (2012). Water soluble complexes of curcumin with cyclodextrins: Characterization by FT-Raman spectroscopy. *Vibrational Spectroscopy, 62*, 77-84.

Moongkarndi, P., Jaisupa, N., Samer, J., Kosem, N., Konlata, J., Rodpai, E., & Pongpan, N. (2014). Comparison of the biological activity of two different isolates from mangosteen. *Journal of Pharmacy and Pharmacology, 66*(8), 1171-1179.

Moongkarndi, P., Kosem, N., Kaslungka, S., Luanratana, O., Pongpan, N., & Neungton, N. (2004). Antiproliferation, antioxidation and induction of apoptosis by Garcinia mangostana (mangosteen) on SKBR3 human breast cancer cell line. *Journal of Ethnopharmacology, 90*(1), 161-166.

Murakami, K., Aoki, H., Nakamura, S., Nakamura, S. I., Takikawa, M., Hanzawa, M., .& Ishihara, M. (2010). Hydrogel blends of chitin/chitosan, fucoidan and alginate as healing-impaired wound dressings. *Biomaterials, 31*(1), 83-90.

Nypelö, T., Berke, B., Spirk, S., & Sirviö, J. A. (2021). Periodate oxidation of wood polysaccharides—Modulation of hierarchies. *Carbohydrate Polymers, 252*, 117105.

Obolskiy, D., Pischel, I., Siriwatanametanon, N., & Heinrich, M. (2009). Garcinia mangostana L.: a phytochemical and pharmacological review. *Phytotherapy Research: An International Journal Devoted to Pharmacological and Toxicological Evaluation of Natural Product Derivatives, 23*(8), 1047-1065.

Ou, Y., & Tian, M. (2021). Advances in multifunctional chitosan-based self-healing hydrogels for biomedical applications. *Journal of Materials Chemistry B, 9*(38), 7955-7971.

Pan, H., Fan, D., Cao, W., Zhu, C., Duan, Z., Fu, R., & Ma, X. (2017). Preparation and characterization of breathable hemostatic hydrogel dressings and determination of their effects on full-thickness defects. *Polymers, 9*(12), 727.

Qu, J., Zhao, X., Liang, Y., Zhang, T., Ma, P. X., & Guo, B. (2018). Antibacterial adhesive injectable hydrogels with rapid self-healing, extensibility and compressibility as wound dressing for joints skin wound healing. *Biomaterials, 183*, 185-199.

Raafat, D., von Bargen, K., Haas, A., & Sahl, H.-G. (2008). Insights into the mode of action of chitosan as an antibacterial compound. *Applied and Environmental Microbiology, 74*(23), 7455–7455. https://doi.org/10.1128/aem.02290-08

Rahmani, A. H., Aldebasi, Y. H., Srikar, S., Khan, A. A., & Aly, S. M. (2015). Aloe vera: Potential candidate in health management via modulation of biological activities. *Pharmacognosy Reviews*, *9*(18), 120.

Ranamukhaarachchi, S. A., Lehnert, S., Ranamukhaarachchi, S. L., Sprenger, L., Schneider, T., Mansoor, I., & Stoeber, B. (2016). A micromechanical comparison of human and porcine skin before and after preservation by freezing for medical device development. *Scientific Reports*, *6*(1), 32074.

Rezvanian, M., Ahmad, N., Amin, M. C. I. M., & Ng, S. F. (2017). Optimization, characterization, and in vitro assessment of alginate-pectin ionic cross-linked hydrogel film for wound dressing applications. *International Journal of Biological Macromolecules*, *97*, 131-140.

Rivera, A. E., & Spencer, J. M. (2007). Clinical aspects of full-thickness wound healing. *Clinics in Dermatology*, *25*(1), 39-48.

Shan-Yang, L., & Yuh-Horng, K. (1989). Solid particulates of drug-β-cyclodextrin inclusion complexes directly prepared by a spray-drying technique. *International Journal of Pharmaceutics*, *56*(3), 249-259.

Sharahi, J. Y., Ahovan, Z. A., Maleki, D. T., Rad, Z. R., Rad, Z. R., Goudarzi, M., & Hashemi, A. (2020). In vitro antibacterial activity of curcumin-meropenem combination against extensively drug-resistant (XDR) bacteria isolated from burn wound infections. *Avicenna Journal of Phytomedicine*, *10*(1), 3.

Sharma, S., Kumar, A., Kumar, R., Rana, N. K., & Koch, B. (2018). Development of a novel chitosan based biocompatible and self-healing hydrogel for controlled release of hydrophilic drug. *International Journal of Biological Macromolecules*, *116*, 37-44.

Shefa, A.A., Sultana, T., Park, M.K., Lee, S.Y., Gwon, J., & Lee, B. (2020). Curcumin incorporation into an oxidized cellulose nanofiber-polyvinyl alcohol hydrogel system promotes wound healing. *Mater. Des*, *186*, 108313.

StatistaMarketInsights. (2024). *Wound care – Thailand.* https://www.statista.com/outlook/hmo/otc-pharmaceuticals/wound-care/thailand.

Sun, C., Jia, H., Lei, K., Zhu, D., Gao, Y., Zheng, Z., & Wang, X. (2019). Self-healing hydrogels with stimuli responsiveness based on acylhydrazone bonds. *Polymer, 160*, 246-253.

Sung, K. Y., & Lee, S. Y. (2016). Nonoperative Management of Extravasation Injuries Associated with Neonatal Parenteral Nutrition Using Multiple Punctures and a Hydrocolloid Dressing. *Wounds: A Compendium of Clinical Research and Practice, 28*(5), 145-151.

Szejtli, J. (1998). Introduction and general overview of cyclodextrin chemistry. *Chemical Reviews, 98*(5), 1743-1754

Tanaka, A., Nagate, T., & Matsuda, H. (2005). Acceleration of wound healing by gelatin film dressings with epidermal growth factor. *Journal of Veterinary Medical Science, 67*(9), 909-913.

Toohey, K. S., Sottos, N. R., Lewis, J. A., Moore, J. S., & White, S. R. (2007). Self-healing materials with microvascular networks. *Nature Materials, 6*(8), 581-585.

Trigo-Gutierrez, J. K., Vega-Chacón, Y., Soares, A. B., & Mima, E. G. de O. (2021). Antimicrobial activity of curcumin in nanoformulations: A comprehensive review. *International Journal of Molecular Sciences, 22*(13), 7130. https://doi.org/10.3390/ijms22137130.

Urciuolo, F., Casale, C., Imparato, G., & Netti, P. A. (2019). Bioengineered skin substitutes: the role of extracellular matrix and vascularization in the healing of deep wounds. *Journal of Clinical Medicine, 8*(12), 2083.

Velnar, T., Bailey, T., & Smrkolj, V. (2009). The wound healing process: an overview of the cellular and molecular mechanisms. *Journal of International Medical Research, 37*(5), 1528-1542.

Vowden, K., & Vowden, P. (2017). Wound dressings: principles and practice. *Surgery (Oxford), 35*(9), 489-494.

Wan, Z., He, J., Yang, Y., Chong, T., Wang, J., Guo, B., & Xue, L. (2022). Injectable adhesive self-healing biocompatible hydrogel for haemostasis, wound healing, and postoperative tissue adhesion prevention in nephron-sparing surgery. *Acta Biomaterialia, 152*, 157-170.

Wang, J., & Windbergs, M. (2017). Functional electrospun fibers for the treatment of human skin wounds. *European Journal of Pharmaceutics and Biopharmaceutics, 119,* 283–299. https://doi.org/10.1016/j.ejpb.2017.07.001.

Wang, X., Xu, P., Yao, Z., Fang, Q., Feng, L., Guo, R., & Cheng, B. (2019). Preparation of antimicrobial hyaluronic acid/quaternized chitosan hydrogels for the promotion of seawater-immersion wound healing. *Frontiers in Bioengineering and Biotechnology, 7,* 360.

Wathoni, N., Sari, D. P., Suharyani, I., Motoyama, K., Mohammed, A. F. A., Cahyanto, A., Muchtaridi, M. (2020). Enhancement of α-Mangostin wound healing ability by complexation with 2-hydroxypropyl-β-cyclodextrin in hydrogel formulation. *Pharmaceuticals, 13*(10), 290.

Wei, L., Tan, J., Li, L., Wang, H., Liu, S., Chen, J., & Liu, T. (2022). Chitosan/alginate hydrogel dressing loaded FGF/VE-cadherin to accelerate full-thickness skin regeneration and more normal skin repairs. *International Journal of Molecular Sciences, 23*(3), 1249.

Xiao, G., Wang, Y., Zhang, H., Chen, L., & Fu, S. (2019). Facile strategy to construct a self-healing and biocompatible cellulose nanocomposite hydrogel via reversible acylhydrazone. *Carbohydrate Polymers, 218,* 68-77.

Xue, H., Hu, L., Xiong, Y., Zhu, X., Wei, C., Cao, F., & Liu, G. (2019). Quaternized chitosan-Matrigel-polyacrylamide hydrogels as wound dressing for wound repair and regeneration. *Carbohydrate Polymers, 226,* 115302.

Yang, B., Song, J., Jiang, Y., Li, M., Wei, J., Qin, J., & Gu, Z. (2020). Injectable adhesive self-healing multicross-linked double-network hydrogel facilitates full-thickness skin wound healing. *ACS Applied Materials & Interfaces, 12*(52), 57782-57797.

Yang, R., Li, P., Li, N., Zhang, Q., Bai, X., Wang, L., & Yan, J. (2017). Xanthones from the pericarp of Garcinia mangostana. *Molecules, 22*(5), 683.

Yu, H., Xiao, Q., Qi, G., Chen, F., Tu, B., Zhang, S., & Duan, P. (2022). A hydrogen bonds-crosslinked hydrogels with self-healing and adhesive properties for hemostatic. *Frontiers in Bioengineering and Biotechnology, 10,* 855013.

Yuan, Y., Shen, S., & Fan, D. (2021). A physicochemical double cross-linked multifunctional hydrogel for dynamic burn wound healing: shape adaptability, injectable self-healing property and enhanced adhesion. *Biomaterials, 276*, 120838.

Zhang, S., Ding, S., Yu, J., Chen, X., Lei, Q., & Fang, W. (2015). Antibacterial activity, in vitro cytotoxicity, and cell cycle arrest of gemini quaternary ammonium surfactants. *Langmuir, 31*(44), 12161-12169

Zhang, W., Qi, X., Zhao, Y., Liu, Y., Xu, L., Song, X., & Hou, M. (2020). Study of injectable Blueberry anthocyanins-loaded hydrogel for promoting full-thickness wound healing. *International Journal of Pharmaceutics, 586*, 119543.

Zhang, Z. X., Liow, S. S., Xue, K., Zhang, X., Li, Z., & Loh, X. J. (2019). Autonomous chitosan-based self-healing hydrogel formed through noncovalent interactions. *ACS Applied Polymer Materials, 1*(7), 1769-1777.

Zhang, Z., Bu, J., Li, B., Xuan, H., Jin, Y., & Yuan, H. (2022). Dynamic double cross-linked self-healing polysaccharide hydrogel wound dressing based on schiff base and thiol-alkynone reactions. *International Journal of Molecular Sciences, 23*(22), 13817.

Zhao, N., & Yuan, W. (2022). Highly adhesive and dual-crosslinking hydrogel via one-pot self-initiated polymerization for efficient antibacterial, antifouling and full-thickness wound healing. *Composites Part B: Engineering, 230*, 109525.

Zhao, X., Wu, H., Guo, B., Dong, R., Qiu, Y., & Ma, P. X. (2017). Antibacterial anti-oxidant electroactive injectable hydrogel as self-healing wound dressing with hemostasis and adhesiveness for cutaneous wound healing. *Biomaterials, 122*, 34-47.

Zhou, L., Dai, C., Fan, L., Jiang, Y., Liu, C., Zhou, Z., & Tan, G. (2021). Injectable self-healing natural biopolymer-based hydrogel adhesive with thermoresponsive reversible adhesion for minimally invasive surgery. *Advanced Functional Materials, 31*(14), 2007457.

Zhu, D. Y., Chen, Z. P., Hong, Z. P., Zhang, L., Liang, X., Li, Y., & Guo, J. (2022). Injectable thermo-sensitive and wide-crack self-healing hydrogel loaded with antibacterial anti-inflammatory dipotassium glycyrrhizate for full-thickness skin wound repair. *Acta Biomaterialia, 143*, 203-215

# APPENDIX A

# PHYSIOCHEMICAL AND IN VITRO BIOLOGICAL EVALUATION OF AN INJECTABLE SELF-HEALING QUATERNIZED CHITOSAN/ OXIDIZED PECTIN HYDROGEL FOR POTENTIAL USE AS A WOUND DRESSING MATERIAL

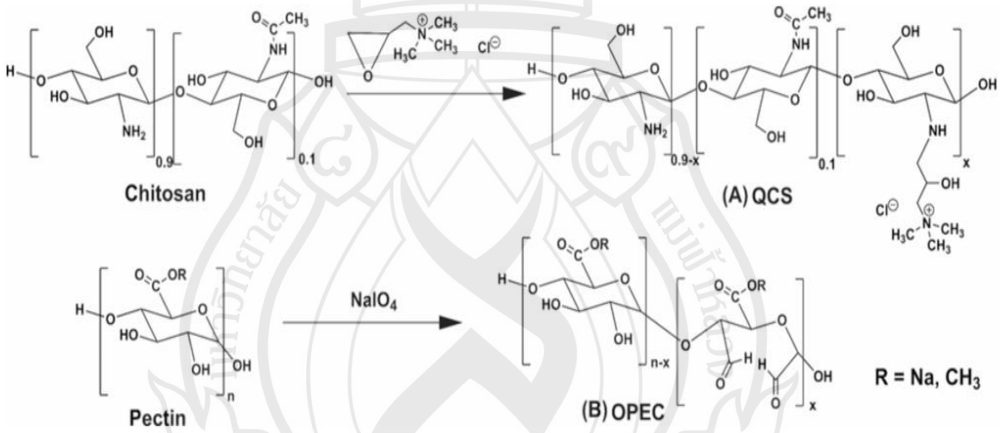


**Figure A1** Reaction Schemes for the Synthesis of (A) QCS (x Refers to The Degree of Quaternization) and (B) OPEC (x Refers to The Degree of Oxidation)

**Table A1** Preparation of α-Mangostin Inclusion Complexes and Antioxidant Activity using DPPH Assay

| **Name** | **MT (g)** | **CD (g)** | **Solvent** | **Sonicate** | **Filtration** | **Dry method** | **Antioxidant activity ($IC_{50}$)** |
|---|---|---|---|---|---|---|---|
| MTx | 1.62 | 0.5 | Methanol and distilled water | 15 min | 0.45 µm cellulose acetate syringe | Evaporate with rotary evaporator (65 rpm, 70 °C) | 3.23 |
| MTx-DI | 1.62 | 0.5 | Distilled water | No | 0.45 µm cellulose acetate syringe | Freeze-drying | 7.98 |
| MTx-NS | 1.62 | 0.5 | Methanol and distilled water | No | 0.45 µm cellulose acetate syringe | Evaporate with rotary evaporator (65 rpm, 70 °C) and freeze-dry | 8.75 |

**Table A2** Preparation of Injectable Self-Healing Hydrogels Containing α-Mangostin Inclusion Complexes

| Name | QCS (mL) | OPEC (mL) | MTx (mg) | CMx (mg) | Gelation (min) | Self-healing (min) |
|---|---|---|---|---|---|---|
| HG | 0.6 | 0.4 | - | - | 1 | 10 |
| HG_MTx2 | 0.6 | 0.4 | 2 | | 1 | 20 |
| HG_MTx4 | 0.6 | 0.4 | 4 | | 1 | 20 |
| HG_MTx6 | 0.6 | 0.4 | 6 | | 1 | 30 |
| HG_CMx2 | 0.6 | 0.4 | - | 2 | 1 | 20 |
| HG_CMx4 | 0.6 | 0.4 | - | 4 | 1 | 20 |
| HG_CMx6 | 0.6 | 0.4 | - | 6 | 1 | 30 |
| HG_MTx/CMx2 | 0.6 | 0.4 | 1 | 1 | 1 | 20 |
| HG_MTx/CMx4 | 0.6 | 0.4 | 2 | 2 | 1 | 20 |
| HG_MTx/CMx6 | 0.6 | 0.4 | 3 | 3 | 1 | 30 |

# CURRICULUM VITAE

**NAME** Mueanchan Chanmontri

**EDUCATIONAL BACKGROUND**

2020 Bachelor of Science
Applied Chemistry
Mae Fah Luang University, Thailand

**INTERNSHIP EXPERIENCE**

2019 National Nanotechnology Center (NANOTEC), National Science and Technology Development Agency (NSTDA)

**WORK EXPERIENCE**

2020-2022 Teaching Assistance in Principles of Chemistry
Mae Fah Luang University

**SCHOLARSHIP**

2020 Post-Graduate Tuition Scholarship (MFU-2021)

**PUBLICATION**

Chanmontri, M., Swilem, A. E., Mutch, A. L., Grøndahl, L., & Suwantong, O. (2023). Physicochemical and in vitro biological evaluation of an injectable self-healing quaternized chitosan/oxidized pectin hydrogel for potential use as a wound dressing material. *International Journal of Biological Macromolecules, 242*, 124984.

**PRESENTATIONS**

| | |
|---|---|
| 2023 | Oral presentation<br>Postgrad Symposium 2023, School of Science, Mae Fah Luang University, Thailand |
| 2024 | Flash Talk<br>The 2nd Graduate Symposium 2024, Mae Fah Luang University, Thailand |